Hindawi
Advances in Materials Science and Engineering
Volume 2021, Article ID 9723450, 60 pages
https://doi.org/10.1155/2021/9723450

Review Article

Recent Advancements in the Field of Ni-Based Superalloys

Senthil Kumaran Selvaraj,[1] **G. Sundaramali**,[1] **S. Jithin Dev**,[2] **R. Srii Swathish**,[2] **Rahul Karthikeyan**,[2] **K. E. Vijay Vishaal**,[2] **and Velmurugan Paramasivam**[3]

[1]*Department of Manufacturing Engineering, School of Mechanical Engineering (SMEC), Vellore Institute of Technology (VIT), Vellore 632014, Tamilnadu, India*
[2]*School of Mechanical Engineering, Vellore Institute of Technology (VIT), Vellore 632014, India*
[3]*School of Mechanical and Automotive Engineering, College of Engineering and Technology, Dilla University, Dilla 419, Ethiopia*

Correspondence should be addressed to Senthil Kumaran Selvaraj; senthilkumaran.s@vit.ac.in and Velmurugan Paramasivam; drvelmuruganp@du.edu.et

Received 21 October 2021; Revised 19 November 2021; Accepted 2 December 2021; Published 27 December 2021

Academic Editor: Fuat Kara

In this review article, research papers related to recent developments in Ni-superalloy technologies have been reviewed in order to provide an insight into recent achievements and the potential for further study, research, and development in this field. In this paper, studies on various aspects of Ni-based superalloys are reviewed, such as production methods, which include widely used casting methods, as well as unconventional alternative procedures, novel techniques, or simulation and prediction of certain alloy casting properties. Reviewing was done by categorising the papers into 4 major categories: manufacturing of Ni-based superalloys, effects of alloying elements, physical and mechanical properties of Ni-based superalloys, and defects in Ni-based superalloys. The process used to make Ni-superalloy parts can have a huge impact on the production process efficiency, the final product's quality and properties, and the defects formed in it. Investment casting is one of the most common methods for making Ni-superalloy parts. Manufacturing covers studies on various casting methods used to make Ni-based superalloy components, novel techniques and methods developed to improve casting procedures to produce better products, and alternative manufacturing methods like AM and HIP processing. Similar to production process, the role of alloying elements is also very important. Even minor changes in their compositions can cause significant changes in the final product. Simultaneously, these alloying elements appear to be more efficient in the development of new methods to control product quality, suppress defect formation, and improve material properties such as the creep and fatigue. As a result, the effects of various alloying elements used in castings of Ni-based superalloys are thoroughly examined. A material's properties are its most important components. They assist the industrialist in selecting or developing a material based on the needs of the application/use. With this in mind, many researchers have conducted extensive research on physical and mechanical properties, as well as how to improve them. Fatigue life, stress rupture, creep properties, impact ductility, strain response, stress relaxation behaviour, and so on are some of the most important physical and mechanical properties of Ni-superalloys. This article thoroughly reviews various studies on these properties, how and by what factors they are affected, and how they can be improved. Another important factor to consider when making Ni-superalloy castings is defect formation, which can affect the properties of the final product. Freckle defects, hot tears, porosities, and slivers are some of the major defects that occur in Ni-superalloys during the casting process. This article also reviews in detail about these defects, how they form, and how they affect the final product. These defects were found to have a significant influence on a variety of properties, such as creep, fatigue behaviour, and fracture mechanism. Topics and areas such as reinforcement of Ni-superalloys with the help of CNCs and 3D printing of Ni-superalloys that can provide scope for potential future research are highlighted based on the above-reviewed papers.

1. Introduction

An alloy is a mixture of metals and/or other elements in specific proportions. An alloy's properties will differ a lot from those of the individual alloying elements and can be altered using a various techniques. Superalloys are a type of alloy that is specifically designed to make parts that will be subjected to extremely harsh conditions that ordinary metals and alloys cannot withstand, thus failing prematurely. Due to superior mechanical and physical properties, superalloys

can endure harsh environments like those seen in gas turbines, rocket/aeroplane engines, nuclear power plants, military vehicles, and satellites. They can survive extreme temperature, pressure, and highly corrosive/erosive environments while giving great mechanical performance and a long life. They have high mechanical strength and creep resistance at high temperatures, good surface stability, and improved oxidation and corrosion resistance. Ni-based superalloys that have nickel as the main constituent are the most commonly used superalloys, due to their superior physical and mechanical properties, which give them a wide range of applications. This paper solely targets Ni-based superalloys. Table 1 lists the various Ni-superalloys used in the studies discussed in this article.

2. Objective of the Study

Use of Ni-superalloys has sky-rocketed in recent years due to their versatility, wide range of demands and applications, and superior physical and mechanical performance, particularly at high temperatures. This has prodded researchers to elaborately study the various aspects of Ni-superalloys (as depicted in Figure 1), to better understand their making, uniqueness, superiority, and improvement/development. This caused numerous advancements in their manufacturing and performance. The goal of this paper is to review recent technological advances and achievements in the field of Ni-based superalloys and to provide guidance on scope for future research. Extensive research has been conducted over the last decade on various manufacturing processes for making Ni-based superalloy components, different manufacturing methods and their optimization, the effect of alloying element compositions, the physical and mechanical properties of these alloys, and the impact of defects on these alloys. In this article, we reviewed 102 research papers that investigated and experimented on such aspects of Ni-based superalloys of the 1^{st}–4^{th} generation. We present an in-depth narrative review article underlining many recent discoveries that have aided in the advancement and improvement of Ni-based superalloy technology.

3. Manufacturing of Ni-Based Superalloy Components

The majority of nickel superalloys are made using an investment casting procedure in a Bridgman furnace. First, the molten metal is poured into a casting shell made of investment slurry, which is kept the furnace's hot chamber. After the metal is poured, the shell is gradually drawn into a cold chamber separate from the hot chamber, where the casting is cooled. A variety of casting techniques and methods can be used in conjunction with the process to improve certain aspects of the casting process, which can affect the final product's properties. Some casting parameters or conditions can also have an impact on the properties of the final casting. Aside from casting methods, some research on alternative methods for producing Ni-superalloy components has also been reviewed in this paper.

Table 1: List of Ni-superalloys used in the papers reviewed and in which study they have been used.

Ni-superalloys	Papers or studies in which the alloy is used in
AM1	[1]
MAR-M 247	[2, 3]
B1914	[3]
CM 247 LC	[4, 5]
IN 738 LC	[6, 7]
DD33	[8]
IN 718	[9, 10]
IN 713 LC	[11–14]
CMSX-4	[15–29]
PWA 1483	[30]
IN 100	[31, 32]
DZ24	[33]
K24	[33]
K 4169	[34]
RENE N4	[35]
DD6	[36–38]
IN 792	[39, 40]
CMSX-2	[41, 42]
K 465	[43]
IN 713 C	[44–47]
ZVhM4	[48]
DD3	[49]
CMSX-6	[17, 50]
CMSX-10	[50, 51]
Alloy 625	[52]
MAR 247	[53]
K 417 G	[54]
U500	[45]
K 4750	[55]
MAR-M 200	[41]
DD98	[56]
IN 939	[57]
EPM-102	[23]
DZ4	[58]
GH 4037	[59]

3.1. Casting of Nickel Superalloys: Influence of Casting Methods, Techniques, and Parameters on Final Products. Components made of Ni-superalloys are typically cast in a Bridgman furnace using investment casting process, as it is one of the most cost-effective, simple, and efficient production methods. A variety of techniques, such as high rate solidification (HRS), liquid metal cooling (LMC), and directional solidification, can be used in conjunction with the process to improve certain aspects of the casting process, such as withdrawal rate, thermal gradient, cooling rate, and cooling isotherm shape. All of these factors can cause the final product to have different properties. Some casting parameters, such as mould geometry and shell slurry contents, can also have an impact on the properties of the final casting or product. Thus, when it comes to casting Ni-based superalloy components, there are two very important factors that play a major role in influencing the properties of the final product. They are the casting method and the various casting techniques used, and the casting parameters and conditions used for casting. Directional solidification (DS) refers to the process of ensuring that grains grow in a single

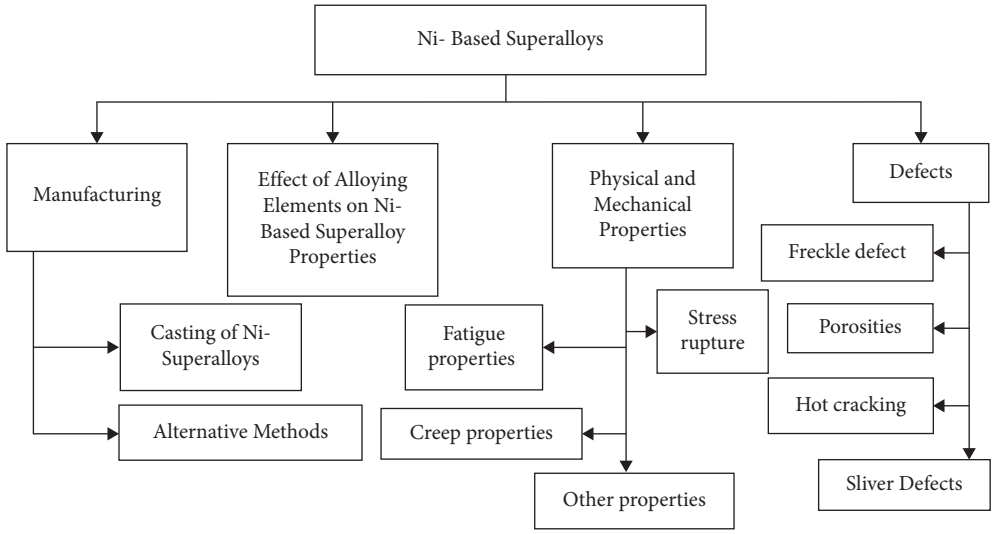

Figure 1: Grouping of the papers reviewed in different major categories. Further classification can be done in terms of area of research as given in Table 2.

Table 2: A broad grouping of papers reviewed in this article based on unique research areas.

S. No.	Research area	Papers pertaining to the respective area
1	Simulation studies: any study in which simulations were performed in order to reproduce or simulate different casting features, grain structures, skin formation, like the progression of S/L interface, shape of liquidus isotherm, etc.	[2, 8, 36, 37, 41, 42, 54, 56, 60–68]
2	Prediction studies: any study in which various methods were used for predicting the features of the cast specimens like pore size, freckle formation, grain structure, grain size, and fatigue life	[9, 17, 20, 28, 37, 41, 43, 58, 69]
3	Conventional investment casting (Bridgman furnace): any study that focuses on the conventional casting process where a Bridgman furnace is used	[16, 44–46, 70]
4	LMC process: any study in which LMC process was used or was talked about in depth	[1, 30, 35, 36, 71]

Table 2: Continued.

S. No.	Research area	Papers pertaining to the respective area
5	HRS process: any study in which HRS process was used or was talked about in depth	[8, 30, 36, 71]
6	Radiation baffles: any study that has used baffles or talked in depth about them	[16, 35]
7	Directional solidification: any study that talks in depth about the process and its effects and benefits on the final casting	[4, 5, 12, 15–17, 23, 26, 27, 48, 49, 56, 57, 71, 72, 100]
8	Single crystal: any study that talks in depth about the single crystal process and the procedure for producing a single crystal structure or its effects and benefits on the final casting	[4, 17, 19, 24, 26, 27, 33, 38, 41, 48, 49, 56, 57, 62, 72–74]
9	Polycrystalline: any study that deals with a superalloy having a polycrystal grain structure	[3, 5, 7, 12, 33, 46, 47, 53, 55, 57, 67]
10	Comparative studies: any study that has done a comparison on different properties, manufacturing methods, casting conditions, alloys, or any other parameters	[1–3, 10, 11, 13, 16, 19–23, 25, 30, 33–36, 39, 45, 47, 52, 53, 57, 66, 74–78]
11	1^{st} generation superalloy: any study that has used a 1^{st} generation superalloy	[1, 3, 5–7, 10, 11, 13, 30–35, 40, 42, 43, 49, 79]
12	2^{nd} generation superalloy: any study that has used a 2^{nd} generation superalloy	[16, 19, 20, 22, 23, 28, 29, 33, 36–38, 43, 56, 68]
13	3^{rd} generation superalloy: any study that has used a 3^{rd} generation superalloy	[8, 21, 50]
14	4^{th} generation superalloy: any study that has used a 4^{th} generation superalloy	[23, 51, 77]

Table 2: Continued.

S. No.	Research area	Papers pertaining to the respective area
15	Novel methods: any study that developed new methods to tackle various problems faced in the manufacturing of Ni-based superalloys	[13, 25, 39, 59, 69]
16	Microstructure: any study that talked in depth about the microstructure of the alloys used and its effect on alloy properties and quality	[7, 9–12, 15, 16, 18, 20, 22, 23, 29, 31, 32, 34, 35, 39, 46, 52, 54, 55, 57, 59, 67, 68, 72, 74, 76, 77, 79–84]
17	Fracture mode: any study that talks about the fracture mechanisms, modes, and crack propagation taking place in superalloys	[3, 10, 11, 13, 19, 20, 22, 30, 31, 37, 41, 43, 47, 53–55, 58, 59, 67, 77, 85]
18	Ductility	[37]
19	Grain or dendrite size: any study that talks in depth about the grain or dendrite size, PDAS value, SDAS value, carbide size, or other precipitate sizes	[11, 12, 16, 22, 34–36, 59, 66, 79, 80, 82, 86]
20	Grain refinement: any study that talks about grain refinement, the process of refinement, and how and why the refinement takes place	[16, 17, 34, 48, 49, 80, 87, 88]
21	Additive manufacturing: any study in which AM process was used	[10]
22	Hot isostatic pressing: any study in which the HIP process was used	[3, 14, 58, 67, 89]
23	Vacuum condition: any study that talked in depth about the effects of using vacuum conditions during casting procedure	[26]
24	Effect of alloying elements: any study that talks about the effects of different alloying elements and how varying their contents can affect the final product	[7, 40, 42, 55, 59, 73, 76, 77, 82, 83, 90]

Table 2: Continued.

S. No.	Research area	Papers pertaining to the respective area
25	Freckles: any study that talks about the formation of freckles, the harm they do, and how freckling can be avoided	[5, 8, 26–28, 35, 42, 85, 90–93]
26	Hot tears: any study that talks about the formation of hot tears, the harm they do, and how hot tears can be avoided	[7, 29, 38, 40, 94]
27	Porosities: any study that talks about the formation of porosities, the harm they do, and how they can be avoided	[20, 21, 25, 34, 37, 39, 43, 50, 54, 76]
28	Slivers: any study that talks about the formation of sliver defects, the harm they do, and how they can be avoided	[16, 68]
29	Fatigue properties: any study that deals with the different fatigue properties like fatigue life and behaviour of various superalloys	[1–3, 11–14, 20–22, 30, 41, 43, 47, 58, 67, 74, 86, 95, 96]
30	Creep properties: any study that deals with the different creep properties like creep life and behaviour of various superalloys	[1, 12, 18, 19, 23, 31, 41, 51, 74, 77, 78]
31	Stress/strain properties: any study that deals with the stress/strain properties like stress relaxation and rupture behaviour of various superalloys	[2, 12, 13, 22–25, 33, 37, 41, 45, 47, 52, 54, 55, 57, 58, 74, 88]
32	Grain selection: any study that talks in depth about the grain selection/competitive growth process that takes place when selecting a single grain while producing SX components	[4, 6, 36, 49, 56, 62, 85, 95, 97]
33	Geometric effect: any study that talks about how the geometry or dimensions of the components, the mould, or the cores affect the properties of the final product	[4, 5, 8, 31, 42, 79, 80, 93]

Table 2: Continued.

S. No.	Research area	Papers pertaining to the respective area
34	Ceramic mould/core constituents: any study that deals with the effects the composition and type of constituents of the ceramic slurry used in making the mould and cores have on the final product	[56, 66, 87]
35	Mould interaction with alloy: any study that deals with the different interactions that take place between the mould and the cast superalloy due to the reaction between the elements in the alloy and mould constituents	[46, 98, 99]
36	Grain orientation and misorientation: any study that deals with the formation of grains that present unacceptable deviations in the grain orientation angles, and studies that have come up with methods to prevent misorientation	[11, 22, 35, 36, 49, 56, 62, 68]
37	Use of supportive unconventional techniques: any study where some techniques or methods like TMF or EMS were used along with the casting process for specific purposes	[17, 27, 32, 41, 74]
38	Casting process conditions/ parameters: any study that talks in depth about the effects of using different casting conditions or parameters	[30, 31, 34, 44, 49, 80, 87]
39	Heat treatment: any study that talks in depth about different heat treatment processes and their effects on the properties of the final casting	[10, 23, 24, 33, 55, 57, 66, 67, 82]

Table 2: Continued.

S. No.	Research area	Papers pertaining to the respective area
40	Cooling rates: any study that has performed extensive examination into the cooling rate observed during the casting procedure and its impact on the casting properties	[1, 15, 16, 35, 42, 54, 66, 79, 80, 84, 85]
41	Withdrawal rates: any study that has performed extensive examination into the withdrawal rate used during the casting procedure and its impact on the casting properties	[8, 18, 26, 32, 35, 49, 50]
42	Coated alloys: any study that deals with alloys that have been given thermal barrier coatings	[12, 13, 22, 74, 81]

direction, resulting in a continuous and unbroken crystal lattice. DS is mostly obtained by casting with the assistance of a Bridgman furnace where the movement of the casting from the hot chamber to the cold chamber during solidification promotes grain growth in one direction. This uniformly oriented crystal structure can help improve mechanical and physical properties. Many experimental and simulation studies have been conducted to investigate and optimize the DS process of Ni-superalloys. The DS process is widely used in the production of Ni-superalloy castings, particularly turbine blades with a single crystal (SX) and columnar grain structure. Controlling solidification process parameters such as solidification rate and temperature gradient ensures that the desired macro and microstructure is obtained in turbine blade castings made of Ni-superalloys. One study [15] used ProCast simulation software to run numerical simulations of the temperature distribution and the DS process. Various parameters influencing the DS process, such as temperature gradient, solidification rate, cooling rate, and the shape of the liquidus isotherm relative to the thermal baffles, were all established along the height of the cast rod using data from numerical simulations. The study discovered that solidification conditions vary continuously along the height of the components as solidification progresses. Furthermore, the cooling rate was found to be highest where the casting and the chill plate came into contact, and the chill plate's impact on the cooling rate and thermal gradient was found to significantly decrease beyond a critical height. The thermal gradient was seen to gradually decrease as solidification and the solidification front progressed, indicating the growing thermal resistance of alloy upon solidification. It was also discovered that the height of the mushy zone increased as the withdrawal rate increased. The liquidus isotherm was also observed to change in response to changes in withdrawal rates and height away from the chill plate. The liquidus isotherm had a concave shape near the chill plate, and it changed to a convex shape as it moved away from the chill plate with solidification progressing. When low withdrawal rates were used, the isotherm inclined towards the chill rings, while inclining towards the central rod at high withdrawal rates. The shape of the isotherm had an effect on the grain growth as well. A liquidus isotherm with a flat shape was observed to induce grain growth in the direction most parallel to the symmetry axis. Occasionally, stray grains were formed during the DS process. These grains should be avoided in order to maintain superior casting quality and properties. As a result, one study [60] focused on using a fuzzy control algorithm to dynamically change the withdrawal rate used to prevent the formation of stray grains. The withdrawal rate changes were calculated using input parameters such as the width of the mushy zone, temperature differences at the cast-mould interface (ITE), and change in ITE. Based on the structural features of the casting, the multivariable fuzzy rule was developed. The study developed a fuzzy control model that analysed data from the simulation process in real time while tracking a few critical variables in order to change the withdrawal rates in relation to some other factors in order to find optimized parameters for the production of defect-free castings. The process was found to aid in the design of DS models with high temperature gradients, the expansion of process windows, and the production of defect-free castings.

Techniques such as the DS process, which helps to orient the grains in a specific direction, can also play a significant role in grain and dendrite growth in Ni-superalloy castings. This was specifically investigated in a study [61]. Using

numerical simulation techniques, the researchers investigated the microstructural evolutions in Ni-based superalloy castings that occur during the DS process. To investigate the microstructural evolutions, a solute diffusion model coupled with a macro temperature field and a meso grain structure model is used in this study. Cooling curves and grain structure data from the experimental results were used to validate the simulation results. The initial nuclei's growth and dendrite arm spacings were also investigated using macrosimulations. The temperature measurements and numerical simulations used in this study were used to validate the model proposed in this study and determine the solidification time during the DS process. A linear decrease in temperature distribution was seen along the mould length. Undercooling at the shell mould and superalloy was observed to be caused by the chill plate at a distance of approximately 20 mm from the casting base. A temperature distribution that was constantly changing was observed. The grain structures that had developed along the direction of the heat flux had the highest probability of sustaining growth. As a result, only a portion of the grain with the preferred orientation continued to grow in the preferred direction. Grains with unfavourable growth directions were observed to stop growing at the expense of columnar crystals with growth directions parallel to the heat flux direction. The decreasing grain numbers observed as the distance between the chill plate and the casting base increased characterized this competitive growth of grains. Temperature gradient and cooling rate were coupled with macro temperature field and grain structure simulation results, and adiabatic boundary conditions were set up on all four sides of the model. The study discovered a 4-fold symmetry of a "cruciate flower" in the secondary dendrite arms, as well as initial tertiary dendrite arms developing immediately behind the secondary dendrite tip, which had grown in a perpendicular direction with random spacing, relative to the secondary arms' growth direction. The competitive growth was also observed to cause a decrease in grain numbers as the cross-section's height increased. As a result, the dendrite arm spacing increases. Dendrite tip growth was sufficiently slowed by intensified solute field interactions between adjacent dendrites and rejection of solute into the melt. Secondary dendrite arm coarsening was observed as a result. As the solidification process progressed, a few dendrites developed misalignment angles. Misalignment angles were seen to significantly affect the competitive dendrite growth. Moreover, for large misalignment angles, the competitive phenomenon was seen to start quickly at grain boundaries (GBs). The secondary arms were also seen to be flourishing and branching at diverging GBs. Observing one initial seed revealed the preferential growth of many typical cross-shaped solidification structures in about a 100 different directions. The free growth of dendrites and coarsening of the primary trunk of the dendrites along with side branching were also seen. Severe competitive growth was seen to take place because of an increase in the number of secondary dendrite arms originating from the primary dendrite arms, as solidification progressed. Also, the uneven fluctuations in the temperature of the components was seen to cause quicker growth of dendrites with the preferred orientation while the elimination of other dendrites took place as a result of their growth being blocked, and adjustments to the dendrite arm spacing was observed to happen accordingly. Finally, stable dendrite growth with equally distributed dendrite arm spacing was observed. Another study [100] was conducted to compare normal DS process taking place in Bridgman furnace with the downward directional solidification (DWDS) technique. In the DWDS technique, the DS occurred in a downward direction along gravity as the chill plate was attached to the top part of the component, compared to the conventional process where DS occurs against gravity. The study revealed that compared to the typical Bridgman DS casting process, DWDS process had the ability to produce thermal gradients that were 10–12 times greater, thus confirming the superior heat extraction capabilities of the DWDS process. The vastly higher thermal gradients obtained during DWDS process was seen to help maintain a stable liquid/solid interface, even at very high withdrawal rates, and thus reduce the formation of defects. Compared to Bridgman samples, significant refinement of the primary and secondary dendrites was also seen in DWDS samples. Bridgman samples were seen to have very few but large eutectic pools, while DWDS samples were seen to have a numerous small eutectic pools. The size of γ' phase in the sample made from DWDS was seen to be 42–48% smaller than the γ' phase present in the Bridgman furnace sample. DWDS also reduced the pore size of the samples' microporosities by 43–57 percent. The segregation coefficients of Cr, Mo, and Co in Bridgman solidified samples were found to be much greater than one, indicating significant segregation of these elements into the dendrite cores. In DWDS samples, the segregation coefficient for the aforementioned elements was observed to fluctuate around unity. These elements also showed no strong tendency to segregate into the dendritic core or the interdendritic regions. Furthermore, when DWDS solidified CMSX-4 samples were compared to Bridgman samples, the segregation coefficients for W and Re showed a smaller deviation from unity.

It is common knowledge that directionally solidified components have superior properties. This was further investigated experimentally and confirmed in terms of stress rupture properties, one of the most important properties of Ni-based superalloys, in one study [33]. The study compared the microstructural and stress rupture properties of DS Ni-superalloy castings and polycrystal Ni-superalloy castings. The K24 superalloy was used to create equiaxed polycrystal materials for harsh environments. However, at extremely high temperatures, the GBs of K24 superalloy with an equiaxed grain structure become a favourable site for damage accumulation, with crack growth appearing even in the early stages of use. The DS process is used to produce blades with a columnar and directional grain structure, which solves this problem. Only a few columnar grains in DS castings have an orientation that is parallel to the preferred crystallographic direction. The absence of transverse GBs was also observed in these castings, and as a result, the stress-rupture life of the DS castings was significantly higher than that of the polycrystal castings. The microstructural and

rupture properties of the new directionally solidified Ni-based superalloy DZ24 obtained by modification of K24 were also compared to the polycrystal K24 superalloy in this study. The DS specimens were made using vacuum precision casting. Rupture tests were carried out at a stress of approximately 196 MPa and a temperature of approximately 975°C. Both as-cast K24 and DZ24 alloys were found to exhibit serious dendritic patterns while studying their microstructure. And their microstructure was seen to be composed of carbides, γ, γ', and γ/γ' eutectic pools. Complete removal of existing dendritic structures was observed in these alloys during heat treatment. And a full dissolving of coarse γ' and γ/γ' eutectic regions into the γ matrix was observed. Further observation of DZ24 alloy's microstructure showed reprecipitation of fine and regular cubic γ' phase. During aging, due to the reaction of carbides with the matrix, enveloping of $M_{23}C_6$ and M_6C carbides and the γ' phase around the MC carbides was observed in the DZ24 alloy. The DZ24 alloy was seen to have a rupture time which was 2 times that of the K24 alloy. Further investigation of the K24 alloy's microstructure showed wider spacing between the γ' precipitates, while the volume of the γ' phase was seen to be small. As a result, no γ' rafting at the time of stress rupture tests were observed. In the DZ24 alloy, due to significantly high volume, the spacing of γ' precipitates was seen to be much closer, and γ' rafting was seen to occur under stress rupture conditions. Higher volume fraction of fine and regular cubical γ' precipitates was seen to provide better and more optimal rupture resistance in these alloys. The study proved superiority of DS castings of DZ24 in comparison with K24 superalloy. A highly similar study [57] did a comparative analysis of the microstructure and the mechanical properties of samples that were conventionally cast, made using the DS process, and made using the single crystal (SX) casting process. IN939 superalloy was used for this study. <100> crystallographic orientation was only exhibited by a few columnar grains in the DS sample, while a SX casting was seen to be made entirely of just only one grain. Mechanical properties were compared in terms of the samples' stress rupture lives. Stress-rupture life, under similar conditions, was calculated for both as-cast (DS samples) and heat-treated (polycrystal and SX samples) samples. Testing of both SX and polycrystal samples took place only after they were heat treated. All as-cast samples were seen to have a cored dendritic microstructure that consisted of γ solid solution, intermetallic γ' phase, and MC-type primary carbides. The γ' phase's volume fraction and the formation of secondary $M_{23}C_6$ carbides were seen to increase during heat treatment. It was also seen that stress rupture life improved as the γ' phase's volume fraction increased with heat treatment. SX castings were seen to have highly superior stress-rupture lives when compared to DS castings, and particularly polycrystal castings. GBs are considered as weak spots in the microstructure. The elimination of GBs in SX castings accounted for the difference in rupture life. Just like the DS process improving the quality of the final product, there are a few other techniques which can be executed along with the DS process in order to produce components of even better quality. One such method is making SX components. These components are made from one single crystal, thus eliminating the presence of GBs and the defects that are associated with it. This can help in enhancing the quality of the final product, as seen in the study reviewed above. SX castings are made by exploiting a phenomenon called competitive growth, where grains that are formed initially at the start of cooling compete with each other to sustain their own growth and thus eliminate the growth of other grains. At the end of this process, only one grain will survive, and this grain will continue to grow in a stable manner to make the entire component, thus forming a single crystal component. Grain selection refers to the process of selecting a grain through competitive growth. Grain selection is done during the DS process with the help of a grain selector unit, which is made up of a starter block and a grain selector. The efficiency of the grain selection process can be influenced by varying the properties of these components, and grain selection research was carried to optimize it. One such study [49] was conducted specifically to gather information on how spiral grain selectors aid in grain selection while casting SX components and how grain orientation can be influenced during the process. SX castings have an advantage over DS or conventional castings in that the desirable [001] crystallographic orientation direction overlaps with the direction along which the alloy component has the lowest Young's modulus value and is parallel to the component's axis. The creep resistance of an SX blade along the longitudinal direction improves as this directional orientation becomes more accurate and close to [001]. Even minor deviations from this axial orientation could result in a significant reduction in creep performance. The process of grain texture evolution in the spiral grain selector during DS was examined in this study to investigate the grain selection mechanism taking place in the spiral passage. The effect of spiral grain selector geometry on crystallographic orientation and grain selection in spiral passage was investigated. Many spiral grain selectors with varying geometries were used for this purpose. The spiral rotation diameter was kept constant, and the average thermal gradient was 45 K/cm. The study revealed the main purpose of the starter block to be optimizing the crystal orientation, with 35 mm being the ideal length of a starter block for achieving optimal grain orientation. During the grain selection, the grain closest to the inner wall of the spiral passage was chosen as the final single crystal. Further research revealed that new tertiary dendrite arms grew from secondary dendrite arms in a direction parallel to the primary dendrites near the inner wall, thus causing dendrite overgrowth far from the inner wall. This study also aided to correlate grain deviation angle to a variety of factors, as shown in Figures 2 and 3. X-ray diffraction analysis of crystal orientation revealed that increasing spiral thickness or angle did not result in any significant change in crystal orientation. An increase in the temperature of ceramic mould and the withdrawal rate, on the other hand, was observed to optimize crystal orientation. However, when the withdrawal rate was increased to 200 mm/s in this study, the selection of an SX structure was found to be impossible. It was also discovered that the grain number decreased gradually as the pouring temperature

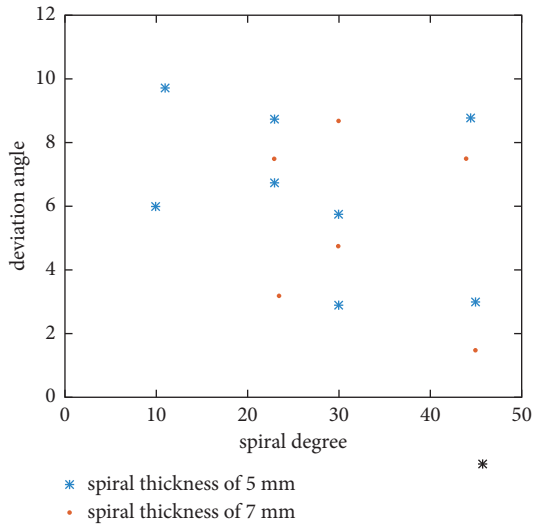

Figure 2: Relationship between the spiral ceramic mould temperatures on crystal orientation.

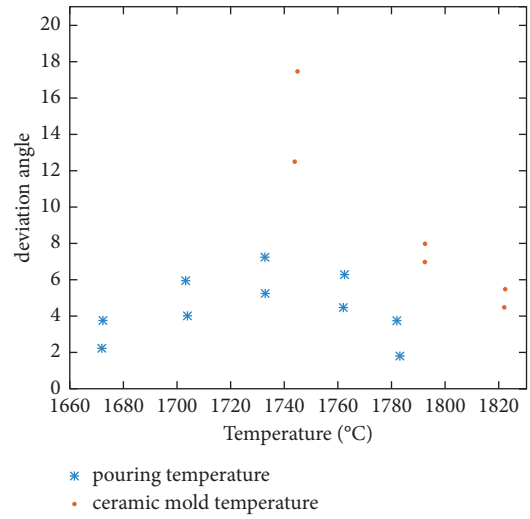

Figure 3: Effect of pouring and geometries and crystal orientation.

increased. The main function of the spiral part was determined to be ensuring the survival of only one grain at the completion of the grain selection process that occurs in the spiral passage. Geometrical blocking caused by competitive grain growth was discovered to be the primary mechanism that aided in grain selection in the spiral part. Grain selection in the spiral selector was found to have no effect on crystal orientation, and spiral geometry was found to have no effect on crystal orientation. The pouring temperature was found to have a large influence on the SX orientation and grain texture in the starter block, and SX castings with small angles of deviation were found to be achievable by causing a decrease or increase in pouring temperature around 1460°C. Another study [56] was conducted to investigate grain selection with the help of simulation and experimental validation of results. ProCAST software was used to run simulations based on a cellular automata finite element (CAFE) model. A spiral grain selector is made up of two parts: a helicoid-shaped spiral part and a cylindrical start block. The initial angle of the spiral, turn of the spiral (r), height of the starter block (H), diameter of the spiral (D), length of screw pitch (Lp), and diameter of the helicoids (d) are the various parameters used to design a spiral grain selector. This study investigated the grain selection process by utilising various spiral designs obtained by tinkering with the aforementioned parameters. The starter block model for this study was a cylinder with dimensions of 15 mm × 100 mm. The DS experiments were carried out in a vacuum furnace. In this study, DD98, a 2nd generation Ni-superalloy, was used. Observations showed that maintaining the dimensions of the selector within a stable range was crucial for proper grain orientation and selection of a single crystal efficiently. With the starter block diameter (15 mm) being fixed, the height of the starter was varied between 20 and 30 mm. And while fixing the turn of spiral part ($1r$) and length of screw pitch (30 mm), initial angle and diameter with values in the range 45°–65° and 10–16 mm, respectively, were used. Simulation results showed that a starter block height of 25 mm, spiral part diameter of 15 mm, and initial angle of 45° were the optimal parameters that encouraged the successful and efficient selection of a single crystal with regard to the thermal conditions and the furnace used in the study. The data pertaining to these findings are depicted graphically in Figures 4–6. These findings were confirmed by experimental results. Changes in the grain crystallographic orientation during grain selection in the spiral was seen to occur as a result of unstable growth of dendrites that was caused fluctuation in local thermal conditions. A similar experiment [62] was also done to study grain selection and grain orientation induced by a grain selector using a different superalloy, DD6. This study also showed similar results as the previous. The simulation results in both studies were seen to agree with the experimental results. There was a very familiar research to the ones above conducted to study grain selection. But, in this study [97], the effect of a grain selector's structural parameters and other aspects of the solidification process on grain selection was also investigated. This study employed experimental and simulation methods to examine the structural design and grain selection of the spiral selector. Two models for the grain selector were developed using the cellular automation-finite difference (CA-FD) method: a heat transfer model and a 3D microstructure growth model. Following that, simulations were used to verify the distribution of grain orientation, temperature field distribution, and microstructure. This study also included a grain growth model based on solute equilibrium and a heat radiation model. The relationship between the DS process and the grain selection mechanism was further investigated using simulation tools. The energy transfer during DS was seen to be extremely complex with 6 ways for heat transfer. It was discovered that radiation and conduction of heat were the two major methods of heat transfer. In this study, SX components made of DD6 Ni-superalloy were used. The cooling rate values obtained from both temperature measurement and simulation results were found to be nearly identical. It was also discovered that the chilling effect caused the simulation fluctuated at the start.

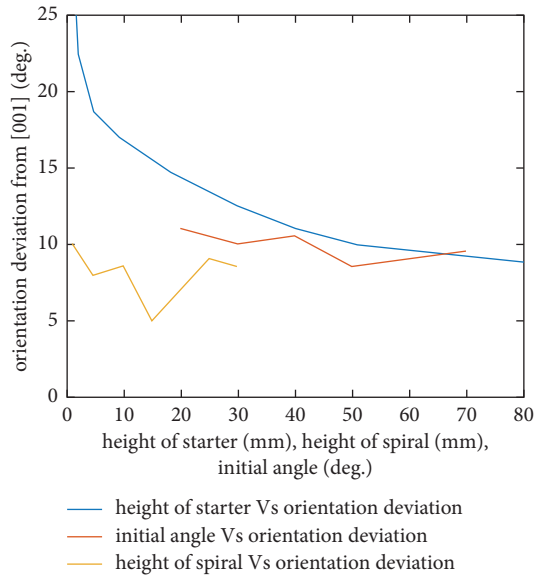

Figure 4: Change in orientation deviation w.r.t. changes in height of starter, height of spiral, and initial angle.

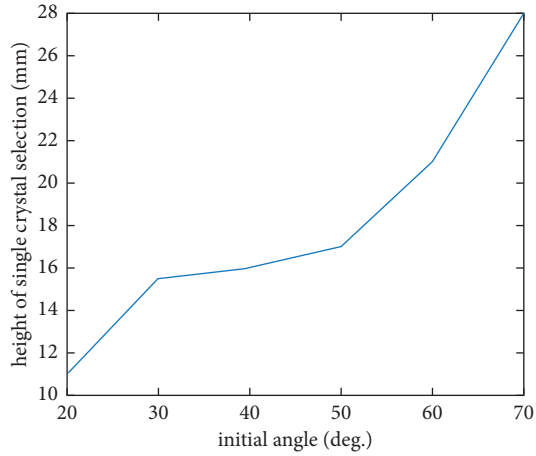

Figure 5: The graph shows how the single crystal selection height changes w.r.t varying initial angle of spiral selector.

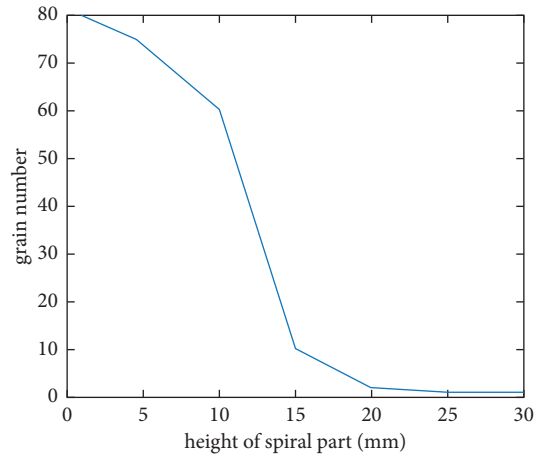

Figure 6: The graph depicts how the change in the height of the spiral part can influence the number of grains found at said height.

During the early stages of solidification, a large number of small grains were observed at the bottom. However, the sizes of these grains were observed to gradually increase with increasing solidification height and progress. However, once the solidification height reached a certain value, the size of the grains did not increase any further and remained constant with further increases in solidification height. The grain density curve of the starter block was observed to have three possible sections based on grain density distribution: the exponentially decreasing zone, the linearly decreasing zone, and the stable zone. The inclined S/L interface along the spiral part was found to be responsible for the complete destruction of the unidirectional heat flow. This was observed as a result of the lower heat transfer efficiency of mould versus heat transfer through metals. The inclination of the S/L interface and the isothermal surface occurred as a result of the majority of the heat flowing along the spiral tunnel. The efficiencies of spiral selectors were found to be highly dependent on their respective geometries. The efficiency of the spiral improved when a smaller take-off angle, a shorter pitch length, a smaller diameter of wax wire, and a comparatively larger diameter of spiral rotation were used for the same pitch lengths. During grain selection in the spiral part, most grains were seen to be strained and eliminated. Horizontal growth and expansion of grains formed near the lower edge of the spiral part's cross-section were observed. Furthermore, decreasing the spiral angle increased the number of grains blocked and eliminated. Therefore, a direct geometric constraint on primary dendrite growth in the vertical direction was seen in the spiral selector. During selection process, higher starter block heights (h_b) was seen to better control and limit the number of grains entering the spiral part, but starter blocks with very large heights were seen to consume a lot of additional metals and thus time for casting. Limiting the number of grains entering the spiral part was also seen to be affected by the spiral tunnel diameter (d_w). Once an SX structure has completely filled a particular section, the distance between the bottom of the spiral part and this section is the single crystal selection height (Hs). Figure 7 depicts the average value of Hs increasing with increasing d_w based on data obtained from this study. The grain selection effect was seen to be weakened as a result of this, due to the low number of grains entering the spiral part. A smaller d_w is due to the low number of grains entering the spiral part. A smaller d_w was observed to aid in a quicker crystal selection process. Moreover, when the d_w value was low, a wider crystal selection range was seen. But however, the seeming position of H_s was observed to be highly unstable. This was observed to be a result of the low number of grains entering the tunnel enhancing grain selection randomness. On the contrary, a high d_w value was seen to reduce grain selection's randomness and make H_s value appear more concentrated. Thus, d_w was seen to largely influence the SX selection process, the selector's structural strength, and selection efficiency. Also, when the spiral diameter (d_s) was fixed, the spiral pitch (h_s) was seen to be proportional to tanθ. Consequently, large material consumption and increased solidification time were observed with high h_s values. Figure 8 shows the effect h_s has on SX

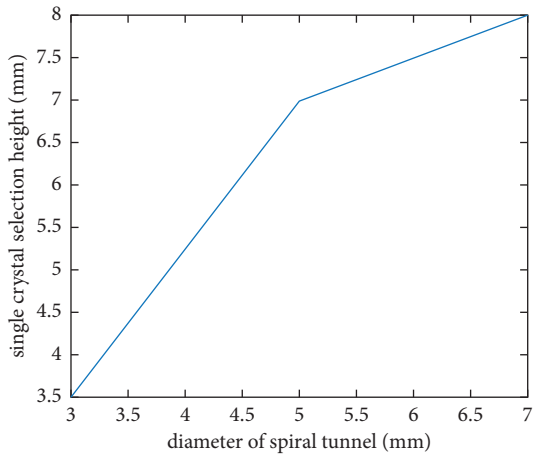

Figure 7: Relationship between the diameter of the spiral tunnel and the SX selection height.

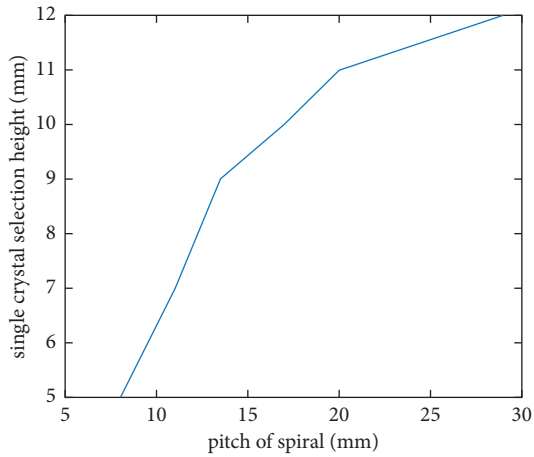

Figure 8: Relationship between pitch of spiral and SX selection height.

selection height to follow a similar trend to the effect d_w has on SX selection height. Furthermore, for a constant h_s value, d_s was seen to be inversely proportional to tanθ. In addition, this solidification sequence was not followed by the liquid region at the top of the spiral part. The study showed that nucleation and growth of stray grains might happen in the undercooled regions, which could significantly increase the chances of a failed grain selection process. As a result of the eccentric arrangement of the crystal, the mushy zone was observed to be slightly convex and inclined. Contrarily, the inclination degree was found to be low and its influence on grain growth and orientation was seen to be negligible. And with it reaching the spiral selector's top, the successful SX selection was seen. Though many studies focus on the grain selection of the grain selector to produce SX castings, the grain selector can also help achieve a particular grain orientation. One study [6] particularly focused on this issue, but instead of spiral selectors used a Z-form grain selector to examine the influence of its take-off angle on the SX grain selection and orientation. Deviations in the orientations of grains are extremely significant defects that occur in SX superalloys during the DS process. SX superalloy samples made of Ni-superalloy MM247LC made using the Z-form grain selector modified Bridgman method was used in this study. The Z-form 2D selector was made of 3 parts: a starter block, a connector, and a z-selector. When the grain selectors' take-off angle was small, as dendrites grew into the Z-form grain selector, growth of many dendrites except for the ones near the Z-form's grain selection side was seen to be limited by the wall. Thus, the small take-off angle was seen to enable the successful SX selection. However, large deviation angles in the surviving dendrites were observed because the surviving dendrites were not from the core of the wire connecting the starter block to the grain selector, but from the outer part. While the outward grains are stray grains, the final main grains that grow are usually the dendrites from the core of the connection tube. And as a result, when using selectors having large take-off angles, small deviation angles were observed. But the chance of selecting a single grain was seen to reduce. The study also revealed that the dendrites most likely appeared on the inner side of the turns, as the coarse phenomenon of dendrites in the <001> direction was observed at the turns after corrosion. Also, the lateral dendrite appeared on the outside of the turn at the second bend of the Z-form. The homogenization effect of diffusion and solute distribution coefficient were the main factors influencing dendritic segregation during the DS process. Changes in elemental segregation were mostly seen to depend on the homogenization effect of the diffusion. However, the spreading distance and the diffusion time were the main factors influencing the dendritic segregation. In addition to this, it was also seen that the competitive growth of dendrites caused by their coarsening was simultaneously accompanied by the nonuniform concentration distribution of elements in the dendritic region. This was seen to positively influence the blocking effect that was seen to occur during the grain selection process. It was also seen that the outer side of the Z-form grain selector's 2nd turning point was where the coarsening of the dendrites took place. Dendrite coarsening was mostly seen to be exhibited by the lateral dendrites. And the 2nd turning point's inner side was observed to be not so prone to dendrite coarsening. The coarsening of turning dendrites was mostly instigated by the very fast changes that occurred to the heat flow vector at these turning points. Further investigations showed that this caused the slow diffusion of solute and their accumulation at these turns, which decreased cooling and solidification rates and ultimately dendrite coarsening. While many studies regarding grain selectors concentrated on the spiral selector part, one particular study [95] focused on the starter block's impact on DS of single-crystal Ni-based superalloys. The effect the starter block parameters can have on grain selection and the selection mechanism was examined in this study. The study used experimental procedures to optimize the starter block parameters properly. In the starter block, the grain selection mechanism is influenced mainly by 2 factors: the competitive growth of grains at the initial stages and the blocking wall at the end. The Ni-superalloy CM247LC was used in this study. Grain selection in the starter block was seen to occur in 2 stages: competitive

growth (1st stage) and mould wall's blocking effect (2nd stage). Electron backscatter diffraction (EBSD) results showed that the average deviation from the <001> orientation of 4 dissimilar grains taken from starter blocks with different diameters was above 20°. Moreover, the grain diameter was seen to have little or no effect on their chilling or nucleation. Various equiaxed crystals with different <001> orientations were seen to nucleate at the seeding section's bottom region. At the same time, the transfer of heat between the molten metal and the chill plate caused the temperature to fall below the alloy's liquidus. Further examination showed that there were changes in the grain's <001> orientation deviation found in the 4 different starter blocks, as their heights varied. Data regarding these trends followed by grain orientation deviation angle is graphically represented in Figure 9. It was also seen that an increase in the starter block diameter led to an increased amount of molten metal to be consumed. Though the reduction in the starter block diameter was seen to improve and further optimize the grain orientation process, having a too-small diameter was seen to harm starter block quality and grain selection efficiency. Minimal diameters were also seen to prevent the necessary amount of grains from gaining entry into the selector. In contrast, a very large starter block diameter was seen to allow an undesirably massive number of grains to enter the selector. Data regarding this are depicted in Figure 10. It was also found that minimal starter block diameters caused severe instability of the liquidus and isotherms, which resulted in the <001> orientation deviation increasing. Another study [4] focused on the efficiency of a 2-D grain selector during the casting and solidification of Ni-based SX superalloys. This study investigated a newly designed high-efficient 2-D selector with varying geometrical parameters regarding the competitive growth and grain selection taking place in it. The study revealed significantly reduced grain numbers as the selector height increased. This was seen to be accompanied by the grains enlarged gradually. The greatly reduced value proved the high efficiency of the new 2D selector for the number of grains found in the selector. Increasing the eccentric distance was seen to cause a reduction in the selection height, as depicted in Figure 11, thus indicating an increase in the 2D selector's selection efficiency as the eccentric distance increased. However, structural instability was observed when the eccentric distance was increased beyond 20 mm. The study revealed that having a large eccentric distance and a small thickness made the grain selection process more efficient. With the 2D grain selector's selector part's stability taken into account, an eccentric distance of 8 mm and thickness of 3 mm were recommended. When the thickness was 3 mm or smaller, a single grain was seen to be selected. Reducing this value was seen to make the grain selector more effective. Similar results were seen when the eccentric distance of 8 mm or more was used.

Apart from using the conventional Bridgman furnace to make DS castings, other techniques are employed to obtain DS castings with the SX structure. Studies have been done on such techniques to find how beneficial they can be to conventional techniques or procedures. One such study [63]

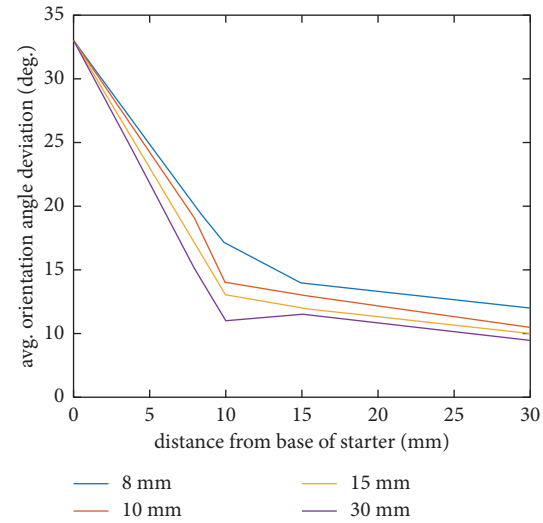

Figure 9: The relationship between the distance of grain from base of starter and average orientation angle deviation for various starter block diameters.

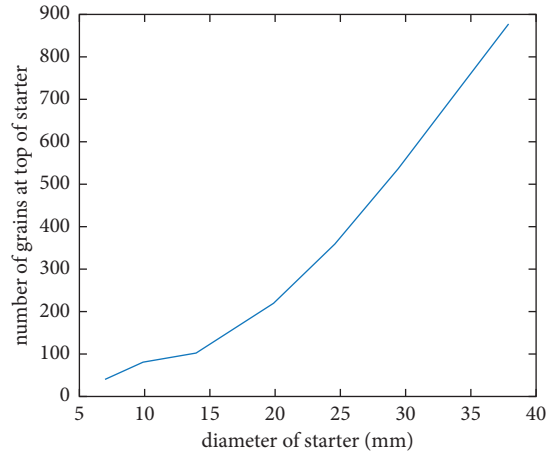

Figure 10: The relationship between the starter diameter and the number of grains present at the end of starter.

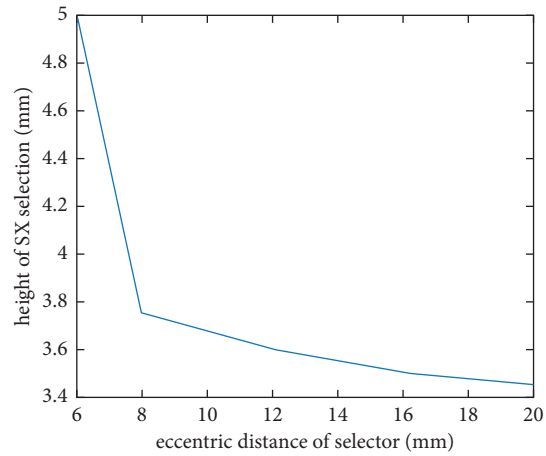

Figure 11: The relationship between the eccentric height and the SX crystal selection height.

focuses on a liquid metal cooling (LMC) process. This study aimed at predicting the microstructure evolution and temperature distribution during the LMC process. In the study, the coupling issues of the macro-micro grids were dealt with by an interpolation algorithm. The solute distribution was also taken into account to define the growth of dendrites. Experimental results were used to verify the proposed model. Varying withdrawal rates were used in the study to perform numerous simulations. A liquid metal with a low melting point temperature is used as a coolant in the cooling zone during the LMC process to extract the heat more efficiently via heat convection and conduction. Employing this method was seen to provide many benefits, especially in maintaining DS and SX microstructures for Ni-based superalloy parts with large transverse sections via immense heat extraction. There are 3 ways of heat dissipation between the mould, the shell, and the ambient environment during an LMC process: radiation, conduction, and convection. Meso grain structure, microdendrites, and macro temperature fields of the plate castings were simulated in this study with the help of a multiscale coupling model. It was observed that the withdrawal rate used had a strong influence over the heating and cooling efficiencies of the DS process. For all withdrawal processes, at the initial stage, the length of the mushy zone was seen to be narrow. As the liquid fraction was seen to slowly increase for all withdrawal processes with progress in withdrawal and solidification, the mushy zone length was seen to increase/widen, proving the chill plate's high heat extraction efficiency at the initial stage compared to the subsequent stages. However, the value of the mushy zone length was seen to vary with varying withdrawal rates considerably. Moreover, slight changes in the mushy zone and large range of fluctuations concerning certain other changes were observed in the study as the solidification fraction increased. Furthermore, having a flat and narrow mushy zone was seen to help reduce solidification defects. In the LMC process, the solute distribution in the vicinity of the dendrite tip where fluid flow occurs was seen to be affected by the mushy zone's curvature formed across the width of castings. The primary and secondary dendritic arm's growth was also seen to be affected by the mushy zone's curvature. Preferential growth of grains and the primary dendrites angled towards the centreline of the castings, and the preferential growth of secondary dendrites towards the centre was seen to be caused due to the presence of a concave interface. The study revealed that the average deviations and number of grains decreased as the solidification rate increased, in the case of all withdrawal rates. The number of grains was also seen to decrease significantly when the height of the interface from the casting base was seen to drop below 20 mm. This was accounted for by the many grains having different orientations fiercely competing with each other during the initial stage of the DS process. Followed by this, rapid elimination of grains having huge deviation angles and grain orientation optimization were observed. With further increase in the distance, the competition between the grains was seen to be relieved and the number of grains was seen to gradually decrease. Likewise, decreasing average deviation angles were also seen due to the increasing distance of interface from the casting base. Dendrites having huge angles of deviation formed by the angle between the z-axis and the desired direction of growth were lagging behind the dendrites exhibiting little or zero deviation angles. A growth advantage was provided to the grain, with the direction of growth being perpendicular to a tangent drawn to the isothermal line. It was also found that the primary dendrite struggle was the main factor influencing competitive growth with a converging relationship. The struggling of the secondary dendrite arms at the contact position below the S/L interface was seen to cause the competitive growth with a diverging relationship. During withdrawal, nucleation in the bulk of the liquid was not considered to have occurred while only the growth of the seeds placed at the base of the DS castings were considered. Therefore, the study concluded that the competition mechanisms and branching exhibited during the growth of initial seeds were the only contributing factors towards the development of the final dendrites. Three other studies compared the LMC process with the HRS process. One of these studies [35] focused on casting that were made to resemble the IGT blades, so that the data collected from the study can be used to find the benefits of using LMC for manufacturing IGT blades. At the beginning of the Bridgman process to produce large IGT blades, initially cooling takes place due to conduction of heat from the solidifying casting to the chill plate. During the withdrawal of large castings, the very low heat conductivity of many Ni-based superalloys makes this heat extraction method highly inefficient. As a result, the dominating mode of heat extraction becomes radiation via a vacuum. This leads to the solidification front experiencing low thermal gradients. Using the LMC process is one way to improve the heat extraction during solidification. One of this study's main goals was to conduct a thorough comparative analysis of the LMC and Bridgman processes. The study revealed that the thermal gradients produced in LMC process were 2 times higher when compared to those seen in Bridgman processes. And for the experimental model examined in this study, the LMC process was seen enable the withdrawal of castings, 2-3 times faster than speeds used in the conventional process. This was seen to help achieve cooling rates that were up to 7.5 times higher compared to conventional processes. The S/L interface, which is affected by casting parameters, like cooling efficiency, heating efficiency, and withdrawal rate, was seen to have a strong impact on the number of grains that were misaligned and the shape of the interface. Freckling was eliminated, and the casting defects were seen to have significantly reduced when the S/L interface was found to be present closer to the floating baffles during LMC processes. Moreover, the study proved that favourable interface location and shape can be maintained even while using significantly high withdrawal rates while casting is done using the LMC process, thus helping in obtaining a highly refined microstructure with significantly reduced primary dendrite arm spacing (PDAS) values. When casting significantly large SX components with a DS columnar grain structure, the LMC process was seen to be extremely advantageous as it helped reduce the time taken for casting, reduce the number

of defects formed during casting, and produce a microstructure that is highly refined. The other 2 similar studies [36, 71] which also compared HRS and LMC processes did not focus on IGT blades but had a more generalized approach as to which one can be beneficial to cast any Ni-based superalloy parts. The LMC-DS and conventional HRS processes were compared in these studies from both experimental and theoretical perspectives. The following analyses regarding the temperature field distribution, crystallographic orientation, and dendrite arm spacing were conducted for both HRS and LMC processes. And the LMC process was seen to produce superior results in all these areas. A more horizontal and narrow mushy zone was seen to have been attained by the LMC process compared to the HRS process. Radiation was seen to be the mode of heat extraction in the HRS process. Unlike in HRS, in the LMC process, castings were lowered into a liquid tin bath and convection was the main mode of heat dissipation. And this was seen to provide a larger thermal gradient in the LMC process in comparison to HRS. The average angle of deviation in grains was seen to be smaller in LMC castings than that in the HRS ones. Dendrites that were observed in specimens made using the LMC process was also seen to have undergone significantly better refinement. More refined dendrites were also observed in the samples produced by the LMC process with reduction in PDAS values by 50%, due to higher thermal gradients, cooling rates, and better shielding of the cooling chamber from the furnace. The study proved the superior use of the LMC technique in casting Ni-based superalloys compared to the HRS method. Another study [16] discusses the effects casting conditions can have on high cycle conditions and microstructural properties of Ni-superalloys. PWA 1483 Ni-superalloy was used in this study. The paper focuses on the changes in the microstructure and how it affects the high-cycle fatigue properties. The HRS process is the most commonly used solidification process in industries today. Two dissimilar casting methods (LMC and HRS) and wall thicknesses for the cast bars and slabs were used to vary the solidification conditions. It was found that, by improving thermal and cooling gradients or by switching the process from HRS to LMC, microstructure refinement takes place and, a decrease in the value of PDAS and SDAS as depicted in Figures 12 and 13, coarsening of carbide, and reduction in the number of microporosities formed and their size were also observed. It was also observed that having more refined microstructure and optimized casting conditions meant better fatigue life; i.e., the component survived the fatigue tests for more number of cycles and was able to endure higher loads. The study revealed that the fatigue life is the key to determine microstructural defects. The largest casting pore and shrinkage cavity are present in the sample when tested under commercial conditions. The fatigue life does not get much affected by the carbide size due to its small size. In the HRS condition, maximum carbide size played a major role, as they can be as large as the largest pore that was the cause for initiation of fractures. Further from this study, it can be concluded that the LMC process increases the fatigue life and reduces the pore size. The above studies on LMC prove

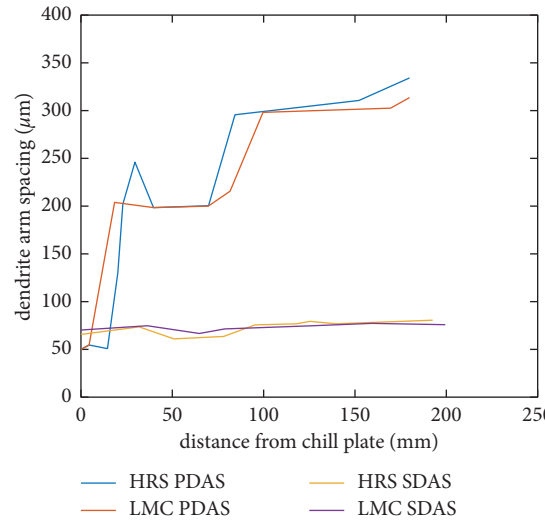

Figure 12: Relationship between PDAS and SDAS values and distance from chill plate.

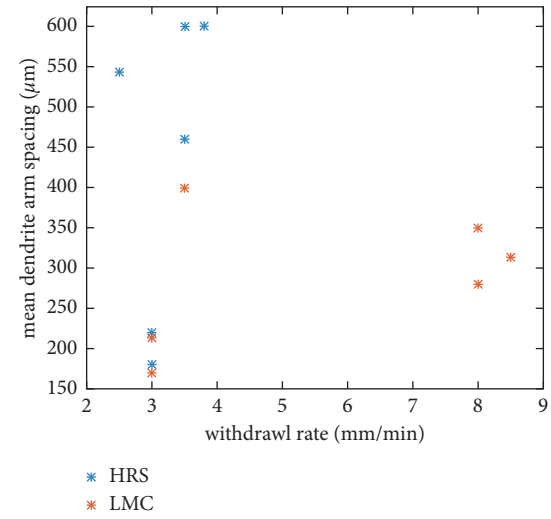

Figure 13: Correlation between withdrawal rate and mean dendrite arm spacing observed in samples made with different methods.

its superiority compared to other casting processes used for manufacturing Ni-superalloy components. The LMC process was seen to refine the microstructure to a greater extent than other processes, supported by the data represented in Figures 12–17. The significantly higher cooling rates and thermal gradients provided by the LMC process (depicted in Figures 14–15) had a significant impact on various aspects of the microstructure, from the dendrite arm spacing to the number and types of surface defects. One of the reasons we strive to achieve a high thermal gradient during solidification is it can be highly beneficial to the quality of the product. It can refine the microstructure control the dendrite arm spacing and thus improve specific mechanical properties. Similar to the use of methods like LMC and HRS, radiation baffles is also a perfect idea to enhance the thermal gradient and the cooling rate. One particular study [101] focused on

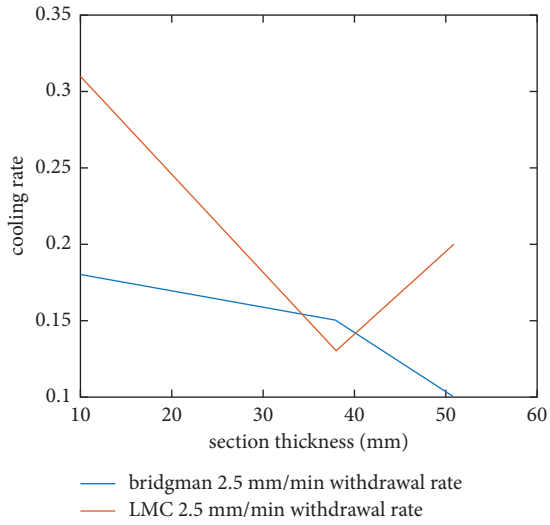

Figure 14: Relationship between section thickness and cooling rate in samples made using different processes.

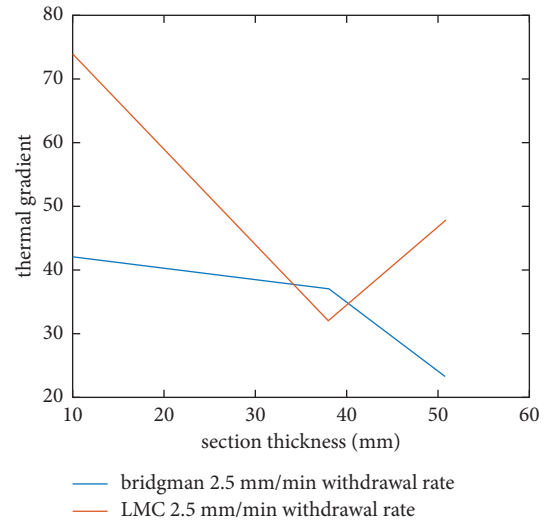

Figure 15: Relationship between section thickness and thermal gradient in samples made using different processes.

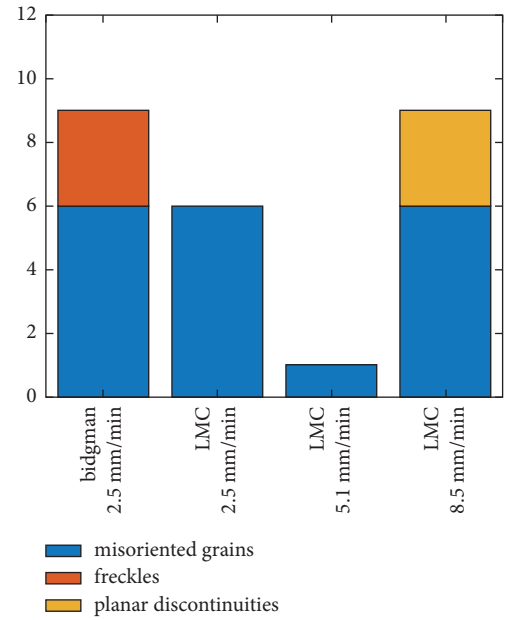

Figure 16: Amount of different defects found in samples made under varying casting conditions.

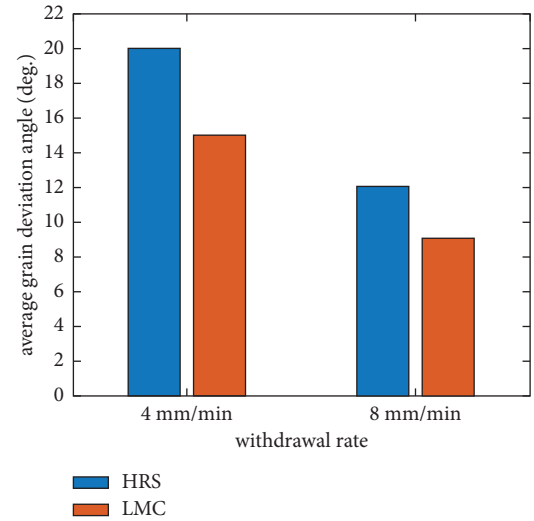

Figure 17: Variation in average grain deviation angle w.r.t. varying withdrawal rates for samples made in different casting setups.

how beneficial radiation baffles can be, particularly inner radiation baffles. Ni-superalloys are used in very harsh environments where enhanced mechanical properties are required. A casting's microstructure has significant influence over a majority of the mechanical properties. In this paper, how the introduction of standard (SRB), adjusted (ARB), or inner (IRB) radiation baffles affected the microstructure and PDAS was studied. CMSX-4 Ni-based superalloy was used to make DS blades needed for this study. The experiment was done three times with different efficiencies in the baffle separation. The 1st experiment was performed with a round mould and a radiation baffle (SRB) having a ring shape and an opening diameter of 230 mm. It was placed on the hot chamber's thermal insulation. In the 2nd experiment, the baffle's opening was adjusted to match the most extensive cross-section of the pouring cup and the casting to adapt the radiation baffle. The mould geometry was modified for the third experiment to have an alumina ceramic tube control rod. Then, in addition to the externally adjusted radiation baffle, inner radiation baffles were also introduced by mounting them between graphite washers placed around the ceramic control rod. Seven such baffles were placed. Analysis of cooling curves for the experiments revealed that the time needed to attain the liquidus isotherm increased from small to large using SRB, ARB, and IRB, respectively, and the experiment that used the IRBs had the highest temperature gradient or cooling rate. The study also revealed that closely matching the contour of the opening in the baffle to the mould's outer surface increased the thermal gradient along with the mould height. The introduction of IRBs also limited the impact of the heaters on the casting portion below the

radiation baffle because of the high thermal gradient. Thus, the casting temperature was reduced to a greater extent than in experiments that used SRBs or ARBs. It was also seen that as we moved from experiment one to three, the thermal separation area increased, which helped raise the thermal gradient. Microstructural studies showed that all samples had a typical dendritic structure with secondary and tertiary dendrites. The PDAS was found to vary along with the height of the cast blade. The largest value was achieved at the bottom of the casting, and the most negligible value was observed at the air foils of the edge for all experiments. It was also found that more favourable microstructure occurred as the baffle geometry matched the mould surface more. And thus the best microstructure was observed in specimens made with the help of IRBs, with ARBs performing better than SRBs. These data regarding PDAS are depicted graphically in Figure 18. The PDAS obtained in this study was compared to that of other studies where castings were made of other methods (comparison of relevant data is shown in Figure 19). And it was found that while the PDAS value obtained in this study was lower than that of a few other studies, some studies which employed the DWDS or LMC procedure had smaller PDAS values, despite the higher thermal gradient obtained while using the baffles. This proved that PDAS is not linearly dependant on solidification parameters. On investigating the casting macrostructure for defects, it was found that defects like freckles, low angle GBs, slivers, nor stray grains were found on the surface. But, the root edges of some blades were seen to exhibit freckling. The largest length of the freckle chain was formed in specimens made using the help of the SRB process, and it was observed to decrease as we used the ARB process. Further decrease in the freckle chain length was seen as we used IRBs. This was seen to occur as a result of the increased cooling rate and temperature gradient. The PDAS value was seen to decrease while using IRBs significantly. And thus, unlike in other processes, promoting thermosolutal convection is low, thus reducing the chances for formation of freckles. It was also seen that the flattening of the mushy zone occurred due to the significantly increased temperature gradient attained with the use of IRBs, thus reducing the radial flow and reducing the chances for freckle formation. But implementing IRBs were not enough to produce freckle-free blades. Some sliver defect formations were also seen in castings made. Although most of the blades obtained by the three experiments were sliver defect free, in the ones where this defect was observed, it was seen in the air foil and just under the platform extending to the blades' top. In these blades, sliver defect formation and dendrite deformation were seen to occur due to increased levels of mould thermal stresses that were caused due to the increase in temperature difference ΔT and thermal gradient, along with the height of the mould and the mould casting. The application of IRBs in producing IGT blades was seen to help attain finer microstructure and less defects compared to other methods. These results were further strengthened/validated by another similar study [39], where IRBs helped attain very fine and superior microstructure.

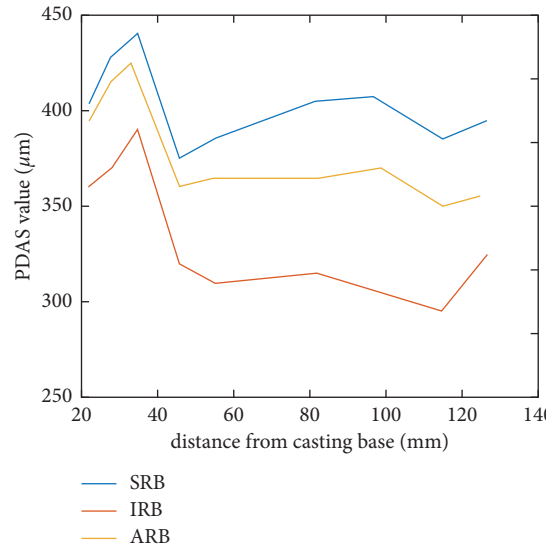

Figure 18: Changes in PDAS of samples produced using all 3 types of baffles as we move away from the casting base.

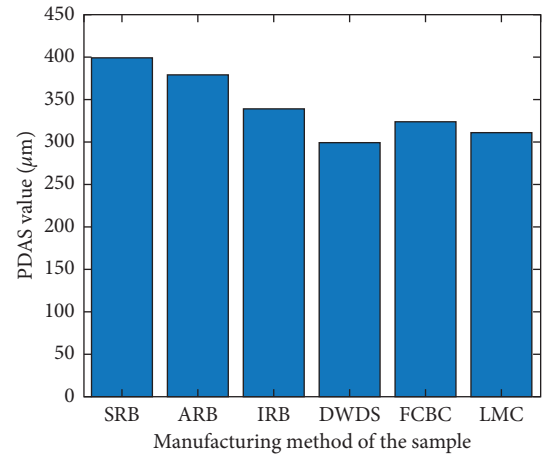

Figure 19: Difference in the PDAS values of samples manufactured using different methods.

So far, studies on how the method or technique used in manufacturing SX superalloys that are directionally solidified influence the final product or its production have been discussed. But all these are generalized studies. Implementing these basic techniques may not be sufficient to produce good quality parts of intricate or complex geometry or sometimes even parts with different grain structures that can be crucially needed in particular cases. To meet these demands, novel techniques are developed to produce castings of desired results. One such study [44] focuses on a particular technique that can be used to make a Ni-based superalloy casting with an equiaxed grain structure. The study developed a novel technique based on interdendritic-melt solidification control (IMSC) to make Ni-based superalloy castings with an equiaxed microstructure and significantly abridged porosity levels. The fundamental concept of IMSC and its influence on the phase formation and porosity formation in IN792 Ni-based superalloy were

examined with the help of synchrotron X-ray diffraction and quantitative metallography methods in this study. The study showed that IMSC, compared to conventional production methods, can produce castings with no shrinkage or porosity defects, lesser microporosities, bigger dendritic arm spacing, and eutectic ($\gamma + \gamma$') regions of slightly larger size and MC carbides. But IMSC was seen not to have any significant influence on the relative amount of phases formed. IN792 is a Ni-based superalloy used in the study. The high content of Ti in IN792 alloy was often seen to impart poor castability to the alloy, thus making these castings more prone to hot tears and porosities. This porosity formation in these castings was characterized and modelled in many previous studies. And some of these studies tried to control the porosity formation by modifying the element composition of the alloy. One such study that was done showed that adding hafnium improves the castability of IN792 superalloy. However, it was also seen to decrease the alloy's incipient melting temperature, and a reaction between Hf and the ceramic mould was also seen. Instead of using a chemical approach, monitoring and adjusting the solidification parameters and maintaining the continuous feeding of liquid into the solidification front is an effective way to reduce porosity. However, in the case of certain crucial structural components, an equiaxed grain structure is preferred. And this prompted the evolution of the thermally controlled solidification (TCS) technique from the usually used DS process. The TCS process was seen to help produce massive and complex thin-walled equiaxed castings more efficiently and effectively. But this technique was found to be incompatible with production of IN792 tube castings that had varying microstructures along the height instead of identical microstructures, which can only be attained by using a uniform mould temperature. Unlike the abovementioned methods, the IMSC process developed in this study was seen to successfully produce IN792 superalloy castings having an equiaxed microstructure and no shrinkage porosities and significantly reduced microporosities. In the conventional investment casting process, after preheating the ceramic shell mould, the molten alloy is poured into the mould maintained at a temperature that is most often below the solidus temperature of the alloy. The main factor distinguishing the IMSC method from the conventional investment casting (CC) process is that the shell mould used in the IMSC technique is retained at a particular temperature between the alloy's solidus and liquidus temperatures once preheating of mould is complete. The microstructure and quantitative examinations performed in this study showed the elimination of shrinkage porosities and the significant reduction of microporosity in castings made using the IMSC process compared to the CC castings. Approximately a 5 times higher value for the volume fraction of microporosities was observed in CC castings compared to IMSC castings. Moreover, in CC castings, the porosity cluster sizes were also seen to be slightly bigger compared to the IMSC castings. Feeding of liquid present in the interdendritic channels into the interdendritic shrinkages was seen to be ensured by the use of IMSC process. Thus, porosity formation was seen to be prevented. The study also revealed that the dendrite arm spacing for IMSC castings were 2 times the value measured in CC specimens. This proved that the use of IMSC can help to reduce the alloy's solidification rate and cause slower cooling. As per the SEM and OM data, a 0.8% volume fraction of MC carbides was seen to be maintained in both IMSC and CC samples. And this showed that the IMSC process did not have any kind of direct influence on the MC carbides' volume fraction. But a small rise in the size of carbides was observed with the use of IMSC. The shape of the precipitated MC carbides was seen to significantly vary for both processes, with bar-shaped MC carbides formed in IMSC castings and block shaped MC carbides formed in CC castings. The eutectic ($\gamma + \gamma$') region's size was larger in IMSC castings than CC specimens. However, the eutectic ($\gamma + \gamma$') region in IMSC specimens was seen to have a slightly lower volume fraction compared to the eutectic regions in CC specimens. Also, the γ phase was present in a relatively very small amount in the IMSC specimens. The microstructural changes observed in this study were attributed to the relatively slower cooling observed in the castings made using the IMSC method. Another study [69] investigated the use of alternative thermal insulating modules for controlling solidification to manufacture thin-walled Ni-based superalloy castings. A component called the insulating module, which was a cylindrically shaped thermal insulation with a varying wall thickness along with its height and can be reused multiple times, was developed successfully and thoroughly tested in this study to examine its ability to help in the manufacturing of castings of plates and air-foils with an equiaxed microstructure. The experiments performed in this study were done with the IN713LC Ni-based superalloy. Ceramic moulds needed for the study were produced in accordance to the investment casting method. In this method, the molten metal was poured into a preheated ceramic shell/mould and allowed to solidify in order to manufacture complex thin-walled castings of turbine blades and vanes with an equiaxed grain structure. Solidification in turbine blade castings was mostly seen to be controlled with the help of a thermal insulation blanket. The insulating blankets were placed on the surfaces of different mould surface areas, so a reduced cooling rate was obtained at certain selected parts of the casting. Developments regarding the production of thin-walled castings having an equiaxed grain structure and are made of Ni-superalloys are still underway, even in recent times. It was emphasized that only a few of the presented methods were suitable to produce Ni-superalloy castings with an equiaxed microstructure. In the LMC process, the boiling point of the liquid cooling media used was very low and thus imparted high cooling rates in the castings, thus making it a not so effective way of producing castings having an equiaxed microstructure. Manufacturing of large and complex castings with the desired microstructure was achieved with the help of the TCS, IMSC, or MTCS methods. But the time the mould was kept in the furnace after the melt was poured into it and the time taken to preheat the mould before pouring were seen to be longer in these processes compared to the process where a thermal insulation blanket was used. However, applying the insulation blanket to the mould surface was seen to be a

difficult and time-consuming task to perform. It was found that providing the same solidification conditions during casting is very difficult, even though similar parameters like mould and pouring temperatures were used during the casting process. This was found to be caused due to the blanket's uneven densification that happened during its installation onto the surface of the mould. The blanket attached shell moulds were seen to have poor recyclability and also pollute the environment. This study came up with a novel insulating module instead of using insulation blankets to control solidification during the casting of blades. The solidification control and control of thermal parameters during the casting process were achieved by selecting the module's appropriate wall thickness and shape while keeping the used gating system's and mould's shapes in mind. The study showed that we could use the insulating module multiple times according to its material and shape. It was seen that mounting and dismounting the module onto the mould can be done very easily, quickly, and repeatedly. Based on these results, the study concluded that the insulating module, which allowed effective solidification control, can replace insulation blankets and shorten the manufacturing process of complex thin-walled Ni-superalloy castings having an equiaxed grain structure. Advancing the investment casting process for manufacturing components with complex shapes and thin elements has always been an incredibly difficult task for industrialists and manufacturers. Mainly, misruns occur quite often in as-cast components having complex shapes due to the development of solid skin due to freezing of melt while coming into contact with a colder ceramic mould. Thus, study [70] was done on MAR-M247 superalloy to develop a new tool that helps physically simulate the skin formation while a component undergoes investment casting. A greeble system was used to perform the study. Ceramic tubes were used to study the effects of casting in the formation of skin. A hole was punched in the midsection of the ceramic tubes for placing a K-type thermocouple. This thermocouple helped measure the temperature at the ceramic tube's primary coat's outer surface, at the distance of about 0.9 mm from the surface of contact where the melt and the ceramic mould meet. And a thin *r*-type thermocouple wire was welded to the midsection of the ceramic tube to control the temperature of the specimen during solidification and melting. The study showed that a sample in a ceramic tube that reached a peak temperature of 1030°C had skin formation, while the sample heated within the solidification temperature range did not have any. It was also found that for the heating regime where a melt temperature of 1360°C was reached, as the withdrawal rates increased the skin thickness was seen to decrease. Morphological studies also revealed that the γ' precipitate size decreased as the cooling rates increased, whereas the γ' precipitates' volume fraction was seen to be unaffected by cooling rates. The results produced by the physical simulation tools were validated against experimental results. Thus, the prediction of the skin thickness of a part having a complex geometry produced by investment casting is possible using the tool developed in this study. But this was seen to be possible only if we were able to reproduce in the experiment the ceramic mould's temperature and cooling rates observed during casting. A huge number of highly costly casting trials are usually performed to find the optimized casting parameters for casting any product. With the help of the information obtained through the study, reducing the number of these highly costly casting trials is possible. Another study [17] investigated the application of machine learning techniques to the production processes. The study aimed to improve product quality, support decision-making, or implement process diagnostics with the help of machine learning tools. Support vector representation machine (SVRM) was used in this study. It was used on production data collected from a turbine blade manufacturing plant that implemented an investment casting method. Scientifically and industrially, many efforts were made to develop advanced casting simulation tools that can help in improving blade production. These tools can visualise several process variables like heat transfer, solidification, molten metal flow within the cavity, formation of grains, stress evolution, and shrinkage. Even the various stages of the moulding process can be reproduced. But, these simulation tools are inappropriate for correlating process variables like defects and desirable qualities. Hence, with these tools, the final product quality cannot be predicted even when process parameter values are known. Thus, the study was aimed at developing a systematic strategy for determining the connection between casting process parameters and final product quality. It was seen to help increase cast blade quality and minimise the amount of scraps. Data from an investment casting foundry manufacturing turbine blades for jet-engines were used. To achieve the goal, machine learning techniques, namely, the combination of a SVM and a one-class SVM called SVRM was used. SVMs were chosen in this study because, even while limiting overfitting, they were seen to be able to handle nonlinearly separable data really well. They are also known for being trainable in polynomial time by solving convex quadratic programming problems. This outcome of the SVM training was seen to make choosing of SVRMs preferable. In SVRM, perfect separation of subsets of data was seen to be possible, and by describing or studying the subset, information regarding many meaningful features was seen to be obtained. A subset was ranked only after the data are classified using the standard SVM, instead of solving a classification/rejection problem. The ranking criterion used in this study was seen to be the distance from an implicitly defined vector that acts as a cluster centre. The decision surface of the original classification problem leaves to one side points belonging to the same class, thus identifying a subset of the data that was easy to classify and make the ranking meaningful. Machine learning techniques like this proved to be useful in the industries that manufacture components using investment casting, where a large variety of heterogeneous data and wide range of production processes were present and where old methods failed due to the immensely complex production processes. Additionally, the results of the SVRM were compared with an alternative method called the decision tree method, which aims to deduce rules from data. Comparing both these methods showed the merits of using the SVRM

and how highly beneficial its use is. Another study [64] investigated a different approach to optimizing the casting of superalloys. This study predicted the grain structure of a specimen during solidification with the help of a highly parallelized mesoscale solidification model based on a combination of a macroscale process model and the cellular automation method. Rene N500's nucleation parameters and macroscale thermal model were verified and calibrated with the help of temperature profiles attained by using thermocouples in castings with a step-geometry and analysing the grain structure with the help of EBSD. To predict the grain structure, the calibrated model was used on laboratory-scale turbine blades. The size of grains that were predicted was seen to match with experimental results obtained after casting specimens under various casting conditions, thus proving that the method used to predict grain structure in this study can be used to predict the grain structure for other castings. With the help of a combined approach that included both the process and grain structure models, a feasible path was seen to be provided for optimizing the DS process, and this application was seen to be very important for Ni superalloy castings as it was seen to provide minimized physical process iterations, optimize casting conditions, better the geometrical design, and prevent the formation of stray grains. In another study [45], for predicting accurately, the thermomechanical behaviour and the viscoplastic flow during the cooling of Ni-superalloys, a thermodynamically consistent thermo-elasto viscoplastic model was developed. To achieve this, a compressible-type viscoplastic yield function was introduced in this study. This function was seen to be based on equivalent stress that depended on the volume fraction of the solid phase formed within the material's liquid phase as a result of dendrite propagation. On a single integration point, an isothermal tensile-compression test was first simulated. Then, a benchmark testing of a Ni-superalloy bar with a rectangular shape in a sand mould was simulated and examined. Limiting mechanical stresses as the metal cooling down and solidified was seen to be one of the challenges faced while industrialising a new part. Thermal stresses were seen to originate due to the difference in the coefficients of thermal expansion and thermal gradients of solidifying alloy, the ceramic cores, and the ceramic moulds. Adjusting the Bridgman DS process parameters or modifying the part's shape was seen to help in limiting the residual stresses and the plastic strain. This study's aim was to develop a modified behaviour model with an additionally modified Norton–Hoff potential, by adapting the modified behaviour model from the classical Voce isotropic hardening model. With the help of both isothermal and anisothermal tests performed on simple specimens, the elementary validation of the present methodology was conducted from room temperature to 1200°C for 2 typical strain rates. An increase in the yield limit for a particular temperature interval and also in the viscosity modulus of that interval can be observed from the results of the isothermal tests. After this, a progressive decrease was observed in these two parameters. In an anisothermal test, the stress and strain curves showed that at the time of the initial phase of compression, the growth of experimental stress was slow compared to simulations. While the experimental stress was seen to grow more slowly in comparison to that observed in simulations, between the time of 2000 and 3500 s, i.e., during the tensile phase's initial stages. Contrastingly, the evolution of computed stress was seen to be constant. After changing from compression to tensile loading paths, which occurs at time 2000 s, stress was seen to still remain positive and increase; it only started to decrease around 3700 s. At the bar's solidification phase, the maximum stress was observed at bar's corners, while the minimum stress was seen to be concentrated in the bar's centre. While performing isothermal tensile relaxation tests carried out at various strain rates and under a wide temperature range, the gap between the experimental and numerical observations was reduced by using this methodology. The anisothermal tension/compression tests results were then validated. All results obtained in the study proved that the methodology developed achieved its goal.

Like the different casting methods and techniques we have discussed, varying the casting parameters and conditions can also result in changing results for the final casting. These parameters and conditions may include mould geometry, mould content, withdrawal rates, pouring temperature, and many more. One such study [65] focuses on how particular casting variables can affect the residual stress and strain formed in a casting, emphasising melt pouring and superheating temperature. Residual stresses can be defined as elastic stresses that remain in the cast component after being taken out of the mould. These stresses occur due to the nonuniform contraction and expansion rates observed at various points in the same casting component. The extent and type of residual stresses present greatly influenced the casting's quality as they can cause unwanted changes in the dimensions and distortions in crucial parts. A cutting technique was used to examine how residual stresses formed in components made of Ni-superalloys IN713C and U500 are influenced by the pouring temperature. Depending on the shape of the casting, the extent of residual stress formed was seen to vary. Residual stress was seen to be highest in triangular samples. Moreover, it is also observed that at constant melt superheat temperatures, residual stress was lower in IN713C that than in U500. Despite the greater flexibility of U500 compared to IN713C, the above result can be explained by the mushy solidification behaviour of U500 and the more drawn-out freezing range present in it. It was also seen that as the melt superheat temperature increases, thermal gradients and cooling rate differences also increase, thus causing higher amounts of residual stresses in castings. The various trends about residual stress are depicted graphically in Figures 20 and 21. Another study [30] focuses on how casting castings' cooling rate can affect process parameters and the final product. To establish a relationship between solidification and microstructure, an experimental high-efficiency method was developed in this study, which helped accelerate the speed to find the optimum casting parameters by using controlled cooling rates. The steady cooling rates used in this study were seen to range from 0.25 to 10°C. To examine the solidification behaviour with correspondence to solidification rate (V) and thermal gradient

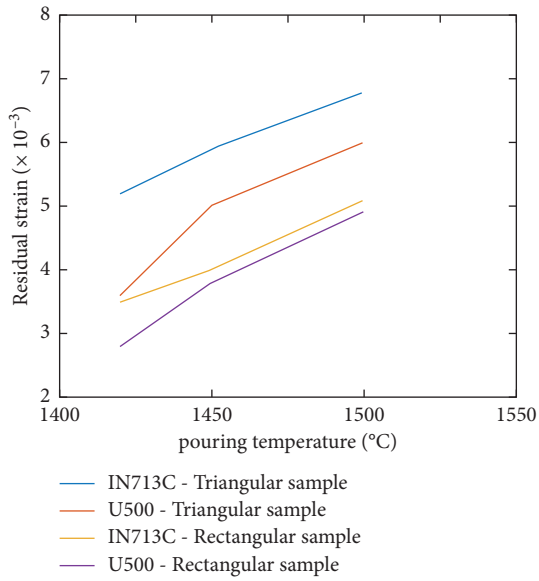

Figure 20: Relationship between residual strain and pouring temperature.

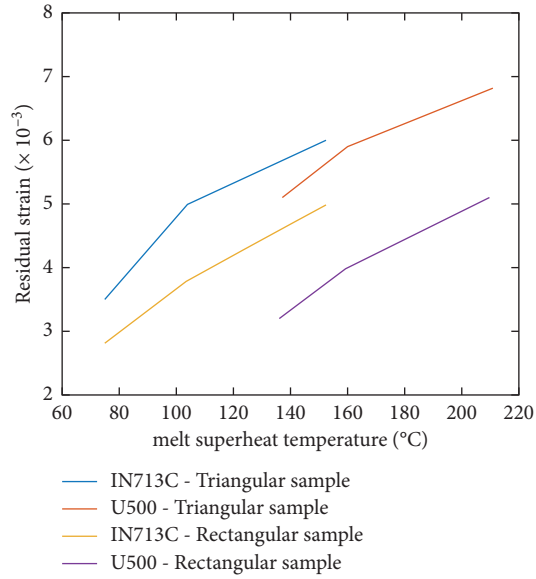

Figure 21: Relationship between residual strain and melt superheat temperature.

(G), a novel high-efficiency experimental method was developed in this study. Developing the method was seen to help in deriving a relationship between resultant microstructure and solidification parameters in investment casting. The procedure is as follows: using UG software, actual castings are constructed—ProCAST is used for prior model's numerical simulation—and finally, the physical simulation was carried out with the help of the high-efficiency experiment design developed in this study. The actual cooling rate can be found with a spot-welded thermocouple. A spot-welded thermocouple was used in the study to keep track of the actual cooling rate. It can be observed that the solid-liquid region's cooling rate was close to a preset value. Thus, it was made clear that the control of the temperature was precise and reliable in the greeble. As the controlled cooling was increased, the temperature gradient was also seen to increase (data regarding this is graphically represented in Figure 22). Steeper gradients were observed in cases of increased cooling rates. Moreover, the increase in thermal gradient was most rapid when the cooling rate was equal to 10°C/s. The temperature gradient at a cooling rate of 10°C/s was seen to be 20.57°C/mm. The solidification rate and temperature gradient were seen to be within a range of 0.05–1.78 mm/s and 1.24–20.57°C/mm, respectively. As the distance (D) from the centre of casting increased, the temperature gradient (G) and cooling rate (R) were seen to slowly increase (data regarding this are graphically represented in Figure 22). However, the solidification rate (V) appeared to follow an opposite trend (data regarding this is graphically represented in Figure 23). At the same cooling rate, the R/G value was seen to change greatly, indicating that the solidification rate was subjected to rapid changes, meaning that the movement of the solidification interface was too fast from a microperspective. This was seen to cause significant changes in the microstructure. Many factors determine the SDAS, but mainly V, G, and R. The study showed that parameters like R and G had a significant say in the resulting microstructural morphology. Increasing cooling rates were seen to the refining the microstructure. The local solidification time was seen to have a major influence on the SDAS growth. Hence, it was clear that good contact with liquid helps in the growth of better secondary branches because the coefficient for solute diffusion for liquids is very high. It shows that as the temperature gradient increases, PDAS of disordered arrangement will slowly grow parallel to each other. When PDAS increased, SDAS was seen to increase simultaneously. As the temperature gradient increased, regeneration of secondary dendrites was seen to get inhibited because of the distribution of solute atoms between the dendrites, leading to coarsening of secondary dendrites. And the rate of solidification was found to be the major reason behind SDAS coarsening. Moreover the study revealed that the SDAS response behaviour changed sharply with an increase in solidification rate. Trends pertaining to SDAS value are graphically represented in Figures 24 and 25. In this paper [87], the physicochemical interaction taking place on contact of the ceramic shell mould having Al_2O_3-Al_2O_3 composition, with the molten high temperature Ni-superalloy poured into the shell during investment casting, is investigated. Unlike shell moulds with Al_2O_3-SiO_2 compositions, investment casting moulds with Al_2O_3-Al_2O_3 composition was seen to exhibit significantly reduced amount of interactions with the melt. While using Al_2O_3-Al_2O_3 ceramic shell moulds, nonmetallic inclusions were seen to be introduced at a depth of 10–20 μm in castings, which is significantly lower compared to castings produced in Al_2O_3-SiO_2 ceramic shell moulds (40–70 μm). Moreover, castings produced in Al_2O_3-Al_2O_3 ceramic shell moulds were seen to have a roughness value of 2.5–5.0 μm. However, this value was seen to be much higher (3.5–6.5 μm) in castings made in conventional Al_2O_3-SiO_2 shells. On pouring of molen Ni-based superalloy into the Al_2O_3-Al_2O_3

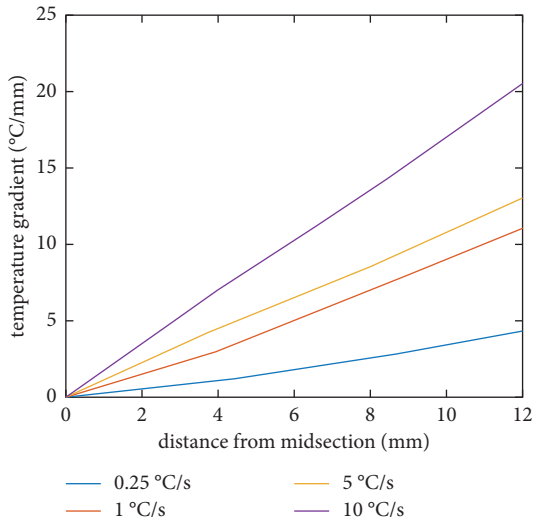

Figure 22: Correlation between temperature gradient and distance from the midsection for various cooling rates.

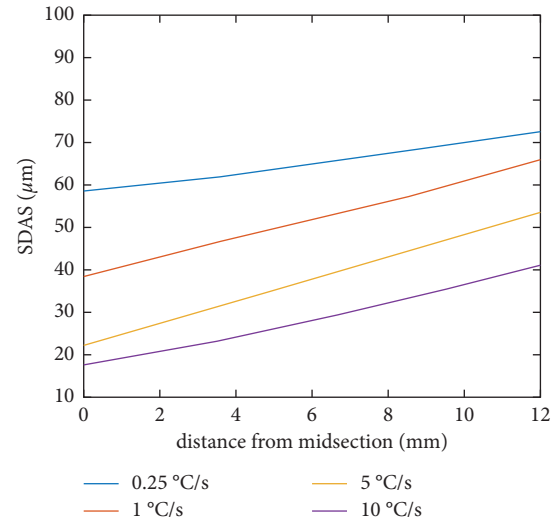

Figure 24: Correlation between SDAS and distance from the midsection for various cooling rates.

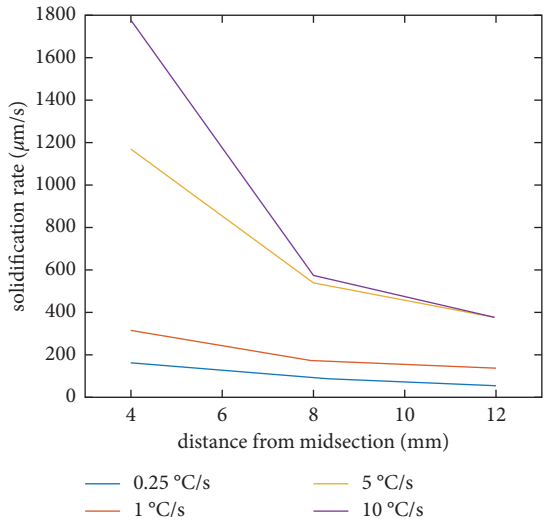

Figure 23: Correlation between solidification rate and distance from the midsection for various cooling rates.

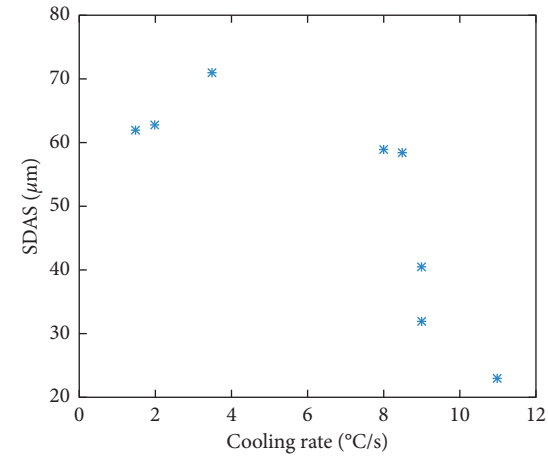

Figure 25: Correlation between SDAS and cooling rate.

ceramic shell, the colour of the shell's front surface was seen to become pink. This was seen to happen because Cr from the alloy formed a number of Cr-based solid solutions with the Al_2O_3 from the ceramic shell. The reaction layer formed between the shell mould and the superalloy was observed to have a very small thickness of 10–20 μm, when using the Al_2O_3-Al_2O_3 ceramic mould, compared to (40–70 μm) Al_2O_3-SiO_2 ceramic shell. Moreover, the reaction left behind on the Al_2O_3-Al_2O_3 ceramic shell moulds after pouring of melt was seen to be easily erased by hand. However, the highly dense reaction layer formed during casting with Al_2O_3-SiO_2 moulds was seen to require sandblasting for their proper removal. And the sandblasting process was seen to affect the mould's cleanliness and also alter its surface roughness. The study also revealed that castings made in Al_2O_3-Al_2O_3 ceramic shell moulds provided much better surface quality and lower roughness. In addition, reduction in the reaction metal oxide layer's thickness was seen to ensure much better dimensional accuracy of castings used for many critical applications and, thus, reduce finishing allowances. Another study [73] that focuses on mould composition focuses on the silicon content and its effect on castings. The element silicon has been proved to be a highly harmful impurity in Ni-based superalloys produced via casting. Si impurities were seen to increase the amount and formation of a low-melting phase and promote the formation of carbides with an unfavourable acicular shape and non-metallic oxide inclusions (CaO MgO $2SiO_2$, MgO SiO_2), within interdendritic spaces. This was seen to decrease the ductility and high-temperature strength of superalloy castings. Topologically close-packed (TCP) phase formation was seen to be stimulated and promoted by Si, during the long-term operation of Ni-superalloy products. Also, large amounts of Si found in casting wastes of SX Ni-superalloys were seen to be related to the specific features of producing aviation GTE parts. Solidification was seen to be fast when producing castings with an equiaxed structure, and this was

seen to weaken the interaction of the melt with the ceramic shell. And thus, the metallic charge used was concluded to be the main source of Si. But in casting blades made using DS and SX processes, the ceramic shell moulds that have free SiO_2 in them were seen to be the main source of Si. During long-term interactions, the Si content in the ceramic mould was seen to reduce, and Si was passed into the single crystal superalloy melt. Moreover, mullite ($3Al_2O_3$ SiO_2) was also seen to increase the Si content in the casting by interacting with the melt at elevated temperatures (1600°C). Experimental investigation showed that silicon saturation in casting made using DS or SX processes occurred due to the interaction of the molten alloy with the free SiO_2 present in the ceramic mould. Also, during casting of SX carbonless Ni-superalloys, the metal was seen to attain Si saturation at a rate 4 times lower than the rate observed for carbon-containing alloys. Another study [98] investigated the effect of using silica-free alumox binder for making a composite ceramic mould that can be used in the investment DS castings of Ni-superalloy components. The study revealed that significant amounts of Si-compounds had formed on the surface of the Ni-superalloy castings made using silica moulds, and thus, the recyclability of the excess charge obtained while preparing crucial components was seen to be reduced significantly. And as a result of this, carrying expensive procedures for refining the alloy was required, which was seen to have a huge impact on the casting cost. The forming of a loose burn-on layer on the surface of castings was observed. This was seen to happen as a result of the oxidized elements present in the liquid melt poured into the ceramic shell mould reacting mainly with SiO_2 and its vapour and partly with Al_2O_3 present in the ceramic mould. This burn-on layer was especially seen on the blade vane region. It was also seen that the burn-off layer's thickness was not uniform in all areas on the casting surface. The burn-on layer and the residual mould material found on the casting surface were seen to have a brownish colour due to the presence of ruby resultant ruby analogs. The regions in the mould that were kept close to heaters prior to pouring of the melt were seen to have burn-on layers with the highest thicknesses. Moreover, the operations performed to remove the burn-on layer were found to affect the casting's geometric precision and thus cause variations in the dimensions of the components made. This was found to induce the excessive consumption of expensive materials used to blast the casting and an overuse of abrasive tools. The study proved that the protective layer formed on the composite mould based on the alumnox binder reduced the amount of the burn-on layer formed, by reducing the mould-superalloy interactions that occur at the the time of pouring and solidification by significant proportions.

Another study [31] examines the effect of surface conditions on creep properties of Ni-superalloy castings. Complex systems of cooling channels are usually incorporated into the design of turbine blades to help them withstand very high temperatures. These hollow blades are made using the lost-wax investment casting method. Other than enhanced cooling efficiencies, thin-walled hollow blades and interior sections can also help with reducing the casting's weight. Turbine blades with a reduced weight that rotate relatively faster are highly preferred, and now, the bearings, shafts, and turbine disks can also be given a lighter design. Therefore, knowing the effect thin section size can have on a material's properties at elevated temperatures is very important, particularly their creep properties. IN100 Ni-based superalloy that was cast using conventional methods was used in this study. The study revealed that very thin castings with a thickness of 0.9 mm had the least creep rates that fell slightly behind the creep rates for 1.3 mm thick samples. Rupture strains were seen to be higher for thin castings, with 1.3 mm thick castings exhibiting maximum values. Porosity content in all alloys used in this study was seen to be between 0.1% and 0.3%, and thin cast samples were seen to have higher roughness than machined specimens. A thin layer of oxide having a 1 μm thickness was seen to have formed on a surface of the casting's typical microstructure. Observations showed that creep cracks usually initiated at the casting's surface. And crack propagation was seen along the GBs. Oxide formation was also found along the crack surface and at the crack tip. The above discoveries infer that the main mode of creep failure in uncoated polycrystalline Ni-superalloys IN100 in the air is stress assisted intergranular oxidation. The influence of the grain size was seen to become more pronounced at lower stress levels. A specimen that has undergone grain or microstructural refinement was seen to possess superior creep properties. Both preparation processes, casting and machining methods used, were seen to impact the section size and thus have an influence on the creep properties. However, this trait was seen to be more pronounced in machined specimens. Creep testing in this study was seen to be done out in the air. And thus, oxidation was seen to affect the creep and creep-rupture behaviour of the specimens. The 0.9 mm thick specimen having a surface-to-volume ratio that is higher in comparison to that of the 1.3 mm thick specimen meant a relatively more significant amount of surface area in contact with the atmosphere in the less wide sample, thus higher oxidation of this specimen. This observation explained the lower creep resistance exhibited by thin specimens due to the oxidation effect. Another paper [66] studied the effects of using different types of moulds on the casting properties. With optimizing casting procedure as the goal, this study examined how the micro and macrostructure and the solidification behaviour of IN738LC Ni-superalloy during investment casting were affected by casting them in 2 different moulds. Alumina and zircon ceramic moulds were used for this purpose in this study. The study compared data regarding the experimental cooling curves, SDAS, and the structure of grains of IN738LC alloy castings made using both ceramic moulds, with the data derived from the simulations performed in ProCAST software and 3-D cellular automaton-finite element (CAFE) model. Parameters like pouring temperature, nucleant types, and mould dimensions were set as constants in this study, and the influence of the thermophysical properties of the ceramic moulds on the qualitative and quantitative changes taking place in the casting's microstructure was examined with the help of simulation. Once simulation was done, alloy that was molten with the help of a

VIM furnace was poured into both alumina and zircon moulds. One sample per mould was made and subjected to heat treatment. While comparing the simulated and calculated SDAS values, it was observed that, as a result of the superior thermal conductivity exhibited by alumina moulds, castings made using the alumina mould was seen to have less SDAS values (data regarding this have been represented in Figure 26) and total local solidification time. This seemed to occur due to the higher cooling rates obtained while using the alumina mould. The cooling rates obtained from both simulations and experimental means were seen to match. The study also revealed that fewer γ/γ' eutectic islands were seen in the heat-treated compared to as-cast samples regardless of the mould they were prepared in. But on examining the effect the type of mould had on the presence of these eutectic islands, SEM analysis showed higher γ/γ' volume fraction present in the microstructure of casting prepared using zircon mould than in the alumina mould specimen (data regarding this are represented in Figure 27). Unlike using the zircon mould, using the alumina mould for casting the specimen was seen to cause a decrease in the γ/γ' eutectic pool size. Due to the increased cooling rates achieved by alumina moulds, the γ' precipitate's size was seen to have decreased from 500 nm in the sample made from zircon mould to 290 nm than in the sample made from alumina mould. In contrast, the γ' precipitate's volume fraction was seen to increase from 46% to 53% during heat treatment. The samples made in alumina mould were also seen to have finer grains with higher grain density, as shown in Figures 28 and 29. Due to preferable microstructural features being obtained using an alumina mould, it was considered a more suitable option for producing IN738LC Ni-superalloy parts using the investment casting method, compared to its zircon counterpart. Another study [46] investigated the effect the constituents of the shell mould used in casting Ni-based superalloys have on the carbides occurring in the component. In this study, aluminosilicate ($mAl_2O_3 * nSiO_2$) and zirconium silicate ($ZrSiO_4$), the main ingredients making up 2 different shell moulds, on the volume fraction, size, morphology, and the carbide's chemical composition was examined. Castings used in this study were made of the Ni-superalloy IN713C. Two types of shell mould systems were used for the casting trials done in this study: (a) Shell 1: it was the usual industrial shell mould system used as a reference. This shell used colloidal silicon binder and zircon filler for the prime coat. The primary stucco applied was seen to be alumina grit. Also, an alumina silicate powder and colloidal silica binder based ceramic was seen to be used to make an eight-coat mould backup. The backup stuccos applied was seen to be an alumina-silicate grit. (b) Shell 2: the prime coat was seen to consist of colloidal silica binder and zircon filler, just like in shell-1. The primary stucco applied was seen to be alumina grit. Also, an alumina silicate powder and colloidal silica binder based ceramic was seen to be used to make an eight-coat mould backup. However, unlike in shell-1, the backup stuccos applied were seen to be SiC. γ' precipitates and carbides were seen to be the strengthening elements present in the microstructure of IN713C nickel-based superalloy castings. In the as-cast samples, they revealed a heterogeneous microstructure with unique segregation of dendrites present. Carbides, coherent γ' precipitates scattered in the matrix,

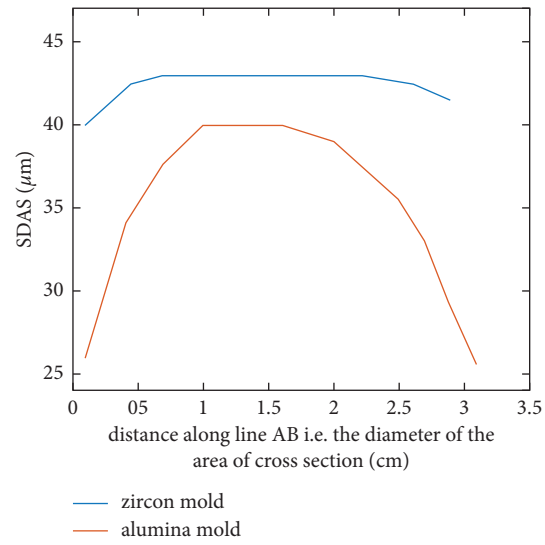

Figure 26: Variation in the SDAS value along AB.

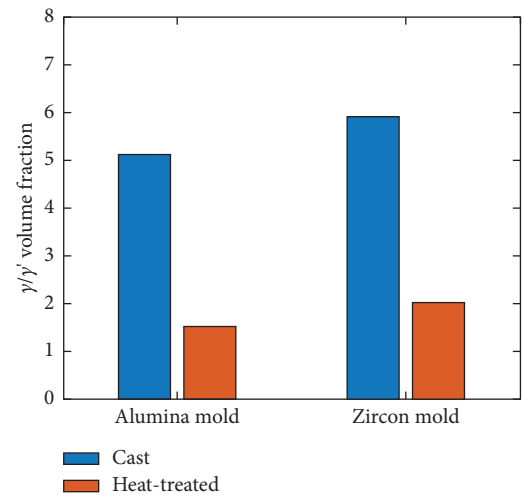

Figure 27: γ/γ' volume fraction in samples made from different moulds.

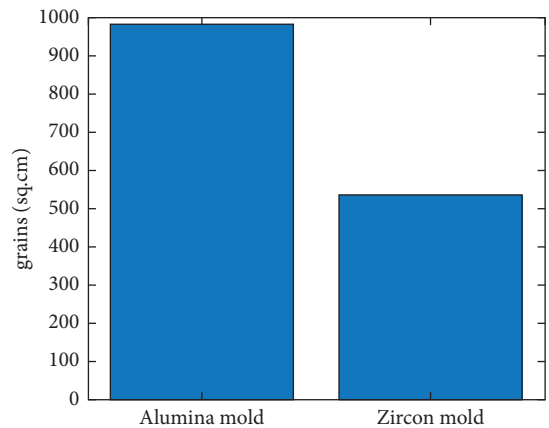

Figure 28: Grain density of samples prepared in different moulds.

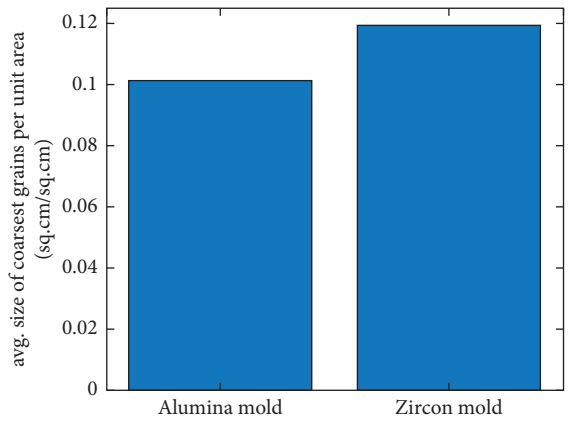

Figure 29: Value of mean size of coarsest grains per unit area in samples prepared from different moulds.

γ-grains with morphologies exhibiting dendritic growth, and γ/MC eutectic materials were all found in the microstructure of all specimens, regardless of the shell material utilized for casting it. The local solidification conditions were seen to have been influenced by the shell chemical composition and wall thickness was found to have greatly influenced the distribution, size, orientation, and morphology of the abovementioned microstructural constituents. With increasing wall thickness, carbides became larger and larger in size, while carbides of finer sizes were seen in castings made in shells of lesser wall thickness. The rates of cooling and thermal gradients were seen to be lower in regions with thick walls. This was supported by the much more coarse γ/MC eutectic materials, γ-grains, and carbides. The impact of heat exchange parameters on the microstructure of castings was validated in the 2nd shell containing SiC that improved the mould's heat conductivity. Thus, shell-2 was seen to be preferable if we want to manufacture a casting with a fine microstructure. Further investigation also showed that the carbide's chemical composition was affected by the constituents of the shell mould used. Just like mould geometry or content, the cooling rate can also affect the casting's properties. One study [79] talks about how the cooling rate can influence the micro- and macrostructure of thin-walled Ni-based superalloys. Mechanical properties are highly influenced by Ni superalloys' macro- and microstructure, particularly in thin-walled ones. Morphology of the micro- and macrostructure was seen to influence the equiaxed grain casting's mechanical properties. In cast-mould environments, the rate of cooling and heat flow was seen to significantly influence the macro- and microstructures formed by the crystallization process. The cooling rate and heat flow under industrial conditions can be controlled by technological parameters, both variable and constant. The specimens that are step-shaped and having circular cross-sections with variable diameters were used. Two casting moulds, one with and the other without ceramic wool thermal insulation, were used. For grain refinement, the prime coat was infused with 5% wt. cobalt aluminate ($CoAl_2O_4$). R-type thermocouples were used to determine cooling curves. A derivative concept was used to identify the solidification process's characteristic temperatures. The number of grains in a given unit area, elongation factor, and mean grain cross-sectional area were all determined using digital image analysis. With an increase in the rate of cooling, enhanced grain refinement and decreased SDAS values were observed (data regarding this have been depicted in Figures 30–32). The casting's diameter, preheat temperature of the mould, and its thermal insulation were found to be influencing the SDAS, as well as the cooling rate. As the casting diameter kept increasing, it was found that the distance till which from the surface grain refinement takes place was starting to become comparatively smaller for the respective casting thicknesses. The study also found that the cooling rate gets affected by mould's temperature and insulation factors. For higher cooling rates, the mould temperature acts as a key factor. For slower cooling, the insulation of the mould is a significant factor. This implies that in the manufacturing of aircraft blades, which are thin-walled castings, the mould temperature must be regulated to a greater extent. Similar to the cooling rate, the withdrawal rate of casting can also have a significant effect on the finished casting. One study [50] regarding withdrawal rate mainly focuses on how it influences the porosity formation in a 3rd generation Ni superalloy. It is difficult to compensate the inevitable porosity formed due to the interdendritic liquid flow during solidification. Porosities can deteriorate thermal-mechanical properties (particularly fatigue property) of turbine blades. Among all the factors that influence porosity formation, the withdrawal rate is highly significant. And thus, optimizing the withdrawal rate is an efficient method for controlling the microstructure for massive industrial castings. A 3rd generation SX Ni-superalloy was used in this study. In this paper, an investigation was made on the size, shape, and distribution of porosities. The optimum withdrawal rate was then found based on the data obtained. The study showed a decrease in PDAS and SDAS values with increasing withdrawal rates. Rising withdrawal rates were seen to lead to a refined microstructure with fewer porosity defects in it. Data regarding this are graphically represented in Figures 33 and 34. The study also helped in concluding that there could be two major factors influencing the porosity levels: (1) using residual liquids to feed volume shrinkages formed by the γ-γ' eutectic liquids that solidified at the end and (2) isolating effect induced by dendrite arms' morphologies. The study also proved researching to find the optimal withdrawal rates for different alloys is a very effective method to minimise porosities in castings, especially in large-scale production. The study also showed that the best creep performance of the alloy was shown by sample withdrawn at a rate of 3 mm/min. An increase in the withdrawal rate was also seen to reduce the surface area and size of the γ' phase. Another study [48] focused on how the conditions during DS process can affect the structure of the carbonless alloys and the SX structured ingot's susceptibility towards defect formation. For experimentation and investigation in this study, rhenium-containing <001> VZhM4 Ni-based superalloy was used to make SX cooled turboprop engine blades. In comparison to SX castings having carbon in them, carbon-free alloy blades were seen to be subjected to

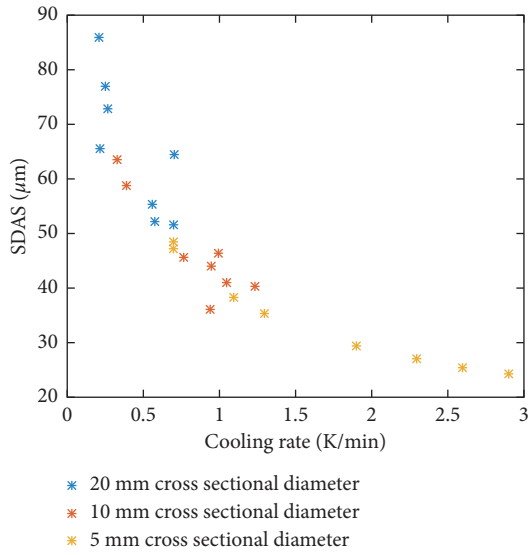

Figure 30: Variation is SDAS value with respect to changing cooling rates for castings having different cross-sectional diameters (20 mm, 10 mm, and 5 mm).

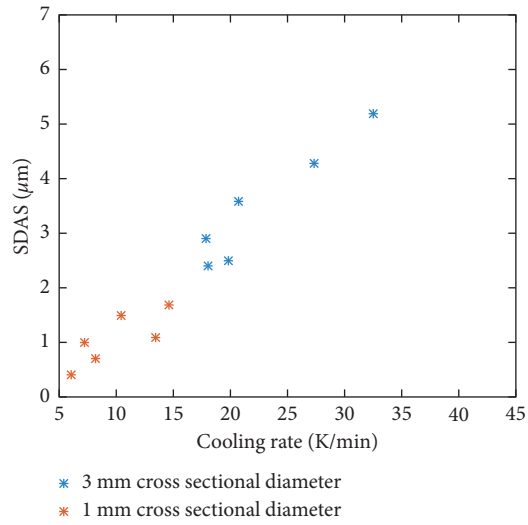

Figure 31: Variation is SDAS value with respect to changing cooling rates for castings having different cross-sectional diameters (3 mm and 1 mm).

more severe structural requirements. GBs, elements that help in hardening GBs, spots, freckles, equiaxed grains, and other casting defects, should not be present in ingots with no carbon content. Also, to prevent recrystallization upon heating, the sand blasting of ingots or any other mechanical processes was seen to be avoided. The deviation of crystallographic orientations (CGO) of the blade ingots was determined using X-ray diffraction patterns. A blade ingot was regarded as good if the deviation α<001> was less than 10° and the block misorientation ($\Delta\alpha$<001>) was less than 3°. The blade ingots that were produced satisfied these criteria, supported by the results obtained from X-ray diffraction tests. SEM studies of the blades showed that they have a cellular-dendritic structure, and in the interdendritic space,

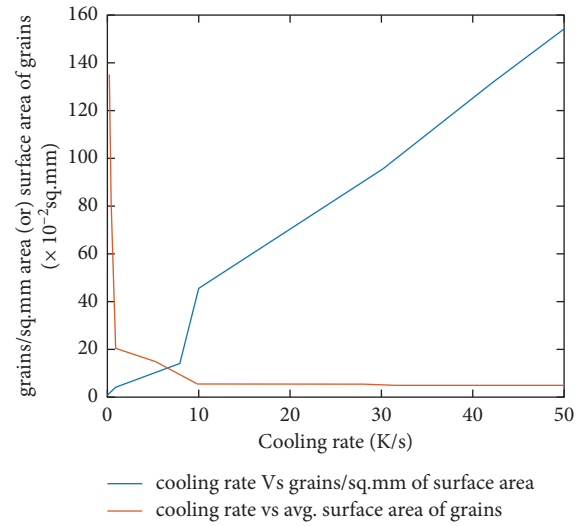

Figure 32: The relationship between the cooling rate and the surface area of grains and the number per sq.mm. These relationships are evident of the refinement that occurs in grains as the cooling rate increases.

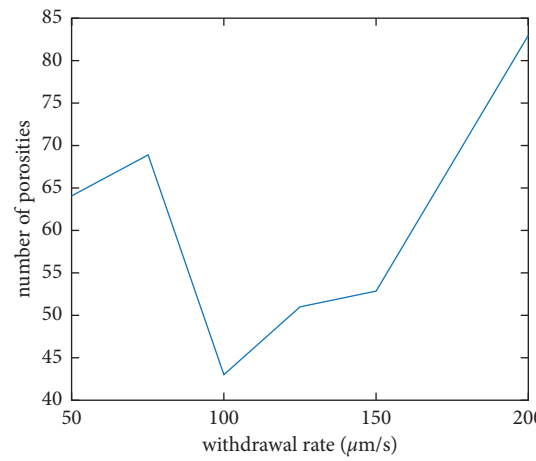

Figure 33: Change in the number of porosities formed as withdrawal rate increases.

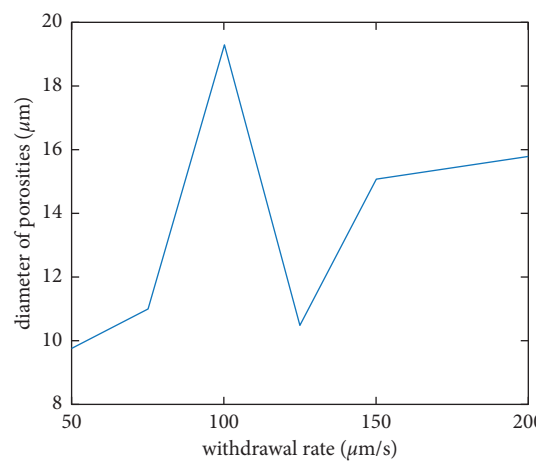

Figure 34: Variation in the diameter porosities formed w.r.t. change in withdrawal rate.

nonequilibrium eutectic γ'-phase precipitates were found. It was also observed that casting micropores of sizes less than 10 μm existed near the eutectic regions. The development of secondary dendrite arms into the blade was around 20–25 μm for the temperature-rate casting parameters employed in the study, which is a favourable sign for the manufacturability of VZhM4 nickel superalloy. After hot isostatic pressing (HIP) heat treatment, the blades were seen to not have any $\gamma + \gamma$' eutectic regions nor any micropores, and the γ' phase was seen to have achieved an optimum cuboidal morphology. Another study [18] focused on how the withdrawal rate can influence the crystal structure perfection, microstructure, and creep properties. The study utilized as-cast SX rods produced using the commercial CMSX-4 Ni-superalloy for experimental purposes. All SX rods that were used were prepared using multilayer ceramic shell preparation and lost-wax casting methods. Based upon the Bridgman method, the DS process was performed with the help of a vacuum furnace at various rates of withdrawal (1, 3, 5, and 7 mm/min). The study revealed a decrease in PDAS as withdrawal rate increased from 1 to 5 mm/min, but the PDAS value for casting made with 7 mm/min withdrawal rate was higher unlike it was expected to be low. The decrease in PDAS values were seen to be due to the growing number of tertiary dendrite arms as the withdrawal rate increased. SEM analysis showed the presence of γ' precipitate with polyhedral shape in both interdendritic and dendritic regions, and their size was seen to decrease as the withdrawal rate increased. Further investigation revealed that when withdrawal rates were increased from 1 to 5 mm/min, the surface area of the γ' precipitates was seen to decrease (data regarding this are graphically represented in Figure 35), but not much variation was seen as we moved to casting being withdrawn at 7 mm/min. The smallest scatter value for the γ' precipitate surface area was seen in casting made with 5 mm/min withdrawal rate. In majority of the castings, the γ' precipitate's volume fraction in the interdendritic regions was observed to be higher than in the dendritic region. In castings made with a withdrawal rate of 5 mm/min, the γ' precipitate was seen to have the largest volume fraction. While for 3 and 7 mm/min withdrawal rates, the smallest values were found (data regarding this are graphically represented in Figure 36). Ni, Al, Ti, and Ta are the major alloying elements found in the γ' precipitates. Among these, the amount of elements other than Ni present was observed to diminish when the withdrawal rate increased. At the same time, the highest and lowest content of Ni were seen for 3 and 5 mm/min withdrawal rates. The lattice parameters for the phases were generally seen to decrease with an increase in the withdrawal rate. It was also observed that the γ' phase present in castings was most ordered when withdrawal rates of 1–5 mm/min were used, and they were seen to become more disordered in casting withdrawn at 7 mm/min. Moreover, when the withdrawal rate was seen to exceed 3 mm/min during the Bridgman process, the ordering of phases was seen to decrease. The amount of porosity formation was seen to decrease with an increase in withdrawal rate from 1 to 5 mm/min, while it was seen to increase when moving on to a withdrawal rate of 7 mm/min. And the size of

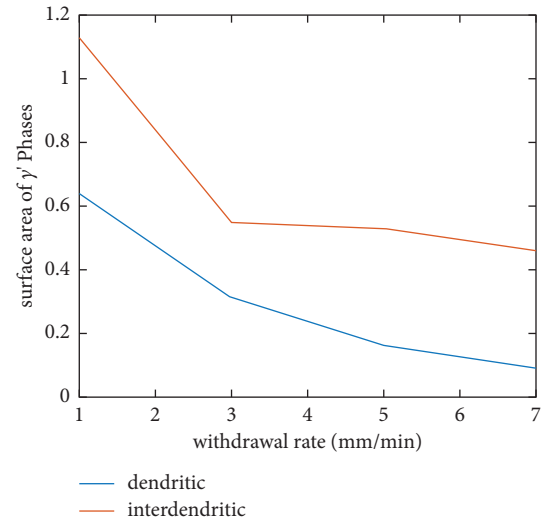

Figure 35: Variation in the surface area of γ' phase precipitates found in both dendritic and interdendritic areas of samples obtained using different withdrawal rates.

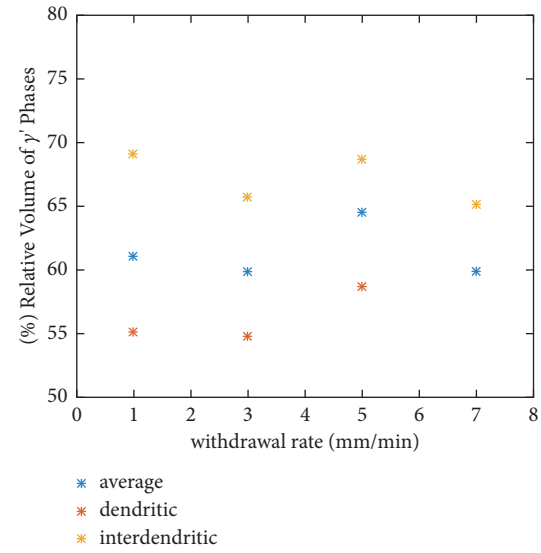

Figure 36: Data regarding relative volume percentage of γ' phase and how it changes with respect to to changes in withdrawal rate.

porosities was seen to decrease with an increase in the withdrawal rate. A casting's creep life was seen to be highly influenced by the presence of porosities. With a decrease in the number and size of porosities, the creep life seemed to improve. The highest creep life was observed for casting made with 3 mm/min withdrawal rate. And the crystal orientation was also seen to be unaffected by the withdrawal rate used. The creep behaviour of samples made using different withdrawal rates has been graphically represented in Figure 37. Another study [99] revealed how the vacuum degree condition used while melting and casting alloys help with the purification of the alloy. This research particularly studied how the degree of vacuum can influence the O and N content in Ni-based superalloys. The study results showed that, compared to rough vacuum conditions, the high

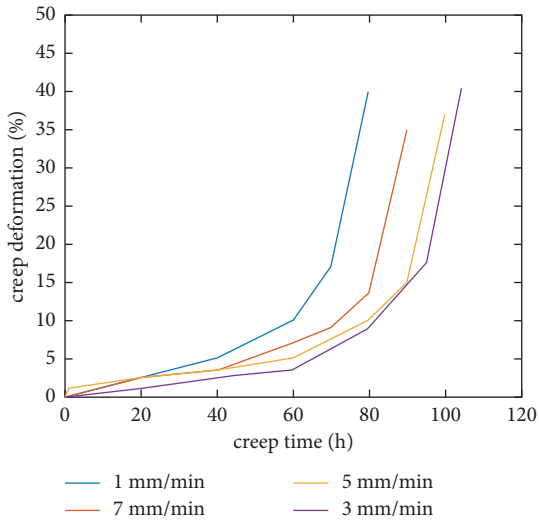

FIGURE 37: The relation between percentage creep deformation and creep time.

vacuum degree was extremely helpful in decreasing the content of O and N present in the superalloy. Moreover, adding the rare-earth element yttrium (Y), the content of O in the molten superalloy was seen to decrease further. However, the N content was seen to slightly increase under high degree vacuum conditions due to the good solubility of N in Y.

Turbine blades are usually cast with a SX structure using Ni-bases superalloys. They are manufactured with the crystal's growth taking place along [001] axial orientation with the help of DS process in a Bridgman furnace. The main reasons for manufacturing the blades with the SX structure are (1) to eradicate the presence of GBs that severely inhibit creep and ductility and (2) to introduce an elastically soft [001] orientation. Although in some particular situations it can become imperative to introduce a particular axial orientation other than [001] on the casting, this was accomplished by using a SX seed that had the correct orientation. Preheating of the whole assembly was performed after the already fabricated seed was planted into the mould to partially instigate the melt-back of the seed's top section during commercial production. Following this, the mould cavity is filled by pouring the molten superalloy into it, and then the withdrawal of the mould is gradually done from the furnace. During the DS process, the melt-back mush was seen as a source for the growth of defective grains that have deviated away from the seed's orientation. This was the subject of one particular study [29]. It investigated the changes that appeared in partly remelted CMSX-4 seeds to evaluate the secondary dendrites' fragmentation's importance in SX processing. The primary objective of this study was to gain a better understanding of the inner workings of the formation of defective grains so as to direct industry practices on measures to avoid such difficulty or complication. The structure of secondary and primary dendrites of the unmelted seed was found to be exactly same as that of the original seed. Examining the melt-back area that is semi-solid revealed a complex dendritic structure. This was seen to have been caused by higher levels of liquid fraction, which was shown to arise as a result of the secondary dendrite arms eroding disproportionately. Islands of misoriented material, which were pinched off secondary dendrites, were seen to have been formed throughout the mushy zone. But those were not regarded as a potential threat that can bring about some casting defect while manufacturing SX Ni-superalloy castings because they were not seen to accumulate at the casting's periphery where stray defect grains are seen to appear. Thus, the part played by seed melt back on occurrence of casting defects was seen to be negligible. Another study [75] focused on determining the impact triggered due to the presence of the inoculant $CoAl_2O_4$ in the shell mould's prime coat and temperature of the melt at the time of pouring on the mechanical and structural characteristics of IN713C Ni-superalloy castings. Inconel 713C superalloy was used to produce eight investment castings, each differing in the temperature of melt on pouring that ranged from 1400 to 1520°C, and $CoAl_2O_4$ inoculant concentration of the prime coat that varied between 0 and 5wt.%. Increasing pouring temperatures of the melt was found to result in decreasing cooling rates. This was seen to lead to larger grains being formed with increasing melt-pouring temperature. In the broad range of pouring temperatures used for IN713C, $CoAl_2O_4$ was seen as a great modifier. This was revealed while the microstructure of castings was further examined. As the molten alloy came in contact with the primary coat, $CoAl_2O_4$ got reduced to Co due to its interaction with highly reactive elements present in the molten alloy. And then, the formation of fine Co particles along the internal surface of the shell mould was seen. These Co particles and Ni γ phase were seen to have a very similar crystal structure. Their lattice misfit was calculated to be only 0.9%, thus showing their effective usage as nucleation substrates and helping increase the cast surface's heterogeneous nucleation rate. Additionally, a higher concentration of vacancies was seen in alloys poured from higher temperatures. Observations showed that the required minimum of yield stress was significantly surpassed in all the samples. The yield stress was seen to decline as the casting temperature increased, for unmodified samples. However, the opposite trend was seen for elongation. The modified castings followed no straightforward trend and the maximum yield strength was observed at sample made with the pouring temperature being 1520°C. The strength of the casting was seen to be mainly influenced by the fineness of the grains. For unmodified castings, as the melt pouring temperature increased, the grain size increased. Except for the casting made with a pouring temperature of 1400°C, the strength of modified castings was significantly higher than the strength of the castings that were unmodified. However, it was the opposite trend in the case of elongations, except castings poured at 1400 and 1450°C. An increase in the pouring temperature of the melt was seen to help in improving the creep life. Additionally, regardless of melt pouring temperature, unmodified specimens were seen to exhibit higher mean rupture time. When the melt temperature increased, the steady-state creep rates declined in all samples regardless of them being modified or unmodified, with the modified

castings having higher creep rates. Another study [80] looked at how casting parameters like rate of solidification and melt superheat affected the microstructural characteristics of IN738LC, an experimental Ni-superalloy, manufactured with the help of investment casting as well as vacuum melting. The as-cast microstructure of the Ni-based superalloy was seen to contain nodular σ phase and plate-like as well as blocky shaped η phase in the interdendritic zones, thus revealing that both and phases solidified in the last stages of the solidification process. Also, the size of the primary γ dendrite was seen to increase and decrease with melt superheat and solidification rate, respectively. This means that the high superheat specimens have coarser primary γ dendrites. In addition, higher cooling rate specimens were seen to have finer primary dendrites than lower cooling rates. It was also seen that a high solidification rate and low melt superheat lead to increased volume fraction (V_f) of interdendritic γ/γ'. The V_f value was seen to decrease with decreasing cooling rate and diminish quickly and drastically with an increase in melt superheat.

3.2. Alternate Methods for Manufacturing of Ni-Based Superalloys. So far, we have discussed how various conventional casting methods are used to make Ni-based superalloy components and how these methods and the parameters used in them can affect the final product. But studies have also been conducted on how Ni-based superalloy parts can be made using methods other than casting and how they are compared to the ones made using casting methods. One such study [32] focuses on vacuum electromagnetic casting of Ni-based superalloy ingots. Ni-superalloys have many alloying elements present in them, and good mixing of these components is required to ensure a good microstructure. Vacuum casting was developed, keeping that in mind. Vacuum-electromagnetic casting uses electromagnetic stirring (EMS) to allow good mixing of all alloying elements. The goal of this study was analysing how EMS affected the inner quality of ingots made of IN100 superalloy. The study showed that, in the absence of EMS during solidification, there were 3 crystal structures found in the ingots: (a) a thin zone made of equiaxed grains at the ingot surface; (b) a zone made of coarse columnar grains; and (c) a zone made of coarse equiaxed grains in the center portion. It was also observed that, after introduction of EMS during solidification, the microstructure got refined. The equiaxed grain's average size was seen to reduce from 2.8 to 0.78 mm, and the ratio of equiaxed grains was seen to increase from 67% to 75%. This result was seen due to the generation of forced convection by the EMS, which, in the solidification front, was seen to cause the breakage of dendritic arms and then disperse them into the melt pool, thus creating a more effective crystal nucleus. It was also seen that without an electromagnetic field, the shrinkage cavity's length and porosity was 87 mm, while in the presence of electromagnetic field, it became 54 mm. EMS during solidification was also seen to improve feeding capacity. In vacuum-casted superalloy ingots, severe element segregation was seen and the introduction of EMS during solidification was shown to relieve this segregation. Another study [81] focuses on the microstructure developed while casting Ni-based superalloy parts using a rather unconventional casting method, centrifugal casting. Inconel 625 was used for the study. The microstructures of all three zones, the chill zone, columnar zone, and the equiaxed zone, were analysed. Four samples were made for the study such that Mo concentration was higher in IN625-2 than in IN625-1. There was higher concentration of Nb in the alloy IN625-3, and there was more C, Si, Nb, and Fe concentrations than the 3 other samples in the fourth sample. With the microstructural analysis, it was observed that secondary phases and microporosity defects were lower in number in IN625-3 and IN625-4 than in IN625-1and IN625-2. But contrastingly, there were almost no niobium carbides (NbC) present. But very small particles were detected in the alloy IN625-4 alone since it had higher C content. It was also seen that after the NbC precipitation, Laves phase started to form due to depletion and decreased concentration of carbon. It was seen that the use of very low cooling rates promoted the formation of Nb-rich phases. Due to low C concentration in the alloy IN625-1, Nb-rich precipitates of two types were detected. The equilibrium condition, along with the microstructure obtained, was seen to be explained by the presence of a bi-phasic constituent containing Nb-rich granules which surrounded the γ-phase nuclei. In higher cooling rates, observations showed that the morphology of the Nb precipitates were elongated. Both these phase morphologies were never seen to be related with microporosities, since compared to globular precipitates, microporosities were seen to have a much higher surface-to-volume ratio. IN625-2 was observed to have the same microstructure even though Mo concentration was higher. Higher Nb concentration was the main characteristic trait of the alloy IN625-3. The C concentration in this alloy was found to be virtually identical to that of the previous two alloys, and the lower rates of cooling promoted the development of the Nb-rich phases. Having the highest C concentration of all the elements utilized for alloying purposes, the alloy IN625-4 was found to have secondary phases with an extremely high-volume fraction located at GBs. When rates of cooling and alloying element concentrations were found to be lower, a rise in the volume fraction of the secondary phase was also observed. Another study [9] compared the microstructure of superalloy parts prepared by suction casting and additive manufacturing. Inconel 718 was used here. The preliminary microstructures belonging to the as-built and as-cast samples were seen to be not the same. This difference was seen to affect the matrix's Nb homogeneity and this was seen to be an important factor deciding grain morphology when homogenization occurs. In suction-cast alloys, Nb homogeneity rises, but in AM alloys, it was seen to decline as the time passed when heat treatment was performed in an isothermal manner at 1180°C. When homogenization happens in suction-casting, the phase changes that occur are unlike those in the AM alloys. It was seen to be this way because the initial solidification microstructure was observed to be divergent in nature. When suction-casted alloys were considered, the Laves_C14 phase was seen to be present even

after short-time homogenization (1 h) occurred, and after long-time homogenization (12 h), they were seen to have been dissolved. But when it comes to AM alloys, they were seen to be dissolved entirely after just 20 minutes of homogenization and a simultaneous growth of carbides (NbC) was also observed. Nb is very important for the development of strengthening phases. And the formation of disadvantageous Laves_C14 phase was seen to occur due to its microsegregation. So the regulation of Nb segregation, when homogenization occurs to make sure that in the γ matrix there is very good Nb homogeneity to encourage strengthening precipitation in the steps that follow after heat treatment, was seen to be important. The alloys made by AM were seen to have good Nb homogeneity initially because of solute trapping effect. This was seen to take place as a result of the swift velocity of the S-L interface that happened due to the rapid solidification during the laser melting process. And, suction-cast alloys were seen to exhibit uncharacteristic excessive grain growth, as well as a rise in the time needed for homogenization. In contrast to this, grain growth was seen to be hindered for AM alloys. Also, for longer homogenization times, the typical grain size was seen to be more refined in AM alloys. It was also seen that the recrystallization process was continuous in alloys made using the AM process. The Zener pinning effect of the NbC carbides was given accreditation for the grain refinement observed in these samples. Many kinds of displacement behaviours were seen in AM alloys, and this can affect alloy hardening. The carbides seen not to be in coherence with the matrix were identified as sources for dislocations. Two main factors causative to the generation of dislocation were seen to be the carbides' growth and the local strains which were released when homogenization processes occurred. In AM alloys, the dislocations created were seen to be actually arrays/loops. The dislocations accumulating at GBs were observed to instigate the creation of additional dislocation arrays in the neighbouring grain located adjacently. This was seen to be beneficial for local strain relief and for assistance in the prevention of fractures, thus helping with alloy-hardening.

4. Effect of Alloying Elements on Ni-Based Superalloy Castings

Alloying elements present in an alloy can cause noteworthy effects to various attributes of the ultimate superalloy casting. These elements can influence the microstructure, mechanical properties, physical properties, and even the formation of defects. Studies have been conducted to determine how much of an influence they have over such factors. We have reviewed some of these recent studies. Nickel-based superalloys' mechanical properties rely on the site and phase preferences of the alloying elements, which can affect the bonding strength inside γ'-Ni3Al precipitates and other characteristics, which give rise to superior mechanical properties. One study [82] done focused on the partitioning actions of elements X = Cr, Co, Ta, To, or Nb amongst γ' and γ phases, their inclinations for site occupancy in γ' precipitates, and how this affects the microstructural development of Ni80Al15X5 alloy systems, as well as the effects their atomic size has on the system. It was observed that the degree of atomic distortions inside the γ' and γ phases decreased, when the presence of alloying elements with larger atomic radii including X = Ta, Ti, or Nb was enhanced in γ' precipitates, while smaller size X = Co or Cr atoms were seen to prefer their precipitation into γ matrix phase. When we observe γ'-Ni3Al precipitates, larger X = Ti, Cr, or Nb atoms were seen to like inhabiting the Al sublattice sites; in the meanwhile, having smaller size, X = Co atoms help in substituting both Ni and Al sublattice sites. Within γ' precipitates, the mechanical strength was seen to be significantly influenced by the bonding strength. Since the alloying element X's atomic radii are nearer to the Al atoms, most of the Al sites of γ'-Ni3Al-X phases are preferentially occupied. It can be seen that the γ' values rely on the alloying element's atomic radii, phase, and inclinations for site occupancy. Mostly when the alloying element's atomic size increases, phase partitioning inclinations of these elements were seen to tend towards the γ' precipitates and the values of energy change parameter were seen to become more negative. As a result of this, there is an increase in probabilities of Al sublattice site occupancy of these elements in γ' precipitates and there is reduced occupation of Ni sites. Due to this, there was formation of stronger directional bonds amongst the X atoms and their NN Ni atoms present in the <110> directions of γ' precipitates, and better hardness properties were seen to be attained in a specific order of additions (X = Co < Cr < Ti < Nb < Ta). And this was seen to lead to strengthening of bonds in γ' precipitates and thus the strengthening of the superalloy. When the alloying elements are inclined to inhabit the Ni sites, a very strong strengthening effect will not be seen since Ni-X bondings are stronger than Al-X bondings. Another study [76] investigated the role of alloying elements like carbon, boron, and zirconium in porosity formation. The alloys' elements were chemically composed as given below in this particular paper: 20.2Cr-4.78Mo-13.7Co-2.34Fe-1.19Al-0.08C-0.69%Ti for Alloy 1 and 20.5Cr-5.03Mo-15.6Co-3.42Ti-1.57Al-1.64Fe-0.15C-0.01B-0.076%Zr for Alloy 2. Since vacuum conditions are used for making alloys, the porosities spotted in the alloy structures were understood to occur because of microshrinkages and not due to evolution of gas when solidification occurs. Small amounts of B and Zr and higher C content in Alloy 2 were found to reduce porosity formation due to the segregating effect of these elements, which help in alleviating microshrinkages during solidification. These elements were also seen to increase the carbide content in the interdendritic region by their segregation and formation of carbides. The study also showed that an increasing Ti and C content increased the MC carbide and γ/γ' eutectic volume fraction, with alloy 2 having 4 times the carbide volume fraction of alloy 1. Creep property of a material defines how well it can work without failing in high temperature conditions. A variety of alloying elements can influence superalloys' creep property, and many studies have been done to understand how these elements can affect them. One such study [77] focuses on a particular alloying element called ruthenium (Ru) and how varying its content in the alloy can affect its creep properties. Two superalloys having different Ru

contents were considered for studying Ru's effect on microstructure and creep rupture life. Using wt% as a scale, both were named alloy 3.5 Ru and alloy 2.5 Ru correspondingly, by the amount of Ru they possessed. After post-heat treatment, the resulting magnitude and volume fraction of the corresponding γ' phase was seen to have reduced with a rise in the content of Ru. It was observed that 2.5 Ru's creep curve consists of three phases and it had one less incubation phase than 3.5 Ru and this was seen to cause a rise in the rate of creep strain in the latter, followed by reduction and steadying and then finally rising again. Due to the reduction of the smallest value of creep rate and extension of the secondary creep stage, the creep rupture life was enhanced with Ru's surge at 1140 C/137 MPa. The increasing of Ru composition was seen to have slackened the movements of the dislocations by improving the γ matrix's strength as well as roughening the γ' phase by lessening the preliminary γ' phase's size (data regarding γ' phase's size and PDAS values have been compared for both alloys in Figure 38), and this was seen to have amplified the primary and secondary creep stage times. The 2.5 Ru alloy's case was not the same. So, it was concluded that rise in Ru-extended creep life (data regarding influence of Ru in creep behaviour are graphically represented in Figure 39) of the alloy but it was seen to be ineffective in avoiding the rare TCP phase development. Another study [19] focused on the effect the alloying element Ti had on creep behaviour of Ni-based superalloys. 2 derivatives of the base alloy, with 1 (Alloy 1) and 3 (Alloy 3) wt% of Ti, were chosen and examined. The difference between the 2 alloys selected for the study was in the number of γ' forming elements, and this study focused on γ' forming element Ti particularly. The stacking fault energy (SFE), lattice misfit between γ' and γ, anti-phase boundary energy (APBE), and creep properties were all seen to be greatly affected by the γ' phase's volume fraction. These are all affected by the Ti content which also affects the γ/γ' misfit. Ti was seen to replace Al atoms in γ', Ni_3Al. There was also a rise in APBE, SFE, and lattice parameter of γ' when the Ti content increases. These trends were seen to have some extent of influence on the shearing mechanisms that are observed in these alloys when temperatures are very high. The number of γ' forming elements and temperature were found to strongly influence microstructure, density of dislocation, APB formation, and SF's existence. It was observed and concluded that Ti addition can improve creep resistance at relatively higher temperatures (about 900°C) due to the detachment of dislocations into small fractional parts which have stacking faults. γ' cutting mechanism was seen to have improved from dislocations attached with SF to APB coupled pairs with rising temperature. But, alloy 3's transition temperature was observed to be more than alloy 1 due to variance in the content of Ti. Due to higher Ti content, there was a decrease in dislocation movement by the detachment of dislocations with SF in alloy 3's γ' phase. So, it was concluded that Ti content's increase can greatly help in bettering the creep properties. After creep (happened at 982°C), the two alloys that were examined showed very similar creep rupture lives and dislocation structures. The creep behaviour of alloys 1 and 3 at different temperatures and stresses are graphically represented in Figure 40. Another paper [72] aimed to study how

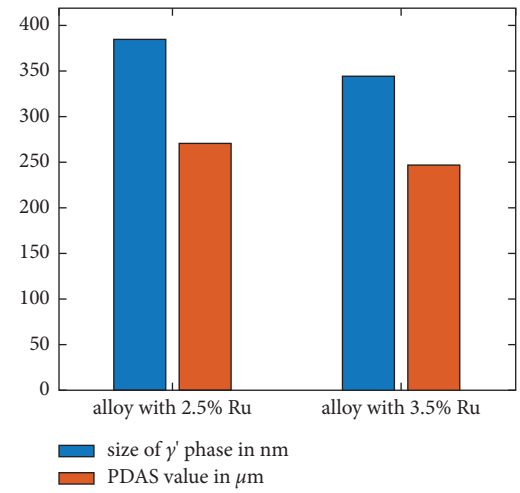

Figure 38: Change in PDAS and γ' phase size values for alloy 2.5Ru and alloy 3.5Ru.

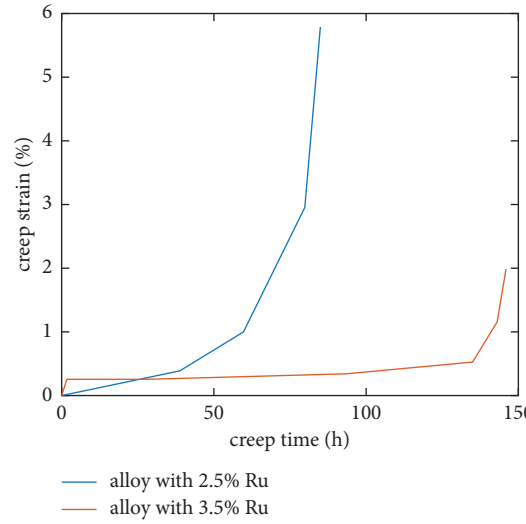

Figure 39: The creep behaviour of both alloy 2.5Ru and alloy 3.5Ru.

integrating calcium (Ca) influences yttrium's (Y's) reduction from a nickel-based superalloy and its alloy's cyclic oxidation. Introducing small quantities of rare-earth elements (REs) can significantly develop/improve the structure of superalloys, cleanse the grain boundaries, enhance their resistance to oxidation at high temperatures, and improve creep resistance of the alloys. Since REs exhibit high reactivity, they mix with S and O and help in the making of an oxide film that is shielding and dense. But substantial loss of REs can happen when alloy is melted and cast because of their volatility and the likelihood of ceramics reacting with them. To reduce these losses, Ca, a much more reactive metal, was added in this study. Here, the effect of adding Ca on enhancing resistance to oxidation of Ni-superalloys was examined using two samples, one comprising of 0.12Y and the other 0.12Y + 0.12Ca (in wt%). They were exposed to many oxidation cycles and then likened for further investigation. It was then witnessed that when solidification happens after melting, the Gibbs free energy of

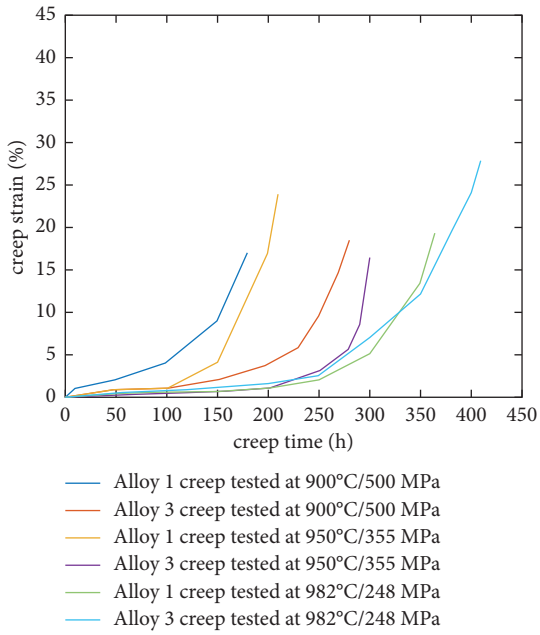

FIGURE 40: Creep behaviour of alloy 1 and alloy 3 at different testing conditions.

combining Ca and O_2 is lesser than combining Y and O_2. So, Ca's consumption of O was seen to have increased and Y's residual content improved. This was proved numerically by performing various calculations in this study. Thus, it was concluded that Ca addition is very useful in improving the resistance to oxidation of the Ni-superalloys. Grain refinement and purification can also be influenced by certain alloying elements or even due to the addition of certain intermetallic compounds. Some studies were done in this regard as well. One such study [34] focused on a couple of intermetallic compounds belonging to Cr Mo Nb's ternary system and Co Fe Nb. These compounds were selected as inoculants for this study, and how they affect the grain refinement of K4169 was examined. It was observed that when these grain refiners are added, size of equiaxed grains can be made in the order of ASTM 3.2. At the cross-section, the equiaxed fraction was seen to have been enhanced from 56% to 99% and the ratios of segregation of elements like Cr, Fe, Mo, and Nb were seen to have declined. There was also grain size reduction seen, which signified that grain refinement through adding refiners can reduce the segregation of the element when solidification occurs, without altering the local solidification time. In conventional castings, the grain morphology was dendritic, and in fine-grained castings, this was changed to granular. Lower temperatures during pouring and grain refiners were seen to reduce temperature gradient in the melt, increasing melt supercooling, rate of cooling, nucleation undercooling, and endurance of many grain-refining particles. All of which was seen to help in achieving grain refinement and grain size reduction. Refiner particles also had excellent lattice compatibility with the γ matrix, resulting in grain refinement. The refinement that took place was also seen to reduce casting pore sizes. Another study [99] focused on how adding yttrium can help with purification of melted superalloys. For that purpose, the study particularly targeted the N and O contents of the alloy. The superalloy K417 was used here. Without including Y, there were four phases present in it, which were γ (FCC matrix), carbide, eutectic, and γ' (Ni_3[Ti, Al]). A novel white contrast phase, which was several microns in terms of size, was observed when 0.1% and 0.5% Y were mixed with the alloy. This new phase was seen to have a smooth block/strip morphology. It was found to be rich in the Y phase as per EDS analysis, and it was further found that the phase rich in Y was a $Ni_{3.55}Co_{0.5}Cr_{0.2}Al_{0.75}Y$ phase with a hexagonal crystal formation. Moreover, adding more Y did not seem to cause the formation of any secondary phases that were rich in Y. It was also noted that N's concentration displayed inclination for slow growth when Y's content increased because it enhanced N's solubility. The study also revealed that Y and Ti have similar affinity for N. Even a small increase in the high vacuum degree was seen to reduce the content of N. Only with the addition of Y did its affinity for N arise and enhance N's solubility in the alloy. By adding Y, at the beginning, the alloy's O content lessened abruptly and it touched a minimum when Y's residue went to around 0.08%. When Y's residue improved from 0.08% to 0.45%, no apparent decrease in the oxygen content of the alloy was seen. Y was observed to have had a purification effect in removing O from alloy and this was seen to be enhanced while performing the melting and casting in a high vacuum degree environment, while the N content was seen to increase slightly due to solubility on N in Y. Certain alloying elements can also be responsible for the formation of defects. One study [90] focuses on this matter. It examines hafnium's (Hf) contribution to the development of defects, called freckles. It was seen that Hf had a very high affinity for partitioning into the solid phase, i.e, the γ-phase, and Hf was not seen in the freckles' dendritic cores. Between freckles and the SC, the elemental distribution was seen to be similar to that amid the S-L phases. This helped to finalize that when solidification happens, the Hf partitions to the solid. Due to this, Hf was seen to have a very significant and possible consequence on introducing the development of freckles. But the concentration of Hf should be more than 1-2% for it to have an effect similar to elements like Re and W. But this was seen to be overcome when the alloy had high amounts of Co or Cr in them. It was observed that the high content of these elements increased the solubility of Hf in the alloy and thus made the effect of Hf in promoting freckling more pronounced. The findings of this study proved that despite the very small concentration of Hf in certain Ni-based superalloys, it can still have a significant effect in promoting freckling.

5. Physical and Mechanical Properties and Behaviour of Ni-Based Superalloys

Ni-based superalloys are superalloys that have Ni as their main component. Amongst all superalloys, Ni superalloys have highly superior mechanical and physical characteristics, thus making them one of the best choices for making components that will have to endure and survive in very harsh environments for prolonged periods. Thus, studying the mechanical and physical properties like, their

microstructure, fatigue life, stress-strain behaviour, creep life, tensile properties, and ductility, of these alloys is very important in order to understand their nature and their behaviour under harsh conditions, so as to help us better optimize their use. This article has extensively and narratively reviewed many studies that have investigated these characteristics of Ni-based superalloys. One such study [83] investigates the characteristics and transformation of the primary phase and its effect on impact ductility on Ni-superalloy K4648, which has enriched Cr content. Here, the primary α-(Cr, Ni) phase was seen to exist in the K4648 alloy's as-cast microstructure, which is an oversaturated solid solution of Ni, W, and Mo in Cr. It was seen to be hard and brittle, and there was an equal tendency for cracking seen in both the alloys that were as-cast and have undergone heat treatment. The beginning of the primary α-(Ni, Cr) precipitation was seen to occur at 1190°C due to late solidification from small amounts of liquid residue in the interdendritic region and also the GBs. And this was seen to be caused by the nonstop segregation of Cr throughout the solidification process. The primary phase solid was then seen to solutionize and subsequently transform into M23C6 carbides between 1180 and 1220°C, and incipient melting was seen to occur in temperatures ranging from 1200 to 1220°C. Here, with increasing the solid solution temperature, the volume fraction of the primary phase was seen to have decreased. Transformed M23C6 carbides or extensively cracked phase were found on the impact specimens' longitudinal sections and fracture surfaces. This was seen to lead to decreased impact ductility of the cast Cr-rich K464 alloy. Another study [59] aimed at testing the practicality of semi-solid processing of Ni-superalloys. Temperature's effect on microstructure and other properties (mechanical) of formed parts are also studied. This study tells the feasibility of using thixoforming for manufacturing a high-performance product made of Ni-based superalloy. An extrusion bar which was made of GH4037, a commercial wrought Ni-based superalloy, was used as the experimental material in this work. At appropriate temperatures, parts made of GH4037 that underwent complete filling and good surface formation were seen to be thixoformed without any problems. 1653 K was seen to be the ideal forming temperature, and good wide-ranging mechanical properties were found on the formed part with an EL value of 41.9% and an UTS value of 960 MPa. Initial thixoforming experiments' results were seen to establish that semi-solid processing is feasible and has potential when used for producing parts made of Ni-based superalloys. A novel route was provided in this work for forming Ni-based superalloy parts, which can offer a foundation for researching the semi-solid processing of Ni-superalloys. But due to the high temperatures during the forming process, there is a possibility of the casting die getting damaged. Another study [84] focused on developing a microstructure and the performance of a casting made of C1023, a polycrystalline Ni-superalloy. The study was conducted by comparing the abovementioned characteristics of the heat-treated and as-cast samples made with the chosen alloy. The effect of carbides and strengtheners on the tensile nature of the heat-treated superalloy castings was also studied for various temperatures. Few carbides were seen to tend to spread their dendritic arms along the GBs. Tiny black spots were detected in the surrounding area of huge primary carbides found in superalloys that were heat-treated, indicating that they were substances precipitated during heat treatment. And the changes the morphology of the primary carbides underwent were seen to be small and insignificant. Huge amounts of γ' phases were seen in the superalloy since it was reinforced by large-scale γ' along with carbides in the austenitic γ matrix. The large-scale carbide which was rich in Mo and Ti was seen to expose the precipitation of (Mo, Ti)C carbides at the interdendritic regions and GBs. Concurrently, Al and Ni's precipitation was witnessed to help with the formation of primary reinforcement/strengthener, which was an irregular round shaped γ'. In the superalloy which was heat-treated, the main MC carbide where Mo and Ti replace M were seen to have gotten decomposed into an octahedral carbide that is rich in Mo throughout the alloy's entirety. Mo's precipitation in the γ matrix when heat treatment was taking place was seen to cause the distinct dispersal of carbides which were rich in Mo. M23C6 carbide's shape changed from octahedron to elongate cube due to its acid resistance characteristic. In heat-treated superalloys, regular shaped and varying sizes of γ' is observed. The γ' particles increasing in size during heat treatment was seen to cause an increase in the volume percentage of γ' and enhanced the superalloy's mechanical properties. Elements like Co, Mo, Al, Cr, and Ti were concentrated in the precipitates like γ', MC, and M23C6 carbides deplete them in the γ base. On the heat-treated specimens, tensile properties were tested at room temperature, 850°C, and 650°C. When done in room temperature, the results of the superalloys' stress-strain diagram displayed that the superalloy showed good yield strength and linear elasticity at yield stage till fracture point. For tested specimens, the elongation as well as decrease in the area at room temperature was seen to reduce noticeably when compared to those at higher temperatures, thus highlighting the presence of casting pores in the sample. At 650°C, the tensile strength was seen to remain at high levels constantly. But the extension and decrease of the area were seen to increase largely with one serrated stage. Tensile strength at 850°C was 23% lesser than that seen at room temperature with two serrated stages. However, excellent plastic deformation ability was seen to promote the extension and decrease of the area near 850°C. Another similar study [55] investigated the effects of microstructure evolution that increased ageing time on all tensile properties. Tensile properties near room temperature for a new cast nickel-based superalloy when the ageing process happens at 800°C for 0–1000 h were investigated. The precipitation and coarsening of M23C6 carbides were observed with increasing ageing time and were seen to show a granular and dispersed morphology. The formation of γ' precipitation free zones due to the formation of η phase at the γ' phases' expense was also seen in samples subjected to high ageing times. This was attributed to the massive precipitation and M23C6 carbides' development and the massive Cr absorption. γ' phase coarsening was also observed with increasing aging time. And excessive coarsening due to

overageing was seen to be detrimental to tensile properties. This was proved by the increase in alloy strength and tensile properties, with the increase in aging time, and reaching peak performance after aging of 20 h, followed by severe deterioration of tensile properties with aging beyond 20 h. Another study [88] investigated the effect the grain refinement had on the structure of cast and other properties brought about by the addition of two intermetallic compounds CO3FeNb2 and CrFeNb to the K4169 alloy as refiners. Without grain refinement, only columnar grains were observed. By adding refiners, an equiaxed grain region was seen to have formed and the average sizes of grains were seen to have reduced. This was seen to be so because the refines behaved like the γ matrix's nucleation substrates. Without grain refinement, porosity with highly developed branches was observed. When grain refiners were added, the primary dendrite length was seen to decrease. And a decrease in porosity was seen due to the increase in alloy flow distance and grain refinement. Due to the refiners, very fine carbides that were dispersive in nature were found in the grain sample. The yield strength was seen to increase along with an increment in the value of ultimate tensile stress due to grain refinement. Another study [102] examined the mechanical and microstructural properties of IN718, which were made by selective laser melting (SLM) and casting. Strengthening in IN718 is usually done by the precipitation of γ' (Ni3(Ti, Al)) phase and γ (Ni3Nb) phase in the γ matrix. Delta phase (Ni3Nb) is a very vital precipitated phase for the IN718 alloy, and this was not seen to be in coherence with the matrix. Observations revealed maximum temperature gradients at the S-L interface when SLM happened, and the value was observed to be very high compared to that seen during the casting process. This indicates that the heat flux rate is very large when the SLM process takes place, while casting process was done, it was much smaller. Accordingly, due to this higher cooling rate attained by SLM compared to the casting process, the SLM-manufactured grain size was seen to be much finer in nature. The sample was then heat treated to witness the δ phase's effect on ductility. It is noted that after heat treating was done for the casting sample, in the interdendritic zones there were many huge segregation Laves phases that were irregular, suggesting that the total eradication of segregations is very difficult. Few globular carbides and rough acicular delta precipitates were detected in the interdendritic zones. Defects like porosity were also observed, and this was seen to affect the casting samples' tensile properties and causes early failure. The fracture surfaces of heat-treated casting and SLM-processed samples showed an indented surface, signifying transgranular ductility failure. The depression size of the SLM-processed samples was seen to be minor when likened to the casting ones because of the finer microstructure. The SLM-processed samples having better mechanical properties were accredited to grain strengthening triggered by the microstructure that had rapidly solidified with a very high cooling rate and temperature gradient. But the huge precipitated quantities of fragile Laves phases in the interdendritic region were seen to have made the instigation and spreading of cracks to be easier. SLM-processed samples' elongation was seen to be higher than for cast specimens because of more fine microstructure and precipitated phase being smaller. It is also concluded that huge quantities of precipitation of delta phase in the matrix will depreciate the SLM-processed samples' plasticity, while the decrease in delta phase was seen to increase plasticity as well as the strength of the material at the same time. Also, having no delta phase was seen to improve the notch sensitivity of the sample examined. So, it was seen to be crucial to have precipitation of an average amount of delta phase since it undertakes a huge part in the plasticity of SLM-processed sample. The study [10] investigated how the fracture behaviour at room temperature for IN718 superalloy is affected by manufacturing processes. This analysis was performed on samples acquired using both casting and Power Bed Fusion additive manufacturing (PBF-AM) methods. Tensile tests and fracture toughness estimations were done on the specimens. Microstructural analysis revealed anisotropy in grain morphology of AM samples. From mechanical tests, it was observed that the cast samples had higher ductility with elongation at break. This finding revealed that additive manufacturing of samples modifies plastic deformation mechanisms. SENB tests revealed that, when compared to cast specimens, the maximum strength and yield of AM specimens reduce, but the maximum strain was seen to increase, indicating mechanisms of plastic deformation being highly varied. Cast specimens were seen to attain ultimate failure but this was not seen to happen in AM specimens after the test finished. Mechanical tests showed that, in cast specimens, initiation of cracks begin a little earlier. This showed that, in AM-PBF samples, local plastic deformation that happens earlier near the crack tip due to lower yield strength might play a part in delaying crack initiation. The crack propagations were also found to be different for AM and cast samples. The crack length value was observed to be a little lower in AM specimens in which, at the bending test's end, ultimate failure was not seen. Testing the fracture toughness showed that, in cast specimens, crack blunting was seen with two varying slopes. This was not the case in AM specimens. This was not expected since cast specimens' yield strength was more than that of AM specimens. This helped to conclude that, near the crack tip, extensive plasticity is not instigated by plastic deformation. The beginning of plastic mechanisms within the materials does not indicate the lower value of fracture toughness when initiation occurs. Tests also revealed that, compared with cast specimens, fracture toughness of AM specimens increases a lot at crack initiation. Fractographic analysis done showed that cast specimens' fracture mechanism was mode-I fracture mechanism, while AM specimens had a mixed fracture mechanism. SEM observations showed that AM specimens have more striations whose formation interrupted crack front advancement and this was seen to provide them more fracture toughness when compared to cast specimens.

5.1. Fatigue Life of Ni-Based Superalloys. Fatigue life is a mechanical property that tells us how long an object or material can last before failing. Fatigue testing is a common practice done to study the fatigue life and behaviour of

various superalloys. There are various types of testing practices. The most common methods of assessment are LCF, HCF, and VHCF testing. Table 3 shows the various papers in which the different types of testing methods are focused on. There are many factors that influence the fatigue life and behaviour (some of the most influential factors are shown in Figure 41) of various superalloy components. The abovementioned factors are some of the most influential factors. Elaborate reviewing of papers discussing the impact of these factors has been performed in this article. Studying the fatigue property and, how and by what parameters it is influenced, can help us optimize the use of a certain material and put it to better use, and hence a lot of research has been done on this regard. One such study [11] focuses on the influence the microstructural parameters have on low cycle fatigue life. This study particularly focused on IN713LC, a Ni-based superalloy. The performance of three alloy batches with different microstructural characteristics such as equiaxed, columnar, and transition were used for standard low cycle fatigue (LCF) testing done at room and high temperatures. Strain controlled LCF testing was used in this study to examine the fatigue life reduction. For all the 3 different microstructures, fatigue life at room temperature (20°C) was seen to be 2-3 times longer when compared to results obtained at higher temperatures (650°C). This was seen to occur due to more slip activation and increased ductility at high temperatures, for any given strain rate. This also helped in proving the influence of temperature on the fatigue life. An equiaxed microstructure was found to have 1.3 times the life of transition ones and 2–7 times longer life than the columnar one. This disparity was seen to increase with increasing strain rates. The relative difference in grain sizes associated with the microstructures was revealed to be the primary reason for this increase. The columnar grains were seen to be the biggest while the grains in the equiaxed microstructure were the smallest. It was also seen that the length of dendrites and elongation along the loading direction were controlled by the size of grains. Both these were seen to increase with increase in grain size, thus facilitating failure. An abundance of precipitated carbides between dendritic arms, formed due to alloy segregation in all three microstructures, which are highly brittle in nature, were seen to provide a crack propagation path and function as origin sites for secondary cracks. Primary sites for initiation of cracks were found to be grains at the surface that have <100> fibre texture components, i.e., Goss and Cube, which is the most preferred direction for the quickest growth of dendrites. This was found to pave the way for the initiation of cracks at the time of LCF testing, in Goss and Cube oriented grains. An identical study [86] was performed, but with cast bars made of IN713C, which was tested under both LCF and HCF conditions. The results similar to the ones seen in the previous study were observed in this study for specimens subjected to both LCF and HCF testing conditions. Three types of samples with varying microstructures (equiaxed, transitional, and columnar) were seen to be used in this study. It was also seen that the columnar microstructure had the largest size of grain amongst all the 3 different microstructures produced. It was seen that for both HCF and LCF tests, the presence of grains with smaller sizes improved fatigue life. Thus, samples with equiaxed microstructure and the smallest grain size were seen to have longest fatigue life, followed by transition and then columnar microstructured samples. It was also observed that rate of crack propagation after its initiation at a casting pore seemed to rise with a rise in the size of grains. When the LCF samples were compared with the HCF samples, after the stage involving the initiation of cracks, the rate of propagation of cracks was observed to be higher in the former because of the higher value of loading stress used compared to the latter. The study [41] also examined the LCF properties of a particular SX Ni-superalloy, AM1. In this alloy, a γ phase matrix having a FCC structure and the γ' phase, which are cuboidal precipitates, was seen. This study aimed to investigate the fatigue behaviour of the AM1 superalloy at high temperatures and develop a method for predicting the LCF lifetime for Ni-superalloys at elevated temperatures. For this purpose, a damage model that describes the growth of microcracks, while assuming that cracks initiated at pores present in the casting was developed. The damage model developed for prediction was based on a process zone concept that described damage contributions along various slip systems in the form of a crystallographic constitutive model. Embrittlement of the material zone lying ahead of the microcracks helped in explaining the interaction with oxidation. In this study, for simulating the behaviour of microcracks at pores, sharp notches were employed. Under small-scale yielding, sharp notches were regarded as cracks at medium temperatures. But at elevated temperatures, as a result of oxidation and local viscoplasticity, an abnormal growth rate of cracks was seen in the region surrounding the notch. This abnormal growth rate of fatigue cracks at elevated temperatures was explained by the local viscoplastic strain field that was calculated using FEM, data regarding oxidation, and the crystallographic viscoplastic constitutive model. It was observed that simulated and calculated results matched the experimental results. Another study [58] focused on the very high cycle fatigue (VHCF) behaviour of castings of DZ4 Ni-superalloy manufactured using the DS process. It also showed how pores in these castings affect it. A very high fatigue cycle loads were imposed on HIP-processed (Hot-Isostatic Pressed) and cast specimens. Cast DS samples were manufactured by employing the HRS method in a vacuum induction DS furnace, followed by heat treatment. HIP was used to process some specimens, in order to eliminate casting pores. The experimental results demonstrated that both HIP-processed and cast samples showed continuously descending S-N curves. Fatigue fracture was observed in both specimens made using HIP processing and castings. Fracture was seen to take place once the number of cycles crossed 10^7 cycles, although for HIP-processed samples, there was seen to be a shift of more than 50 MPa for a period of 10^7 cycles to failure. Thus, by eliminating casting pores, the HIP-processed samples were seen to achieve superior fatigue properties than the samples made using the casting method. It was also observed that the initiation site for subsurface cracks was inner casting pores in the case of cast specimens. And this was seen to take place in the range of 10^5

Table 3: Various papers in which the different types of testing methods are focused on.

LCF	[1, 11–13, 21, 41, 47, 67, 86, 96]
HCF	[3, 21, 47, 86]
VHCF	[20–22, 58]

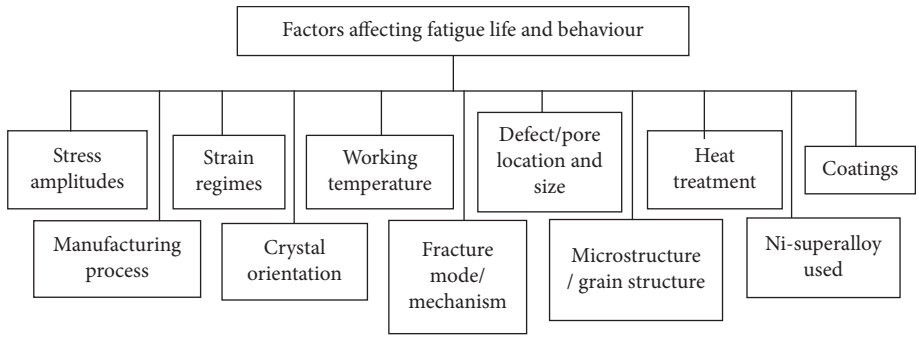

Figure 41: Some of the most influential factors affecting fatigue life and behaviour.

to 10^9 cycles at lower stress amplitudes than HIP-processed samples, whose fatigue cracks initiated from crystallographic facet decohesions. It was also seen that as the area of the casting pores increased, the cycles to failure decreased. In conclusion, the benefits of HIP treatments regarding the removal of casting defects and improved fatigue properties have been thoroughly proved in this study. Another study [20] focuses on VHCF life evolution after microstructure degradation. The main focus has been given to VHCF properties of CMSX-4 a 2nd generation nickel-based SX superalloy, in this study. Tests were performed with the help of 4 different CMSX-4 castings with varying microstructures (thermally aged at 1100°C/300 h, as-received, and creep deformed in tension at 1100°C/120 MPa for 24 h and 100 h) to calculate the influence the degradation of microstructure has over VHCF lifetime to failure and the mechanism for fracture. The coarsening of the microstructure was seen during thermal aging. A numerical simulation was seen to be needed to design the specimen properly. And this was carried out with the help of a finite element model. The VHCF lifetime's prime dependence was seen to be on the crack initiation phase, which was in turn controlled by creep damage. However, pores were seen to have control over micropropagation in mode I. Lifetime was also found to be independent of any influence by oxidation and γ/γ' morphology, and failure was seen to be mainly caused and controlled by casting pore sizes. Moreover, the VHCF lifetime was observed to be negatively impacted by precipitation degradation because of the increase in mode I cracks which were a result of reduction in yield strength and formation of pores of larger sizes, caused by coarsening during aging. Another study [21] aimed at investigating the variability in the fatigue lives under LCF, HCF, and VHCF conditions for CMSX-4, a 3rd generation SX Ni-superalloy based on microstructural defects formed during solidification after application of various solution heat treatment procedures. 3 heat treatment procedures were followed to make 3 types of samples, namely, HT1, HT2, and HT3. HT1's design was seen to focus on the dendrites' structures achieving great chemical homogenization, with neither any remaining γ/γ' eutectic pools nor IM (incipient melting) being present. However, HT2's design focused on presenting a lower level of chemical homogenization, in contrast to that of HT1, and also retain some γ/γ' eutectic pools. In HT3, the alloy's design was constructed to make sure that a huge area fraction (20%) of IM will be present in the casting, without resulting in any sort of easily identifiable growth in the sizes of pores. It was seen that solution heat treatment improved creep and tensile properties, but they were not seen to have been significantly affected by the type of heat treatment applied. The LFC tests revealed that HT1, HT3, and non-treated samples, all had similar LFC life. LFC life for HT2 was seen to be less at very high stress amplitudes, due to HT2 microstructure presenting a pronounced cyclic ratcheting. All cracks that led to failure were seen to have originated from casting pores. This was followed by HFC tests conducted for all samples. And again only HT2 was seen to perform bit worse compared to the other two. Cracks in HT1 and HT2 were seen to originate from internal casting pores, but cracks in HT3 were initiated from oxide layers. Short HCF life and failure of HT2 were explained by the comparatively huge number of surface cracks, even at low applied stress amplitudes. The same set of samples was subjected to VHCF tests, and it was found that there was no significant difference in any of their VHCF durability. It was seen that, in castings that have undergone solution heat treatments, the size of solidification pores was seen to be the major metallurgical defect guiding the VHCF life. And hence, the VHCF life was seen to mostly be influenced by the solidification constraints used in comparison to solution heat treatments. Another study [47] examined the fatigue behaviour of IN713C Ni-superalloy under LCF, superimposed LCF/HCF, and HCF loading. The testing conditions used in the study were an air environment having a temperature of 600°C under total strain control. It was observed that while undergoing loadings under HCF conditions, the strain fatigue limit was seen to decline as the mean strain went up. But once the value of the average strain

was seen to hit a particular limit, going beyond it was seen not to induce any significantly higher mean stresses. If the superimposed loading's amplitude was high enough, the lifetime during superimposed HCF loading was observed to have significantly reduced compared to pure LCF loadings. Under pure LCF loading, casting defects found below the surface were the initiation sites for loading cracks. During LCF/HCF loading, cracks were seen to have been initiated due to the presence of slip bands or from the casting defects found in the tested samples. Due to crystallographic and noncrystallographic initiation of cracks and their propagation, the strain-life curve of the tested specimen was seen to have a very wide scatter. Slip band cracks initiated by crystallographic means were seen to exhibit extended stage-I growth of cracks that were seen to cause huge cleavage facets at and below the surface, or the propagation and growth of cracks in a perpendicular direction to the direction in which the load was applied. The initiation of cracks was seen to occur at pores present below the surface due to stage-II crack propagation when the initiation of crack was following noncrystallographic means. The minimum and maximum stresses induced over the number of cycles under LCF and HCF/LCF loading conditions were observed to be steady and not change much. The lifetime of pure LCF was seen to be relatively higher when compared to LCF/HCF loading conditions. And this was seen to happen because of the excess growth of cracks resulting from HCF loading, even after reaching an adequate crack length. A considerable increase in lifetime was witnessed when superimposed HCF loading was reduced, and lifetime was seen to have reached the life while undergoing loadings with the nature of pure LCF conditions eventually after superimposed HCF loading was eliminated. Various methods for initiation of cracks, crack propagation, and a coaxing effect that may have been caused due to the superimposing of the HCF loads were seen to explain the discrepancies in the lifetime exhibited by both specimens that underwent pure LCF loading and LCF/HCF superimposed loading. Under LCF loading, all cracks were seen to have been initiated beneath the surface at pores. Transgranular propagation of cracks was observed at low LCF amplitudes, while a blend between transgranular and interdendritic crack propagation along pores was seen to occur when high LCF amplitudes were used. Under LCF/HCF loading, only transgranular propagation of cracks was detected, caused by the alternating unloading and loading actions. Results dictate that superimposed HCF loading can strongly influence lifetime before a particular crack length is attained. Another study [74] discusses the industrial perspective of SX Ni-based superalloys' thermal-mechanical fatigue (TMF). The TMF life was seen to be greatly influenced by a given set of test conditions used. This included (1) $T_{\max}$ (maximum temperature), (2) $T_{\min}$ (Minimum temperature), (3) $\Delta\varepsilon$-strain range, and (4) t-hold time. This study primarily focuses on TMF behaviour exhibited by bare alloys at high stress regimes and crack intiation and propagation in coated alloys. One of the conclusions observed from this study was that TMF life of a Ni-superalloy was heavily influenced by the given set of conditions used for testing. The TMF lives were seen to have been significantly reduced as $T_{\max}$ was enlarged from 850 to 1000°C or when $T_{\min}$ declined from 400 to 100°C. It was also seen that the harmful influence of a high $T_{\max}$ value was more noteworthy in lower strain ranges when compared to high strain regimes. When the specimen was held at maximum temperature, there was a dramatic reduction in the TMF life under compressive loading. This was seen to occur as a result of a large plastic deformation during the time of compressive holding. Additionally, holding it at very high temperatures was seen to enhance the damage inflicted by oxidation. It was revealed in the study that the creep capability does not single-handedly determine the TMF life. Proper microstructural heterogeneity and good crystal orientation were observed to have a higher positive impact on the TMF life. For a given strain range, the TMF life was seen to be higher for specimens with a crystal orientation of <001>. However, the orientation effect is less influential than the influence of mechanical stress on TMF life. This was seen to be so due to the lower value of Young's modulus along <001> compared to other crystal orientations. In bare alloys, initiation of the TMF crack was accredited to the following reasons in bare alloys: (1) the interactions between deformation twins or slip bands and (2) formation of micropores or oxidation spikes on the surface of the specimen. The TMF failure mode was also strongly seen to depend on strain range. An experiment with CMX4 superalloy revealed that the fracture mode changed from crystallographic to noncrystallographic with a decrease in strain rate. And, the specimen with the crystallographic fracture mode was seen to have highly reduced life when compared to samples following a noncrystallographic fracture mode. In coated alloys, the cracks were seen to be initiated at the surface of the coating, even at relatively low strain rates. And these cracks were then seen to propagate into the substrate. In coated alloys, crack propagation was also seen to accelerate due to a process called crack coalescence. Another study [2] focuses on fatigue strength and life of gas turbine blade castings made of MAR-M247 a Ni-superalloy with multiple carbide precipitates. The blades used were divided into 3 parts, as shown in Figure 42. During the casting process TaC, WC, TiC, HfC, and other MC carbide types were found to have been formed in the blade material. 50% of the revealed carbides were seen to be TaC carbides. In contrary to their relatively low percentage in the composition, carbides nevertheless have substantial influence over the material properties and enable the initial formation of cracks and their propagation. The yield strength was found to be 883 MPa, which was higher than the values of maximum stress.

The minimum fatigue life at 657, 382, and 545 MPa was found to be 1.17×10^6, 10^7, and 5.89×10^6 cycles, respectively, in the blade body's top, middle, and bottom. So, the total blade's life is inhibited by the fatigue life of $1.17 * 10^6$ cycles of its top part which is the shortest. In the case of carbide defects, in the calculations using FEM a 0.02% volumetric ratio was preset. From the bottom point of the blade to its top, there was an increase in positive stress values, and a maximum of 657 MPa was achieved. Using stress analysis, the fatigue life of the blade can be assessed using the given fatigue curve. A vibration-tensile combined experimental

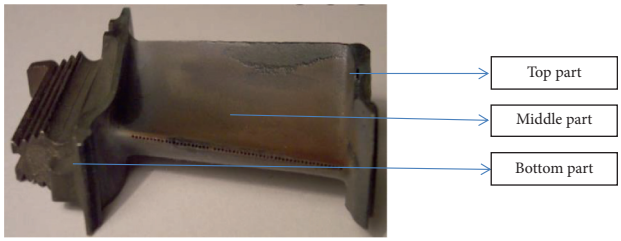

Figure 42: The 3-part division of the turbine blade.

setup that could measure stress with the help of strain gauges was used on different parts of the blade and was used in assessing the blade's conditions. The fatigue life of the blade was to be determined using the respective von Mises equivalent stresses acquired from the experiment and the available fatigue curves and Palmgren–Miner rule of damage accumulation. In conclusion, the experimental results accurately acquired the relation between the blade's defect volumetric ratio and its fatigue life. This relationship was further used to predict the least fatigue life values and maximum stress for models of blades with varying defect volumetric ratios.

Another study [96] investigated how the LCF behaviour of SX Ni-superalloy castings was influenced by temperature. Samples were subjected to LCF testing under two temperatures. One was a lower temperature of T_0°C and another a higher temperature of $T_0 + 250$°C. On examining the cyclic deformation behaviour exhibited by the samples, it was revealed that the temperature during testing and strain amplitudes was seen to influence the cyclic stress response exhibited by the alloy greatly. An initial rapid cyclic hardening was observed for every level of strain while undergoing compression and tension at T_0°C. But an initial cyclic softening at a higher temperature of $T_0 + 250$°C was observed. The samples were seen to achieve saturation typically at T_0°C, after the initial cyclic hardening. This result was seen in samples except for those fatigued on application of the highest strains and showed constant hardening in tension before finally rupturing. Under the higher strain levels, cyclic softening during tension and a consecutive hardening during compression were seen to take place in some exceptive samples that fatigued at $T_0 + 250$°C. Usually, the casting microspores found at the subsurface or the surface were seen as sites for cracks initiation during every LCF test performed at both temperatures. When observed at T_0°C, all specimens were seen to have single fatigue crack origins on them. At $T0 + 250$°C, a few of them are even inclined to exhibit multiple cracks from micropores present in the subsurface. Localized plastic deformation and stress concentration were seen to have taken place in the surrounding micropores to instigate the creation of microcracks and incipient cracks while undergoing the cyclic loading process. And this was seen to be characterized by a rough surface that was observed to be surrounding the micropores. It was also revealed that higher levels of plastic deformation took place in samples tested at higher temperatures, thus leading to fatigue life reduction compared to those tested in lower temperatures. The study also revealed that crack initiation in HIP-processed samples mainly happened at the Ta-rich carbides present in the subsurface, due to the absence of casting pores, as all the pores were eliminated during HIP processing. Further investigation showed that the temperature change resulted in a change in the fracture mode. Observations regarding the overall appearances of the fracture surfaces of specimens tested at T_0°C was seen to point to the fact that predominantly fatigue failure took place on 1 or 2 crystallographic facets. Now, coming to the the direction of the crack propagation, it was found to have been declined at an angle of about 50° from the specimen axis's direction of [001]. This was known as octahedral crystallographic cracking (Stage I). For Ni-superalloys with an FCC structure, this direction of crack propagation was usually seen to be preferred when subjected to high frequencies and low temperatures. Even when subjected to low frequencies and a fixed strain rate of $10^{-3}s^{-1}$ during LCF testing, the Ni-superalloy was seen to prefer the crystallographic cracking mode (Stage I). Another point to be noted was that the failure of facets displayed a classic cleavage type failure along with associated river-like patterns, which were usually seen to be reliant on the component representing normal stress acting on the fracture facet. The stress acting normally on the slip planes aiding failure by avoiding the closing of cracks as the resolved shear stress destroys the slip planes in front of the crack tip was seen to be an observation supported by results from the fractographic analysis. When the specimens were tested in T_0°C and $T_0 + 250$°C, their fatigue surfaces were dissimilar to each other. Microscopic analysis showed that the fracture sections were mostly observed to be flat and displayed Mode-I fracture. A fully functioning noncrystallographic mode for failure was discovered when magnification was increased. And this mode was seen to be comprised of coarse features that were dispersed in a homogeneous manner. The surface showed an absence of fatigue striations, and the cross-sectional area was seen to be reduced only by a minimal amount along specimens exhibiting no substantial elongation. A study of the microstructure was seen to have revealed the failure mechanisms for two cracking modes observed in the study. The failure mechanism for cracking at T_0°C was seen to be the precipitated γ' phases' shearing taking place along with the γ matrix. And for $T_0 + 250$°C, the cracking was seen to be limited to the γ matrix and the γ/γ' interface. Mechanical performance and fatigue properties were heavily dependent on inherent defects induced in the samples used during the casting process. The casting alloys were seen to be porous and have a myriad of defects, such as shrinkage porosities, voids, and gas porosities. The casting components suffering fatigue loading were seen to be negatively affected by the presence of these defects. And as far as fatigue life of casting parts was concerned, it is seen to be heavily dependent on the size and location of the defects. One study [43] particularly focused on this. K465, a polycrystalline Ni-based superalloy, was used to make samples to work with for this study. 2 types of samples were casted for this study. In terms of microstructure observed, the samples used in the study were seen to be split into two categories: fine (FG) and coarse (CG) grained samples that were seen to have considerable

differences when it came to the sizes of their grains. This variation in grain size and microstructure was observed to be the result of using different cooling rates to manufacture the samples. The defects found in these casting alloys were seen to be classified into one of two categories: gas pores or shrinkage voids. Defects in CG samples were seen to be found both inside the grains and on the GBs, while they were only seen to be found in the GBs of FG specimens because of the relatively far smaller and finer grain sizes. The γ' phase and MC carbides were seen to be the main strengthening agent of the alloy. The strengthening of the alloys at very high temperatures was seen to occur as a result of the precipitation of carbide particles, along the GBs and in interdendritic microstructures. However, because of the brittle nature of the carbides, they were seen to act as the sites for the initiation of the cracks and also provide paths for crack propagation. Carbides in CG samples were seen to be found within the grains and on the grain boundaries, while they were only seen to be found in the grain boundaries of FG specimens due to fine grain size. The distribution of carbide precipitates was seen to be uniform and homogeneous in FG samples while it was seen to be highly non-uniformly scattered in CG samples. LFC tests were performed on all samples, and it was found that the CG samples had better fatigue life compared to FG samples. This is graphically represented in Figure 43. Factographical studies revealed that this was due to the higher defect area and defect ratio of FG samples compared to CG samples. The same trend was also seen in maximum defect distribution. In FG samples, the cracks were initiated at the interdendritic defects and propagated through the script-like carbides. In CG samples, cracks were seen to initiate from the grain boundary defect and propagate through these grain boundaries. Microstructural investigations revealed that fatigue failure was dominated by grain boundary defects. This study also revealed the effect of grain fineness on the fatigue behaviour. Another study [12] focuses on the LCF and dwell-fatigue (DF) behaviour of diffusion (Al-Cr) coated IN713LC Ni-superalloy. The study revealed that precipitate coarsening takes place during both LCF and DF testing regimes. Cyclic straining during LCF tests was seen to elongate width along the loading axis at the expense of the width perpendicular to the loading axis. The cubic γ' precipitates on elongation accompanied by increasing strain amplitudes were seen to get rounded at the edges and were also seen to coalesce. DF tests were also seen to lead to grain coarsening, along a direction perpendicular to loading axis. After DF tests, many irregularly shaped cavities representing creep damage had formed along the grain boundaries. The coalescence of these cavities during testing led to further weakening of the material and thus initiate crack formation. They were also seen to facilitate crack growth. Three distinctive zones were observed in the Al-Cr diffusion coatings, based on their unique metallographic features: (1) the outer diffusion zone (ODZ), (2) the inner diffusion zone (IDZ), and (3) second reaction zone (SRZ). The ODZ was seen to possess a coarse-grained structure along with nanoparticles being dispersed in a fine manner inside the grains. But the IDZ was seen to have a fine-grained structure, along with the

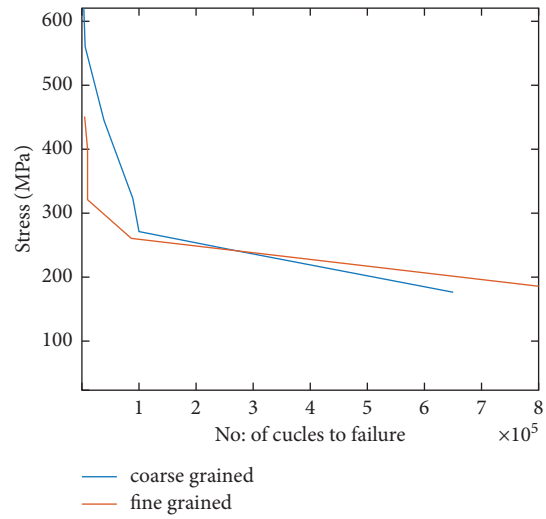

Figure 43: The relationship between applied stress and the number of cycles to failure for fine and coarse-grained samples.

grains having intermetallic particles that were polygonally shaped. Extended γ' precipitates were found when it comes to SRZ. At the boundary of the Inconel 713LC substrate and the SRZ, pointed particles with a needle-like shape and occasionally displaying dendritic morphology recognized to be topologically closed packed (TCPed) sigma phase were seen. In the ODZ, several weak points represented by rounded defects were observed after LCF testing. GBs present at the surface were seen as sites for the origination of fatigue cracks in both ODZ and IDZ. And the direction of propagation of these cracks was seen to be perpendicular to the loading axis. Same results were seen with DF tests, and this was due to the creep damage. It was also observed that both LCF and DF tests lead to fatigue softening. Tests also showed that the DF test condition can decrease stress amplitude compared to LCF samples. The study revealed that DF test conditions improved the fatigue life of diffusion-coated alloys compared to cyclic LCF loading. A similar study [22] regarding another coated superalloy focused on the damage mechanism. In this study, the VHCF properties of CMSX-4, a SX Ni-superalloy coated with a NiCoCrAlYTa coating and grit-blasted, were examined. The specimens cast for this study underwent 2 types of heat treatment: solution heat treatment (T1) and ageing heat treatment (T2). Different polishing durations were used on the specimens in order to vary the thickness of their recrystallized layers between 50 and 200 μm. Under completely reversed conditions ($R = -1$), strain-controlled fatigue testings were performed in this study at 20 kHz and 1000°C. Initially, the heating of all specimens for 45 min was done for stabilizing of temperature profile along the entire sample and obtaining a stable layer of oxide on the surface. For uncoated samples, the study revealed that a layer that had formed as a result of recrystallization with thickness greater than that of the biggest casting pore found specimen's surface (>50 μm) was seen to behave as the main site for initiation of cracks and be the reason behind the decline in the fatigue life. And fatigue life was sent to improve as the recrystallization layer became

thinner (<50 μm). The coated specimens were, however, seen to have reduced VHCF life, particularly for high stress amplitudes. Studying the failed specimens exposed that the cracks originated at the surface of the coating were seen to propagate via a mode aided by oxidation. The cracks were seen to have easily propagated into the coating. They proceeded to enter the interdiffusion zone present along the cellular boundaries while avoiding the penetration of the substrate. The recrystallization layer was observed to have cracked only in the surrounding area found near the cracks initiated at the surface. The environmental resistance of CMSX-4 was seen to have been degraded by the grit-blasting that was performed to introduce roughness via precipitation of AlN nitrides and by increasing the oxide layer's thickness. When comparing with specimens that underwent polishing, the fatigue life or the rupture mode was seen to be virtually independent of any influence by environmental degradation, without the presence of surface recrystallization. It was observed that roughness coupled with surface recrystallized layer degraded fatigue life by speeding up the formation and propagation of cracks formed on the surface, thus causing the concentration of stresses and finally rupture along the crystallographic planes. The interdiffusion zone, which was a site for damage accumulation as a result of cracking caused due to the oxidation of GBs and precipitation of internal nitrides in the recrystallized layer, was seen to have significant control over the coated specimen's fatigue life. Another study [3] studied the fatigue behaviour of a particular Ni-superalloy having elevated amounts of boron and carbon, B1914, which has a satisfactory quantity of carbides and borides in the castings' structure warranting enhanced creep properties. This study was done to understand fatigue properties of the alloy at elevated temperatures. For the study, precast bars of B1914 superalloy were used. The bars used were heat treated using the HIP process, followed by solution annealing and precipitation annealing. The processed B1914 Ni-superalloy was seen to have a final structure made of coarse dendritic grains. The material structure was seen to contain γ' precipitates, a γ matrix, γ/γ' eutectic pools, and many borides and carbides formed along the GBs and in the interdendritic areas. Casting defects varying in sizes between 150 and 800 μm were also observed in the structure of both HIP-processed and cast samples. Fatigue tests were done until failure occurred. The S-N curves obtained from the tests for various specimens tested under various temperatures were plotted and compared. As the temperature during testing increased, the amount of maximum strain the specimen could handle while the number of cycles until failure decreased. Then, the factographic analyses of fractured specimens were done using SEM. This revealed that stage I mechanism of propagation of fatigue cracks which was characterized by the presence of facets in the fish eye was detected on the fractured surface only at 800 and 900°C. The size of the facet was seen to decrease when the temperature during testing increased. Fracture surfaces of the samples that underwent testing at 950°C were not seen to have any facets. When the testing temperature was 950°C, the crack propagation was seen to take place via stage II mechanism only. The study also showed the effect of temperature on the fatigue life. Another study [67] examined initiation of cracks and its propagation during LCF testing of a polycrystalline Ni-superalloy. LCF testings' were performed on specimens that were exposed to various heat treatment processes like HIP, standard heat treatment (SHT), and combined heat treatment (HIP + SHT). Specimens for the experiment were made from an Inconel alloy. The LCF test results showed that SHT specimens endured a great amount of stress but underwent failure at a low number of cycles, HIP treated specimens endured small amounts of stress but withstood high number of cycles before failure, and specimens that underwent SHT + HIP treatment endured lower and higher stresses when compared to SHT and HIP, respectively, but withstood higher and lower number of cycles compared to SHT and HIP, respectively. By studying the microstructure and morphology of the specimens, it was found that subjecting a specimen to SHT enhanced alloy strength by a transformation of Laves into δ particles. At the same time, HIP processing was seen to improve the specimen's fatigue life by eradicating the microporosities present in the casting. In the case of SHT specimens, studying the fracture surface revealed that microporosities acted as sites for the initiation of cracks and provided propagation paths. Secondary cracks initiating from the surface of microporosities were also observed. In HIP-processed samples, the crack initiation zone was seen to display intergranular fracture morphology. As a result of brittle precipitates and microporosities eradicated from the casting's structure during HIP processing, GBs were seen to function as initiation sites for cracks, and cracks' propagation along GBs with low strength were found seen to cause the failure of HIP-processed castings. The macro fractography of the HIP + SHT revealed that the carbide and carbon nitride inclusions acted as crack initiation sites. According to the microstructure observation, other than γ' and γ'' strengtheners, carbides and small scale δ particles were identified to be the major precipitates in castings subjected to HIP + SHT. However, virtually zero evidence supporting the fact that small-scale δ acting as sites for initiation of cracks or channels for propagation of cracks was found. The combination of HIP and SHT was seen to help in achieving a balance between fatigue life and strength in samples. Another study [1] investigated the benefit of using high gradient solidification on the LCF life of AM1 Ni-based superalloy. LCF tests were done on AM1 alloy samples cast using conventional Bridgman process that uses radiation cooling and LMC process that provides improved thermal gradients in order to manufacture castings with coarse and fine dendrite structures, respectively. Test results proved that using the LMC method to attain high thermal gradient, which in turn led to low PDAS and SDAS values and finer micro structure, had 4 times the fatigue life as the Bridgman cast specimens. In samples made of both methods, cracks were seen to have initiated at surface casting pores. The smaller size of these pores in samples made using LMC combined with the finer microstructure produced was seen to help prolong the fatigue life of these specimens. Creep tests of the specimens were also conducted to see if the creep life or properties were affected by using a high thermal gradient solidification technique. But the difference in

observed test results was seen as negligible and not worthy of being noted. Another study [13] examined the effect of applying thermal barrier coatings on the LCF behaviour of Ni-superalloys made using the investment casting process. Superalloys are usually used to make components that work in very harsh conditions. One of the major problems that every part made of nickel superalloys has in common is that they work in very high temperatures. Long-term exposure to very high temperatures can eventually cause damage to any material. Giving these alloys thermal barrier coatings (TBC's) can increase the alloys life much more. Aside from increasing the life of the component, the application of thermal barrier coating can also modify some mechanical properties. One such property the authors studied is the LCF performance of coated specimens VS uncoated specimens, all of which were made of investment casting procedure. The TBC included a CoNiCrAlY bond coat (BC) deposited with the help of air plasma spraying (APS) and a thermal coating (TC) made of a powder mixture of YSZ and EUCOR with the ratio 50/50 wt%, which was plasma sprayed subsequently. The LFC tests revealed that a process called rafting took place testing of both coated and uncoated specimens. It was also revealed that crack initiation in uncoated specimens primarily took place near defects. In coated specimens, the crack initiation was always either at the TC/BC interface or the BC/substrate interface. Findings of the study dictated that the density of the fatigue cracks that made it to the substrate after penetrating through the TBC was seen to be almost 10 times bigger compared with observations about uncoated superalloys. This result helped conclude that there was a more even distribution of the plastic strain along the entire gauge length of coated specimens than in uncoated specimens. This conclusion also revealed that, for the identical levels of stress amplitudes, the plastic strain amplitude levels seen in coated specimens are much higher than the values recorded for uncoated specimens. The curves representing fatigue lives of the specimens in Coffin–Manson representation showed that both uncoated and coated superalloys had the same fatigue lives when undergoing testings at the highest amplitudes. But as the number of cycles increased, the coated specimens were able to withstand higher stress amplitudes, thus leading to a better fatigue property. The fatigue life curves of specimens in total strain representations were almost identical for both coated and uncoated specimens. Very few deviations were seen on reaching a very high number of cycle values. These deviations were found to be due to scattering in Young's modulus of uncoated and TBC-coated superalloys. But the final results concluded that there was no significant increase in fatigue life because of applying a coating. But the TBC used does show to be a promising tool for protection of alloy from harsh environments with very high temperatures.

After elaborate study of the papers related to fatigue behaviour, using the data obtained in these studies, the graphs showing fatigue behaviour of some commonly used Ni-superalloys (Figure 44) and effect of temperature conditions on fatigue life, in terms of number of cycles to failure and stress induced (Figure 45) has been plotted.

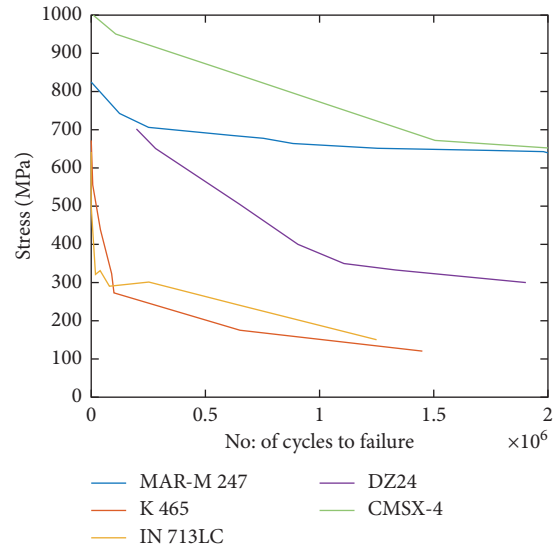

Figure 44: The fatigue lives of various Ni-superalloys.

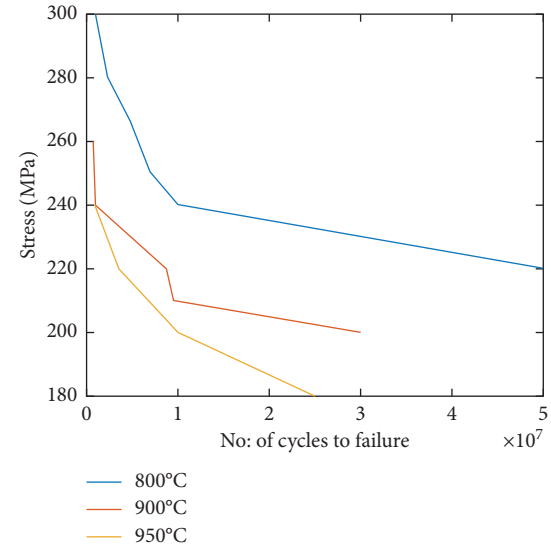

Figure 45: Results produced by Ni-superalloy B1914 at various temperatures.

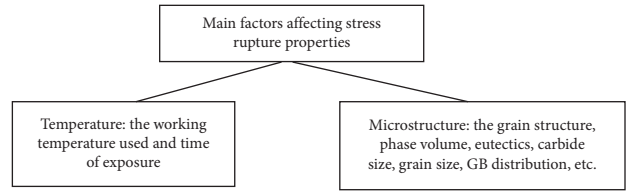

Figure 46: Most influential factors affecting stress rupture properties.

5.2. Stress Rupture Properties of Ni-Based Superalloys. Just like fatigue life the stress rupture properties of a material is also fundamental. Stress rupture is the sudden and complete failure of a material under stress. The stress rupture properties were seen to be governed by two main factors (as shown in Figure 46). Since Ni-based superalloys are used to

make parts that work in very harsh environments, they would likely be under enormous amounts of stress. Therefore, it is paramount to investigate the stress rupture properties of these materials in order to understand better how they perform under various situations, how their applications can be better optimized and how some of their characteristics can be improved. And for these reasons many studies have been done in this regard. One such study [52] focuses on the stress rupture embrittlement of a Ni-superalloy, called Alloy 625. Specimens extracted from sections of huge blocks of cast Ni-superalloy Alloy 625 having a columnar grain structure were subjected to microstructural investigations and stress rupture tests. It was found through metallographic investigation that the castings had two separated: equiaxed and columnar zones. The specimens were taken out from the castings' columnar zone in a way that the grain's width was seen to align in a parallel manner with the direction of loading. This section was selected since it is similar to the microstructure of the inner part of casings like turbine blades where a microstructure having columnar grains is more desirable. Thirteen stress-rupture examinations were performed at temperatures of 650°C, 700°C, and 750°C. The microstructures that were both as-cast and solutionized were seen to have an equiaxed zone with many defects in it and a zone with a columnar grain structure that was completely free of any defects. When inspected with the aid of stress rupture tests, a columnar zone that is free from defects was also observed. The influence imposed by temperature and aging time was combined in this study in order to obtain the Larson Miller parameter for Alloy 625. Through further computation using this parameter, the potential application of Alloy 625 in any structural design, having a design stress of 100 MPa for 100,000 h at 720°C, was found. As a result of the larger size of grains observed in specimens with a columnar structures, it was found that for any given value of service time and temperature, the rupture stress of the sample was significantly greater than any of its other counterparts. However, it was found that there was a negative relation between rupture ductility and exposure to high temperature for an exposure time of 1000 h. Any amount of ageing beyond this time limit was seen to cause rupture embrittlement. This embrittlement was seen as a result of precipitation in GBs. The fracture due to embrittlement was seen to be intergranular with the surface of these fractures being faceted and the side surfaces showing cracks propagating along the GBs. The same trend was observed in all samples, thus suggesting that the reducing of ductility observed was not caused by secondary carbides precipitating at the GBs. Even though a significant increase in secondary carbides precipitating in GBs was seen to happen as a result of a higher duration of ageing, they were still seen to have negligible effects on the rupture ductility. In contrast, the γ" phase's formation was seen to result in the decrease of ductility and then its conversion to the δ phase was seen to induce embrittlement. To avoid the latter, a compromising either the service temperature or duration was seen to be necessary. If compromising the former, it was seen that lowering service temperature to below 600°C was the only option, or in case of the latter, compromising the service time a component can function efficiently for at temperatures above 600°C was seen to be the only option. The δ phase content was seen to increase with increasing rupture duration. The preferred location of δ-phase to precipitate was seen to be near microsegregated Nb found in the microstructure. The study also revealed the influence of applied stress and temperature on the rupture life of Ni-superalloys. Increasing the temperature or the stress applied was seen to reduce the rupture life significantly. This was confirmed by the data collected in the study via the various rupture tests. The data regarding this are graphically depicted in Figure 47 Another study [33] discusses about DZ24, a SX Ni-superalloy obtained by modification of polycrystalline K24 superalloy, and the rupture properties of this alloy. K24 is a conventionally cast Ni-superalloy widely regarded for its properties including its tolerance of average temperatures between 900 and 1000°C. Its equiaxed GBs become sites for accumulation of damage which includes sudden occurrences of crack growths in early stages of use. As a solution, the DS process is used for producing blades having columnar grains with a directional structure. And thus the stress-rupture life of DS castings with columnar microstructure was seen to be much higher than that of polycrystalline castings. The rupture time of DZ24 alloy was seen to be twice that of K24 alloy. The volume of γ' precipitates in K24 alloy was seen to be small, but the spacing between these precipitates were seen to be really wide, and at the time of stress rupture tests, no γ' rafting was seen to take place. In DZ24 alloy, precipitated γ' phase was seen to be very closely packed, as a result of their very huge volume, and γ' rafts were seen to form when undergoing stress rupture conditions. This was seen to indicate better ductility of DZ24. Alloys DZ24 having a large volume fraction of fine and regular cube shaped precipitates of the γ' phase was seen to offer better resistance to rupture. Another study [23] examined the response to stress relaxation and microstructural changes in SX Ni-superalloys and the influence of time and temperature on stress relaxation for SX Ni-superalloys CMSX-4, NASAIR 100, and EPM-102. CMSX-4 (2^{nd} gen) is a superalloy having 3.0% Re content and exhibits a decent creep resistance. It has a density of 8.69 g/cm^3. Meanwhile, EPM-102 (4^{th} gen) is a superalloy, with a density of 9.16 g/cm^3, a slightly greater Re content of 6%, and better resistance to creep. Both of them were made as rectangular-shaped slabs with the usual SX casting methods, then homogenized, solution heat treated, and finally gas fan quenched. NASAIR 100 was seen to be a 1^{st} gen SX superalloy. Data regarding stress-strain rate obtained after relaxation testing was performed was seen to match with results obtained from constant load tests. Stress relaxation and microstructure responses were observed to change as the conditions under which the alloy was tested changed. EPM-102 was seen to exhibit higher resistance towards stress relaxation compared to CMSX-4 at temperatures of 982°C and above. Both alloys after stress relaxation testing were seen to show directional coarsening at high temperatures. Resistance to stress relaxation was almost the same at 871°C for both CMSX-4 and EPM-102. But at elevated temperatures, EPM-102 showed enhanced creep properties and smaller values for stress relaxation rates

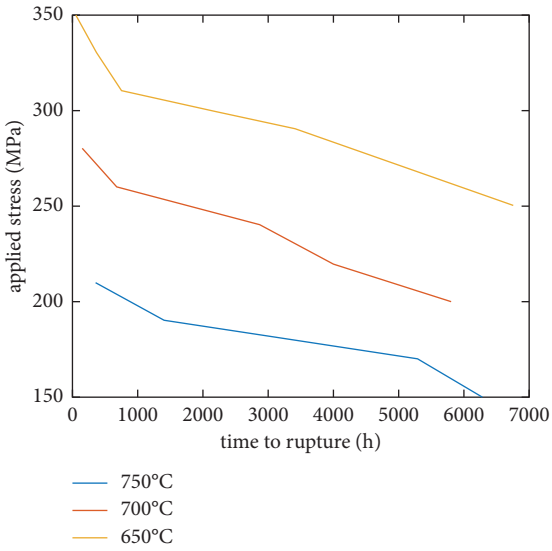

Figure 47: Relation between the stress applied and the time to rupture for tests performed at varying temperatures.

compared to later generation Ni-superalloys. This was also seen to explain why later generation superalloys had better creep resistance compared to older generation superalloys. All three superalloys exhibited coarsening while undergoing stress relaxation and testing temperatures beyond the final ageing temperature. In addition, after unloading at the time of testing, time-dependent strain recovery called "visco-elasticity" was detected. Stress relaxation was seen to progress over passing the time and at what rate depended on temperature. It was seen that with an increase in temperature there was a decline and increase in creep properties and stress relaxation rate, respectively. And also, the potential improvement of resistance towards stress relaxation by prior exposure towards creep was confirmed by NASAIR100. Another similar [24] study was focused on the stress and strain development in CMSX4, a SX Ni-superalloy, while carrying out stress relaxation tests. Avoiding the formation of sliver defects and stray grains at the time of recrystallization and solidification while undergoing successive heat treatment can be regarded as the most important microstructural control for SX Ni-superalloys. This is because the presence of additional GBs has a negative influence on fatigue and creep properties. The formation of GBs is connected with local casting conditions while the creep and fatigue properties are associated with the localised development of strain and stress happening while cooling and solidification take place. The stresses are developed during solidification and cooling of melt due to the different thermal expansion coefficients exhibited by the molten alloy and the ceramic shells and cores. The magnitudes of these stresses can potentially be enough to make SX castings to yield plastically. The magnitude of plastic strain also can instigate recrystallization at the time of heat treatment performed after solidification. Recrystallisation happening in CMSX4 Ni-superalloy was seen to be heavily influenced by the amount of plastic strain introduced and the temperature at which this strain is presented. For recrystallization, the critical value of plastic strain was identified to be 6% in the least. At high temperatures, several stress relaxation and creep tests were performed. These tests revealed that the creep flow at different temperatures was dependant on time. In order to accurately define the evolution of strain and stress happening while cooling occurs over an extensive temperature range, many Norton's or steady-state creep equations were developed with the help of experimental data and was used as a constitutive law of plastic flow. In addition, the equations acquired for steady-state creep were not completely correlated to cooling from solidification as the local solidification/cooling time was seen to be very small than that measured in creep. Furthermore, the stresses applied during creep testing were seen to be less than the yield stress. This was seen to be in contrast to the stresses developed during cooling after solidification, which was always seen to more than the yield stress. Experimental results identified that the growth of macroscopic strain happening while stress relaxation tests were conducted, and the cooling of SX Ni-based superalloys heavily depends on time, thus making them viscoplastic. The viscoplasticity law that was constructed with testing of specimens under displacement control as the basis confirmed that viscoplasticity was more stress dependant than it was time dependant. Whenever the yield stress was surpassed by the accumulated stress when cooled at a specific temperature, time-dependent elongation became very dominant because if the sample was constrained, it must be compensated for the thermal strain. The calculations obtained using the constitutive equation for many stresses and temperatures within a particular range in time were found to match with the results of the isothermal experiments carried out. But they were also seen to show considerable deviation from the measurements obtained via in situ cooling experiments conducted under strain-controlled mode to simulate the casting conditions under which cooling and solidification of melt in a ceramic mould take place. Delving further into the study, the results of experimenting under strain-controlled mode showed that stress relaxation is twice as observed when experiments were conducted under displacement control mode. Stress relaxation under strain-controlled mode was observed to be a better choice for assessing the viscoplastic response under the conditions used in the study. This concluded that the viscoplastic strain development in the initial stages of cooling when testing of samples was done under strain-controlled mode, which was similar to casting conditions, was mostly controlled by lattice relaxation. Another study [54] focused on the influence a casting's rate of cooling can have on the mechanical and microstructural properties with specific emphasis on stress rupture of the Ni-based superalloy K417G. For this study, 3 different cooling rates of $1.42^{\circ}Cs^{-1}$, $1.06^{\circ}Cs^{-1}$, and $0.84^{\circ}Cs^{-1}$ were obtained using differently designed runners. Tensile tests were done at 900°C while stress rupture tests were done at 950°C using a 235 MPa stress value. The experimental results showed that all the properties under observation varied with cooling rates. When the cooling rate was lessened, γ/γ' eutectic's volume fraction got reduced but there was an increase in the spacing of secondary dendrite arm, γ/γ' eutectic's size, and

the γ' phase's size and volume fraction. With the largest cooling rate of $1.42^{\circ}Cs^{-1}$, the microstructure was seen to become more homogeneous. Since the distribution and volume fraction of carbides and micropores in a casting do not vary much, the mechanical characteristics were seen to be mostly ascertained by the size and volume fraction of the γ' phase and the γ/γ' eutectic. Due to this, the samples made using least cooling rate of $0.84^{\circ}Cs^{-1}$ exhibited superlative properties of stress rupture life and ductility. These samples were seen to have γ/γ' eutectic pools that had the least volume fractions and the largest size of the γ' phase. Taking all of these results and observations into account, the most preferable and optimized cooling rate was found to be the value of $0.84^{\circ}C{\cdot}s^{-1}$.

5.3. Creep Properties of Ni-Based Superalloys. Creep property is another important mechanical property that decides how a superalloy component behaves at elevated temperatures. And significant research done on this area has given us a better understanding about how suitable different superalloys can be at high temperature application, and has helped us improve them, to allow the working of such alloys at harsher conditions or to make alloys with improved endurance to harsh working conditions. We have already seen how creep properties can be affected by certain casting conditions and processes (Figure 48 shows the main factors influencing creep properties). But studying that alone will not be enough. Investigating the creep properties and behaviour of different alloys and how it correlates to factors like casting microstructure are also very important. One such study [51] investigates the relationship between creep characteristics and the γ' precipitates' coarsening in a 4^{th} generation SX Ni-superalloy that takes place at the time of long-term aging that is carried out at 1000°C for 100–1000 h. The study also revealed the relationship between precipitated carbide size and creep life. Data regarding these are represented in Figure 49. It was seen that the mean dimensions of γ' precipitate became larger as the aging time was prolonged, with the γ' precipitates retaining its rectangular prism shape while coarsening all throughout the aging process. The creep life of aged samples was seen to increase initially and then get reduced with the time of exposure increasing. The enhancement in the creep life of castings that were subjected to aging was seen to be a result of a slight growth observed in the γ' phase with its size closely resembling the γ' phases' size corresponding to optimized creep performance, refractory element diffusion, and the amassing of dislocations within γ channels. While the deep coarsening of the γ' phase that occurs due to excessive aging was seen to cause decreased resistance of dislocation movements, thus worsening the creep properties. The excellent creep strength of SX Ni-superalloys at elevated temperatures was seen to be the result of coherent precipitation of γ' strengthening phases into the γ matrix, whose volume fraction was higher than usual. The mean size, morphology, volume fraction, the distribution of the γ' precipitate, and the lattice misfit exhibited by the interface formed by the γ and γ' phases and the elastic modulus were all seen to be very important factors that played a substantial role in ascertaining the mechanical properties and behaviour of Ni-superalloys. The γ' precipitate was observed to undergo coarsening with increasing exposure time and temperature during thermal exposure; this was seen to happen in one of two ways: (1) coarsening of γ' phase precipitates with a cube shape as a result of Ostwald ripening and (2) because of the γ' rafts forming directional clusters in other cases. The γ' phase precipitates' coarsening was observed to be caused by a decrease in the γ/γ' interface's area, γ/γ' interface's lattice mismatch strain, and the modulus misfit. As a direct consequence of this intense γ' coarsening, the coherency of the precipitates were seen to reduce considerably, and high temperature strength was seen to be significantly degraded. The experimental study confirmed that γ' phase precipitate coarsening was the principal reason for the degradation of creep properties in CMSX-10 Ni-superalloy while being exposed to very high temperatures for very long durations. After creep deformation, 2 different types of pores, namely, creep and casting pores, were present on the fractured surface. In comparison to the creep pores, the microcracks that have originated from casting pores were seen to be more harmful to the alloy's creep life. Another study [78] collates the creep and microstructural properties of 2 different types of SX Ni-superalloys. One of these types was seen to be was manufactured in a Bridgman furnace with the help of the traditional DS process. The other type was seen to be produced with the help of selective electron beam melting (SEBM). The microstructures of both the specimens started as directional polycrystalline and then evolved into single crystalline with progressing solidification. And in both specimens, a polycrystalline rim of thickness 1 mm was seen. Creep tests were done on as-cast SEBM bar, heat-treated SEBM bar, and heat-treated Bridgman processed bar. The paper also showed the impact of applied stresses and temperatures on the creep properties (graphically represented in Figure 50). In low-stress regimes with elevated temperatures, all 3 specimens were seen to exhibit similar creep behaviour. In contrast to this, in low-temperature high stress arrangement, a highly noticeable difference in the creep behaviour of the 3 specimens was observed. The as-built SEBM material exhibited the lowest rupture times, tiniest rupture strains, and the largest minimum creep rate values. The SEBM material that was heat treated was observed to perform somewhat better than the material made using the Bridgman process. No discrepancies regarding the minimum creep rates were observed. Moreover, the SEMB material was seen to have a somewhat extended creep life due to the higher rupture strains observed in this material. Also, while both heat-treated samples witnessed γ' precipitate coarsening during creep testing, the coarsening was extra noticeable in the completely heat-treated Bridgman sample than in the heat-treated SEBM sample. This was also seen to help better the creep life of the SEBM sample. The study provided a particular emphasis on how the manufacturing process affects the creep life. And here, samples made from the SEBM process were seen to perform better on heat treatment when compared to heat-treated Bridgman samples. However, as-built SEBM samples

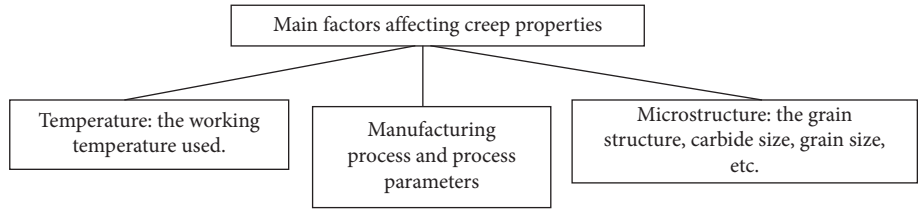

Figure 48: Most influential factors affecting creep properties.

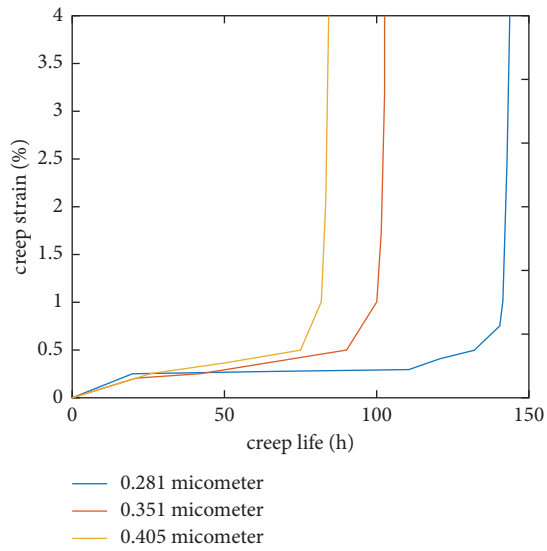

Figure 49: γ' size: (i) blue line is gained by 100 h of aging, (ii) red line is gained by 500 h of aging, and (iii) yellow line is gained by 1000 h of aging.

were seen to show poor creep life. Another study [31] examined the impact of surface conditions on creep properties of Ni-superalloy castings. Complex systems of cooling channels are usually incorporated into the design of turbine blades to help them withstand very high temperatures. These hollow blades are made using the lost-wax investment casting method. Other than higher cooling efficiencies, thin-walled hollow blades and interior sections can also help with reducing the casting's weight. Turbine blades with reduced weight and can rotate relatively more fastly are highly preferred now. This also opens up the possibility to the turbine disks, bearings, and shafts getting a lighter design. Therefore, it is essential to know the effect thin-section size can have on a material's properties at elevated temperatures, particularly its creep properties. IN100 Ni-based superalloy that was cast using conventional methods was used in this study. The study revealed that very thin castings with a thickness of 0.9 mm had the least creep rates that fell slightly behind the creep rates for 1.3 mm thick samples. Rupture strains were seen to be higher for thin castings, with 1.3 mm thick castings exhibiting maximum values. Porosity content in all alloys used in this study was seen to be between 0.1% and 0.3%, and thin cast samples were seen to have higher roughness compared to machines specimens. A thin layer of oxide having a 1 μm thickness was seen on the surface of the typical microstructure of the castings. Observations showed that creep cracks usually initiated at the casting's surface. And crack propagation was seen along the GBs. Oxide formation was also found along crack surface and at the crack tip. Above discoveries infer that the main mode of creep failure in uncoated polycrystalline Ni-superalloys IN100 in the air is stress assisted intergranular oxidation. The effect of the size of grains was seen to become highly important at lesser stress levels. Specimen that has undergone grain or microstructural refinement was seen to possess superior creep properties. Both preparation processes, casting and machining methods used, were seen to have an impact on section size and thus an influence on the creep properties. However, this trait was seen to be more pronounced in machined specimens. Creep testing in this study was seen to be done out in the air. And thus, oxidation was seen to affect the creep and creep-rupture behaviour of the specimens. The 0.9 mm thick specimen having a surface-to-volume ratio that is higher in comparison to that of the 1.3 mm thick specimen meant a relatively bigger amount of surface area in contact with the atmosphere in the less thick specimen, thus higher oxidation of this specimen. This observation explained the lower creep resistance exhibited by thin specimens as a result of oxidation effect. Another study [18] focused on how the withdrawal rate can influence the creep properties. The study utilized as-cast SX rods produced using commercial CMSX-4 Ni-superalloy. The SX rods used were prepared using multilayer ceramic shell preparation and lost-wax casting methods. The DS process performed was based on the Bridgman method and took place in a vacuum furnace while employing different rates of withdrawal (1, 3, 5, and 7 mm/min). The lattice parameters for the phases were generally seen to decrease with an increase in the withdrawal rate. It was also observed that the γ' phase present in castings was most ordered when withdrawal rates of 1–5 mm/min used, and they were seen to become more disordered in casting withdrawn at 7 mm/min. Moreover, when the withdrawal rate was seen to exceed 3 mm/min during the Bridgman process, the ordering of phases decreased. The amount of porosity formation was seen to decrease with an increase in withdrawal rate from 1 to 5 mm/min and increase while moving on to 7 mm/min. And the size of porosities was seen to decrease with an increase in the withdrawal rate. A casting's creep life was seen to be highly influenced by the presence of porosities. With a decrease in the number and size of porosities, the creep life seemed to improve. Highest creep life was observed for casting made with 3 mm/min withdrawal rate. And the crystal orientation was also seen to be unaffected by the withdrawal rate used. The creep behaviour of samples

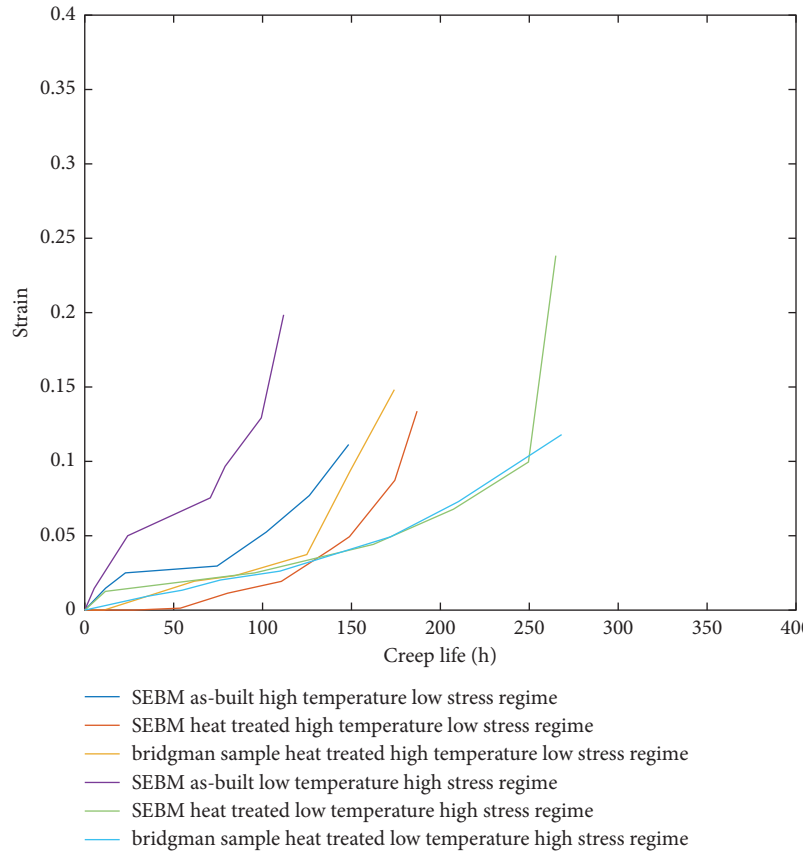

Figure 50: The creep performance of as-built SEBM specimens and heat-treated Bridgman and SEBM specimens that have been subjected to different testing conditions.

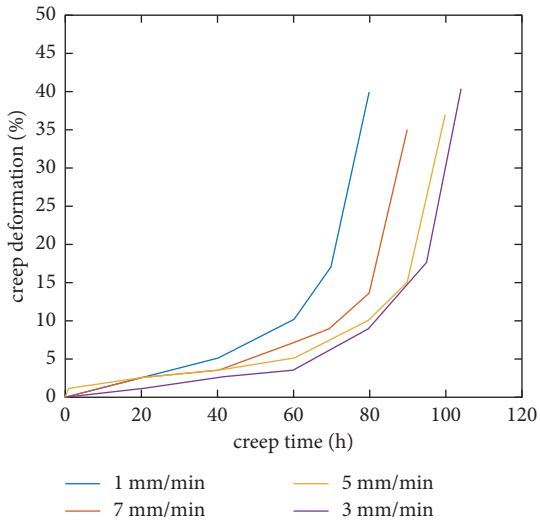

Figure 51: The relation between percentage creep deformation and creep time.

made using different withdrawal rates has been graphically represented in Figure 51. Another experimental study [75] researched the effect of the pouring temperature of the melt on the creep properties of castings made using IN713C Ni-superalloy. Eight investment casting specimens made of IN713C superalloy were manufactured, with each of them being produced using different pouring temperatures of the melt ranging from 1400 to 1520°C. It was also observed that castings made by pouring melt with hotter temperatures had comparatively higher vacancies. Yield stress was seen to decrease as the casting temperature increased, while the opposite trend was seen for elongation. For the castings, as the melt pouring temperature increased, the grain size increased, and the creep life and mean time to rupture were seen to improve with increasing pouring temperature. A decrease in the steady-state creep rate was also seen with an increment in the pouring temperature of the melt. Data pertaining to the improvement in creep life with increase in pouring temperature collected from the study are graphically represented in Figure 52. Changing alloying element compositions can also bring about changes in the creep life of the alloys. One such study [77] focuses on a particular alloying element called ruthenium (Ru) and how varying its content in the alloy can affect its creep properties. Two superalloys having different Ru contents were considered for studying Ru's effect on microstructure and creep rupture life. Using wt% as scale, both of them were named alloy 3.5 Ru and alloy 2.5 Ru correspondingly, by the amount of Ru they possessed. After post-heat treatment, the resulting magnitude and volume fraction of the corresponding γ' phase were found to be reduced with a rise in the content of Ru, but this was not seen to affect both of the alloys' solidus and liquidus temperatures. It was observed that 2.5 Ru's

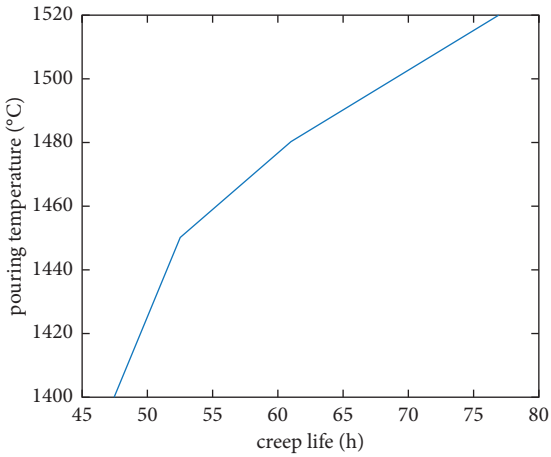

Figure 52: The relation between the pouring temperature and creep life.

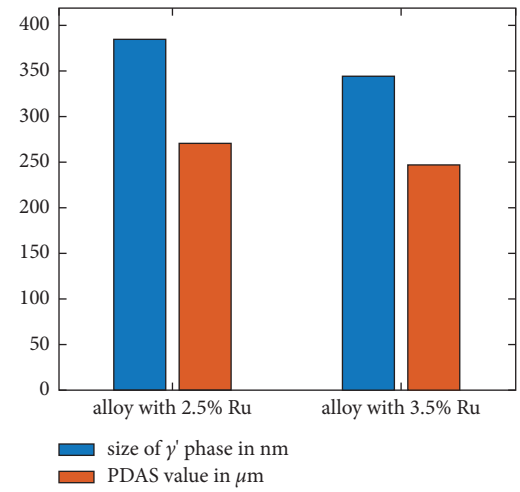

Figure 53: Change in PDAS and γ' phase size values for alloy 2.5Ru and alloy 3.5Ru.

creep curve consists of three phases and it had one less incubation phase than 3.5 Ru and this was seen to cause a rise in the rate of creep strain in the latter, followed by reduction and steadying and then finally rising again. Due to the reduction of the smallest value of creep rate and extension of the secondary creep stage, the creep rupture life was enhanced with Ru's surge at 1140°C/137 MPa. The increasing of Ru composition was seen to have slackened the movements of the dislocations by improving the γ matrix's strength as well as roughening the γ' phase by lessening the preliminary γ' phase's size (data regarding γ' phase's size and PDAS values have been compared for both alloys in Figure 53), and this was seen to have amplified the primary and secondary creep stage times. The 2.5Ru alloy's case was not the same. So, it was concluded that the rise in Ru extended creep life (data regarding the influence of Ru in creep behaviour are graphically represented in Figure 54) of the alloy, but it was seen to be ineffective in avoiding the rare TCP phase development. Another study [19] focused on the effect the alloying element Ti had on creep behaviour of Ni-based superalloys. 2 derivatives of the base alloy, with 1 (Alloy 1) and 3 (Alloy 3) wt% of Ti, were chosen and examined. The difference between the 2 alloys selected for the study was in the number of γ' forming elements, and this study focused on γ' forming element Ti particularly. The stacking fault energy (SFE), lattice misfit between γ' and γ, anti-phase boundary energy (APBE), and creep properties were all seen to be greatly affected by the γ' phase's volume fraction. These are all affected by the Ti content which also affects the γ/γ' misfit. Ti was seen to replace Al atoms in γ', Ni_3Al. There was also a rise in APBE, SFE, and lattice parameter of γ' when the Ti content increases. These trends were seen to have some extent of influence on the shearing mechanisms that are observed in these alloys when temperatures are very high. The number of γ' forming elements and temperature were found to strongly influence the microstructure, density of dislocation, APB formation, and the existence of SF as well. It was observed and concluded that Ti addition can improve creep resistance at relatively higher temperatures (about 900°C) due to the detachment of dislocations into small

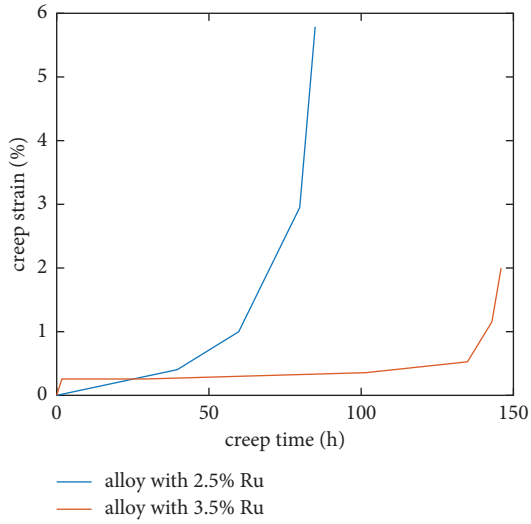

Figure 54: The creep behaviour of both alloy 2.5Ru and alloy 3.5Ru.

fractional parts which have stacking faults. γ' cutting mechanism was seen to have improved from being dislocations attached with SF to APB coupled pairs with rising temperature. But, alloy 3's transition temperature was observed to be more than alloy 1 due to variance in content of Ti. Due to higher Ti content, there was decrease in dislocation movement by the detachment of dislocations with SF in in alloy 3's γ' phase. So, it was concluded that Ti content's increase can greatly help in bettering the creep properties (data regarding this are graphically represented in Figure 55). After creep (happened at 982°C), the two alloys that were examined showed very similar creep rupture lives and dislocation structures.

Application of thermal barrier coats to Ni-based superalloys is a common way to better its mechanical performance by building up its resistance to high temperatures. Studies have been done in this regard to investigate how the application of such coats can affect different mechanical

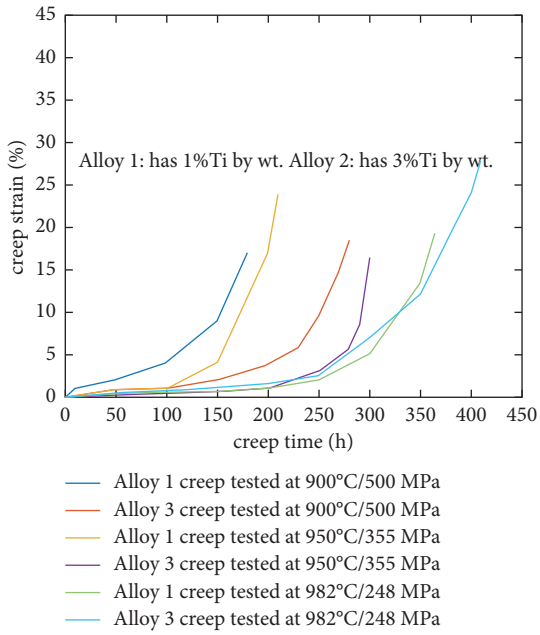

FIGURE 55: Creep behaviour of alloy 1 and alloy 3 at different testing conditions.

properties of the alloy. One such study [53] performed fatigue and creep tests in order to examine, determine, and compare the mechanical properties of the Ni-superalloy MAR247 in its as-cast and coated state where a coating of aluminide layer was given. A 20 μm thick aluminide layer was seen to be given as a coating by means of CVD process. There was not any significant difference in mechanical properties between coated and uncoated specimens at room temperature, where the stress response was almost the same. But during fatigue testing of specimens at an elevated temperature of 900°C, the MAR247 superalloy specimen that was coated was observed to possess the ability to adequately withstand stress amplitude responses in the range of 350–520 MPa, which was double the value seen for uncoated alloys, thus, concluding that the aluminide layer improves the creep performance of the nickel superalloy significantly. Despite the lower hardness and strength of the aluminide layer in comparison to the substrate, the aluminide layer was not found to be the crack initiation site. The good coherence of the coat with the substrate was seen to the raw material against such processes as oxidation, hot corrosion, or wear, and thus, prolong its life. Creep tests revealed that the crack initiation and propagation took place due to grain boundary separation in the polycrystalline MAR247 substrate. In another study [25], TBC specimens with SX substrates coated using thin ODS Co-based flash coats on previously coated coating of Co-based bond coat (Amdry 995) along with a porous atmospherically plasma sprayed yttria stabilized zirconia (YSZ) topcoat were produced, and their thermal cyclic behaviour was studied. When compared to bond coats of just one layer, using thin flash coats that was strengthened by oxide dispersions was seen to increase the lifetime by 2 times. The 2-layered bond coated ODS specimens were seen to exhibit high thermal cycling resistance crossing past the 4000 cycles mark at 1080°C and 1400°C being the bond and top coat temperatures, respectively. The factor limiting a specimen's lifetime was seen to be the oxidation of the bond coat. An increase in thermal cycling performance caused by the ODS flash coat was observed to occur as a result of the growth of the yttrium aluminate in the thermally grown oxide (TGO) being suppressed (called the overdopping effect) and its positive effect on the alumina scale GB oxygen diffusion, which was seen to enhance the resistance towards oxidation of the ODS sample. It was also seen to be so as a result of the better adhesion of the top coat, collective cracking of the TGO allowing stress relaxation, and circumventing failure of the top coat due to higher ODS bond coat roughness. The results from this study proved that the application of advanced bond coatings like ODS flash coats can significantly improve the thermal cyclic performance of the coated alloy. The above two studies showed the impact of different coatings given to the surface of Ni-superalloys on the creep life and properties. Conducting similar studies that study the effect of various thermal barrier coatings can be very important as it can help in identifying a very efficient coating that can be given to these alloys in order to protect it against damage caused by temperature and thus improve creep life and properties. This is because working temperature is one of the most influential factors controlling creep life.

6. Defects in Ni-Based Superalloys

Ni-based superalloys are special alloys designed for making components that can handle extreme conditions. Thus, the presence of any kind of defect can lead to failure of the part manufactured. Defects present in a superalloy casting can have a huge effect on the different characteristics of the castings like, its mechanical behaviour, tensile properties, fatigue life, and ultimately how, when, and why failure of the component occurs. So it is very important to study and investigate the different defects that can be caused in Ni-based superalloys, their cause, and methods we can use to prevent them. We have in this article narratively reviewed recent research work done regarding some of the most important defects found in Ni-based superalloys castings.

6.1. Freckle Defect in Ni-Based Superalloys. One of the major defects in Ni-based superalloys is freckles. Picture of freckles formed in turbine blades has been shown in Figure 56. Freckles appear typically as a long chain of dendrite fragments or equiaxed grains which are formed roughly parallel along gravity's direction. Ever since superalloys were developed, freckling has been a major challenge as it can reduce the life span of any superalloy component significantly and in severe cases render the component completely useless. Thus, many studies have been done to investigate how freckling occurs and how it can be handled. Studies regarding freckling [85–92] showed that freckles were formed as a result of interdendritic microsegregation caused by thermosolutal convection, which in turn is mainly caused by density inversion taking place in the mushy zone.

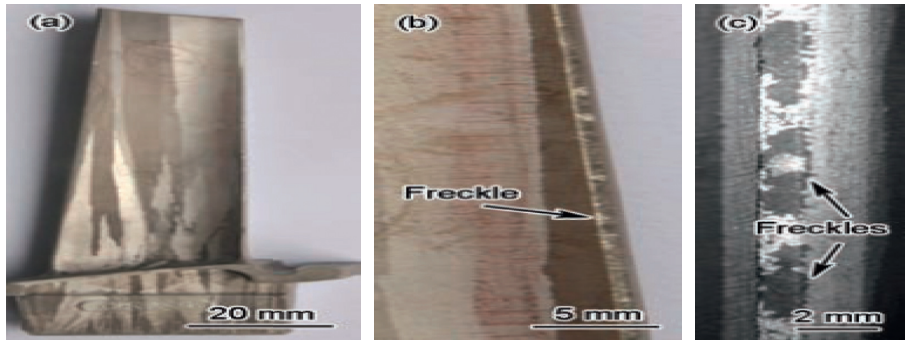

Figure 56: Freckle defects found in turbine blades.

Preferential formation of freckles was seen when the thermal gradient and solidification rate during casting were low. It was also observed that the formation of freckles is highly dependent on the influences of the edges and the curvature of surfaces. One study [93] particularly focused on how the convection pattern can affect the freckling in components with abruptly varying cross-sections. In this study, the evolution of flow and thermal fields was examined numerically with the help of simulation. The thermal distribution's evolution throughout different points in time was studied and noted down. As the solid/liquid interface moved from the region with smaller to larger cross-sectional area, the axial temperature gradients was seen to decrease, while the isothermal lines' curvatures increased drastically, proposing that higher lateral temperature gradients are created at these points. The study of solidification interface and flow fields revealed that, when the solidification interface goes through an expanding cross-section, the interface shape shifts from flat to convex. This behaviour was best described by the high lateral temperature gradients, which were seen to have been induced by asymmetrical cooling conditions observed on either sides of the specimen. The interface deflection also became higher as solidification progressed, along with which a powerful convection zone in close proximity to the solidification interface was brought about as a result of higher interface deflections. There were two vortices moving in an anticlockwise direction in this convection zone, which envelopes the lower part of the large cross-section. As solidification progressed and the height of the liquid metal decreased, the convection style, which was initially a complex 3D flow, was seen to change to an fairly accurate 2-D radial flow. These behaviours were seen to directly influence the distribution of freckles. This study showed that freckles only start to appear as we move between regions with instantaneously changing cross-sections. The study also revealed that freckling can occur as a result of the solidification front experiencing an axial flow. And it was also found that the number of freckles formed was directly proportional to the intensity of the axial flow. It was observed that, as the height of liquid metal decreases, the axial flow changes to radial flow and a lack of axial flow hinders the formation of freckles this is why we see almost all the freckles concentrated at the bottom of the region with the larger cross-sectional area. It was also observed that freckle formation can be increased by increasing the intensity of the axial driving force by increasing melt temperature. It was seen to be possible to improve the intensity of axial flow by using faster withdrawal rates. The PDAS and SDAS values were seen to decrease as the rate of withdrawal increased, and this was seen to cause a reduction in the number of freckles formed. Studies [5, 85–92] also showed that freckles only formed on internal or external surfaces, as thermosolutal fluid flow/convection and channel segregation were only seen to develop a stable flow at casting surfaces and not in the bulk of the material. Some studies [26, 85] also revealed that convex edges are preferred locations for freckling to occur. In components with curved contours, freckles were seen to form exclusively on the surfaces that had a positive curvature and curved outwardly. Freckles were uncommon in components with relatively small cross-sectional areas; this result was associated with the concept of size effect of the formation of freckles. Studies [26, 42, 85] also showed freckles were seen to preferentially form on the vertical and horizontal edges rather than on the plane surfaces of castings. Fluid permeability near the wall, when compared to what was seen within the castings, was seen to be much higher. This was seen to promote thermosolutal convection at the surface more than in the bulk of the alloy, thus inducing preferential freckling in the surface of castings. This was the reason why all freckles are always found on the casting surfaces and never in bulk of the alloy. When it comes to a component's edges, this effect of surfaces was seen to overlap with the influence of convection, thus creating a condition that was significantly more supporting of freckling in comparison to the conditions provided by flat surfaces. One study [26] investigated the impact of ceramic cores on freckling. The results revealed that the number of freckles formed and the ratio of area fractions of the areas where freckles were formed on the castings' exterior surfaces decreased as the interior diameter of these ceramic cores increased. But the opposite trend was seen for the internal casting surfaces where an increase in inner diameter of cores was seen to increase the amount of freckles formed in these internal surfaces. Data regarding these trends are depicted graphically in Figures 57–60. Also, internal freckling was seen to occur only on the outer convex surfaces (as shown in Figure 60) produced by ceramic cores and nowhere else. It was also observed that, when the thicknesses of the walls of ceramic cores increased, the ratio of area fractions of the regions in the casting's outer surfaces that had freckles

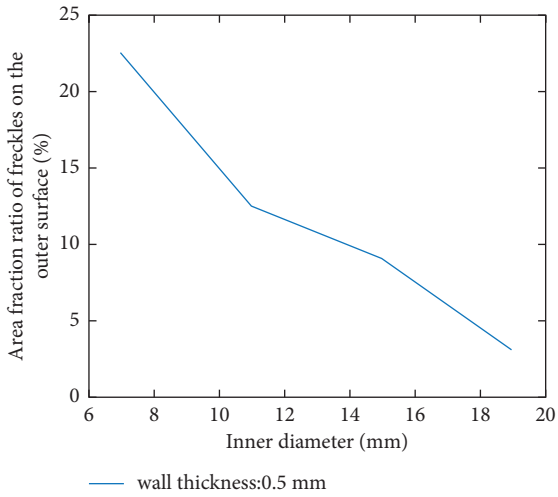

Figure 57: A relation between area fraction of freckles on the outer surface and the inner diameter.

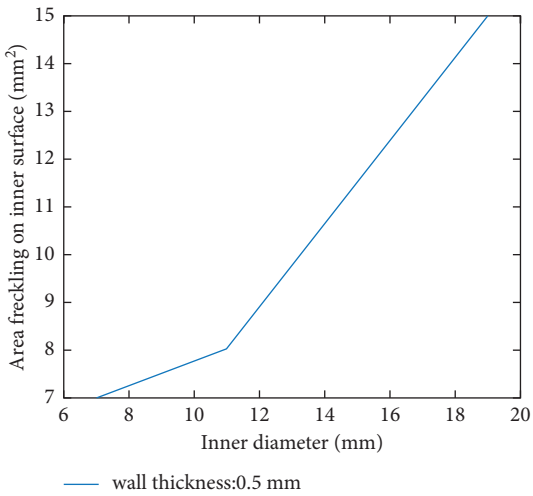

Figure 58: Relation between freckle area of freckles and inner diameter.

decreased. But, at the same time, the area fractions were seen to increase for the freckled regions present in the internal surfaces of castings. One study [91] that investigated how freckling was influenced by sloping surfaces (summarised in Figure 61), provided results proving that the convection channel would be stopped by a surface that has an outward slope, thus inhibiting freckling to some extent. This was backed up by the fact that spots indicating freckling were only seen on the bottom of outward sloping specimens, while having a surface that sloped inwardly was observed to intensify the thermosolutal convection and thus promote freckling. However, in cylindrical bars, freckling was observed to occur and grow consistently throughout the specimen's length in its entirety. The study also showed that the geometrical features of the casting made or the mould used can greatly edit and influence the condition for flow and the reservoir, thus influencing the thermosolutal convection, which in turn can thus more efficiently influence freckling as compared to the local thermal conditions, even

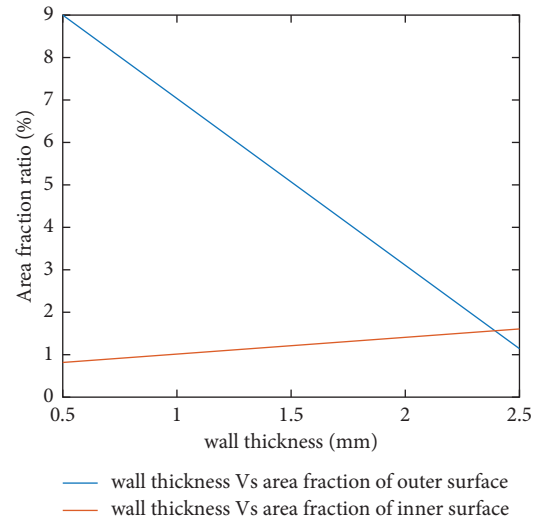

Figure 59: Relation between wall thickness and area fraction of freckles in outer and inner surfaces.

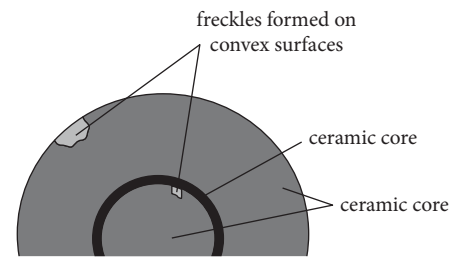

Figure 60: Formation of freckles on convex surfaces.

when the thermal gradient is very high and unfavourable for freckling. Some studies [91, 92] have shown that the causes for freckling, thermosolutal convection/fluid flow, and channel segregations are powered by the buoyancy force of the less-denser solute segregated out of the alloy. Studies [5, 92] also showed that freckling took place preferentially on the castings shadow side. This was seen to be so as a result of the lateral heat flux observed being much stronger on the shadow side. The study also revealed that minimizing lateral heat flux can be a potential way to reduce thermosolutal convection and thus even eliminate freckles. One study [42] showed that, when the casting component has a geometry with abruptly increasing cross-sectional area, the flow intensity in the axial direction significantly increased when the solidification front was transitioning into a cross-section with larger area. The PDAS values were also seen to go up simultaneously. These two factors combined were seen to promote the freckle formation, mostly at the base of the increased cross-section. The study also showed that alloying elements, Al and W, were huge contributors to density inversion and thus promoted freckling. However, contributions of Mo, Cr, and Ti to density inversion were seen to be low enough to make them negligible. Similar results on how abruptly varying cross-sections affects freckling were also seen in other studies [8, 93]. These studies also revealed that that an increase in withdrawal rate can reduce freckling (data regarding this have been graphically represented in

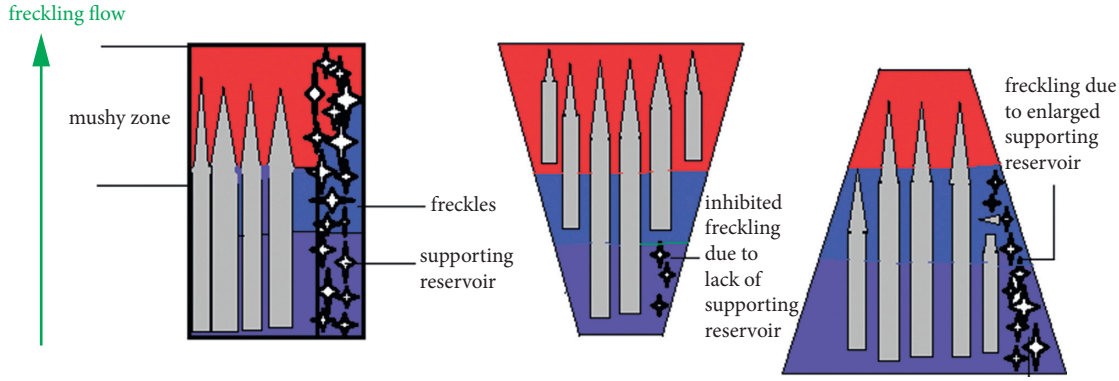

Figure 61: Formation of freckles in cylindrical and sloping surfaces.

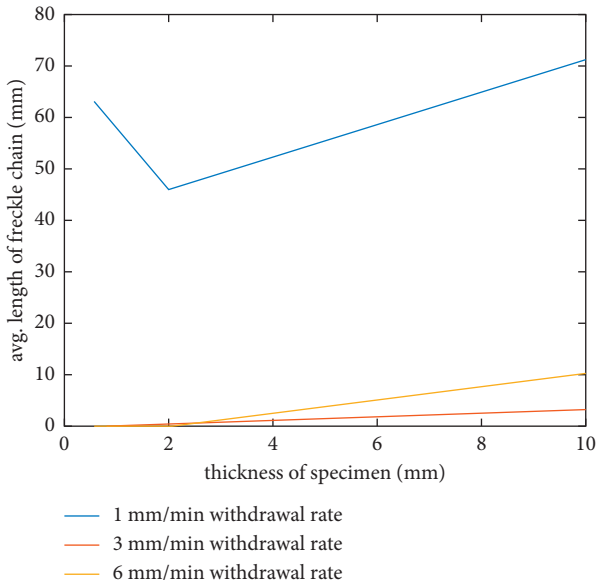

Figure 62: Relation between thickness of samples and average freckle chain length for samples made with varying withdrawal rates.

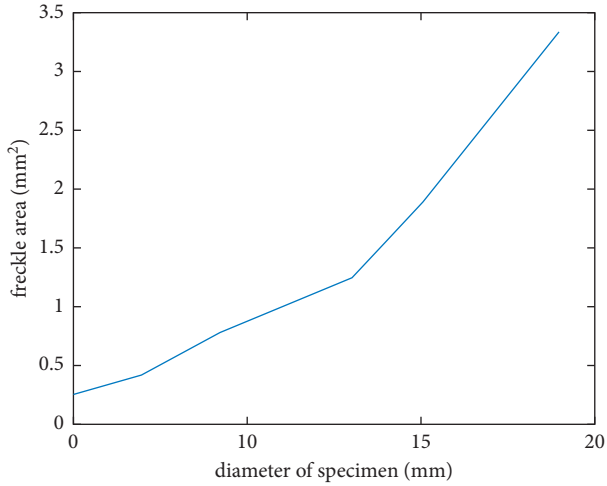

Figure 63: The relation between the diameter of sample and freckle area.

Figure 62), while relatively lesser withdrawal rates were seen to promote freckling due to the dendrites' low growth rate induced as a result of the low cooling rates, which can be easily overpowered by the increased fluid flow rate in the interdendritic region. The study also revealed that, for a given withdrawal rate, a component becomes more prone to freckling with an increase in the thickness of the casting (data regarding this have been graphically represented in Figure 63), as the rate of cooling of the specimens with thicker dimensions was seen to be lower in comparison to that of the specimens with thinner dimensions. It was also found that, at extremely low withdrawal rate, freckles evolved into stray grains. One study [5] also revealed that the components with a larger diameter or cross-sectional area were more prone to freckling. It was also seen that the height of the initiation site for freckles decreases as the rod diameter becomes higher, while the freckle chain width increases. It was also seen that, as the cross-sectional area increased, the area of freckles increased. One study investigated a technique that can be used to prevent formation of freckles. This study [27] examined the influence the use of travelling magnetic fields (TMF) applied to a solidifying casting can have on freckling. The material used for the study was CMSX-4 Ni-superalloy. Further in this study, it was observed that the applied TMF direction and intensity can influenced freckling. When the TMF in the downward direction with an intensity of 1.2–2.8 mT was applied, the re-melting of the segregated liquid was not seen to be much affected, but the overall forces acting on the dendrite arms were seen to have been decreased and this was seen to reduce freckling. When higher TMF was applied, the Lorentz force brought about by the TMF which was acting on the liquid was seen to decrease the thermosolutal convection in interdendritic zone, thus reducing the re-melting of dendrite arms by segregated liquid and the shear force experienced by the dendrites. But the Lorentz force acting directly on the dendrite arms was seen to have been enhanced, thus breaking off the dendrite arms and leading to formation of fragments. When an upward TMF of intensity 2.8 mT was used, even though the convection and force that was applied upon the dendrite arm increased slightly, the enhanced convection was seen to help with the quick removal of the rejected solute, thus decreasing the process of re-melting of

the segregated fluid on the dendrite arms and hence reducing freckling. The study proved that tendency towards freckling in Ni-superalloys that were produced using the DS process could be decreased by using a TMF with an appropriate magnetic intensity. Another study [90] examined the influence of hafnium in the creation of improperly oriented defects, namely, freckles. It was seen that Hf had a very high affinity towards partitioning into the solid phase, i.e., the γ-phase, and it was also seen that Hf was found to be absent on the freckles' dendritic cores. Considering the elemental distribution taking place amongst freckles and SC is exactly the same as that between the liquid and solid phases. The conclusion derived was that as solidification occurs, Hf segregates into the solid phase. By separating the solid phase in the course of solidification, Hf was seen to have a possible influence on beginning the creations of freckles. But as a means to have an influence similar to that of different elements like tungsten and rhenium, the quantity of Hf should go beyond a concentration of 1-2% which is not usually seen in any Ni-superalloy. But this issue was seen to be overcome, when the alloy had high amounts of Co or Cr in them. It was observed that the high content of these elements increased the solubility of Hf in the alloy and thus made effect of Hf in promoting freckling more pronounced. The findings of this study proved that despite the very small concentration of Hf in certain Ni-based superalloys, it can still have a significant effect in promoting freckling. Another study [28] investigated a method that can be used for the prediction of formation of freckles. For the purpose of this study, the relation between the crystal growth and fluid flow during vertical DS process, having a concave-shaped solidification interface, was observed and analysed. With the abovementioned steps concluded, with the help of appropriate equations and numerical formulas, a technique taking the concaved solidification interface and solidification conditions into consideration was developed in order to predict the formation of freckles. The validation results of the study showed that the proposed technique can be used in the predicting the locations where there will be formation of freckles on the castings' with characteristics like a complex shape and large size, except for the regions with not enough height.

6.2. Porosity Defects in Ni-Based Superalloys. Just like freckles, another defect that can have a noticeable influence on cast superalloy components and their parameters and behaviours are porosity defects (Figure 64 shows the presence of porosities within the bulk of the casting) like casting shrinkage defects and voids gas porosities creep cavities. The presence of pores or voids in a casting can be very damaging and can also cause premature failure of the component. In most cases, the pores can be seen to act as sites where cracks initiate and sometimes they even seen to supply a path for the crack to propagate. Thus, many studies have been done regarding casting pores to examine their cause, how they can be eliminated or prevented, and how they can affect the properties of the casting. One such study [14] focuses on how the presence of casting pores can affect the fatigue life of both as-cast and HIP-processed specimens. The superalloy

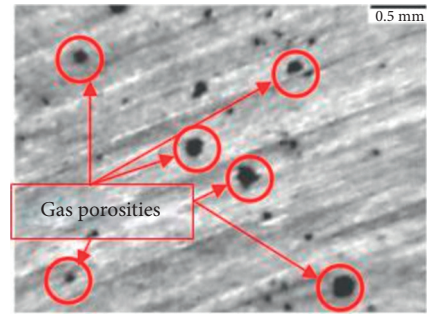

Figure 64: Porosities formed in the bulk of a casting.

IN713LC was used in the study. It was seen that, in both as-cast and HIP-processed specimens, the fatigue cracks were seen to have been initiated at large casting defects which were usually concentrated clusters of many small defects, and the size of these clusters was seen to be reduced by HIP processing of the specimens. And this reduction in defect size was seen to better the performance at higher temperature regions as well as the fatigue life of the HIP-processed specimens relative to as-cast specimens. The stress concentration effect induced by the clusters was seen to promote slip and decohesion in the crystal structure and thus aid the propagation and the growth of the crack. The presence of defects, their role in crack initiation, and the stress concentration effect were all proved by many metallographic methods employed, including the fractographical study of the fractured surfaces. And the betterment of the fatigue life of the HIP-processed samples was proven by the S-N data obtained during fatigue tests and the higher number of cycles to failure observed in these specimens. This healing effect of HIP processing,that can help in curing porosities was further examined by another study [89] that investigated the healing behaviour of micropores under various HIP parameters. The study showed that, with the passing of time, the γ' precipitates were seen to coarsen. The coarsened primary γ' particles precipitated close to the creep cavities were seen to be stretched along its circumference and concentrically arranged under the HIP condition of 1100°C/150 MPa/2 h, which forms the γ' rafting structure which was supposedly concentrically oriented. The γ' rafting structures were seen to have an extra remarkably concentric orientation when HIP temperatures reached 1150–1175°C. A zone with various fine precipitated secondary γ' particles and a smaller number of coarsened primary γ' precipitates were also seen in an area that was in close proximity to the cavity. The zone is given the moniker of "primary γ' denuded zone," appearing between the concentrically oriented γ' rafting zone and the cavity, which was not observed in specimens subjected to the HIP condition of 1100°C/150 MPa/2 h. The movement of solutes in a direction towards the cavity surface was seen to be brought about by the diffusion and the concentration of γ' forming elements, which were in opposite directions. As the temperature of the HIP increases till 1200°C, casting pores and creep cavities were barely seen and the concentrically oriented γ' rafting structure disappeared because the primary γ' precipitates had been totally dissolved into the γ matrix. The experimental results from the

study also depicted that the atomic diffusion greatly influences the micropores' healing process. Another study [37] focuses on casting voids present in Ni-based superalloy castings and how they are affected by tensile deformation at room temperature. At room temperature, it was found that each and every void can act as a crack initiation site during fatigue testing. The study also revealed that voids formed between dendrite arms, a characteristic of casting pore formation. It was seen that there was an increase in porosity in the specimens used for the study after tensile deformation, while the shape of the voids was seen to remain unaffected. The void size growth was also seen to be unaffected by their location of occurrence. The growths of voids were seen to be because of dislocation activities around the void surface. Also at room temperature, during tensile deformation, a cleavage fracture was seen to occur, indicating that voids did not act as crack nucleation sites. Another study [50] investigated how a very important casting parameter the withdrawal rate can affect the porosity present in a 3rd generation Ni-superalloy casting. The study showed a decrease in PDAS and SDAS values with increasing withdrawal rates. This was seen to refine the microstructure and thus lead to less porosity defects in it (data regarding this are graphically represented in Figures 65 and 66). The study also helped in concluding that there could be two major factors influencing the porosity levels: (1) using residual liquids for the feeding of volume shrinkages formed by the last solidified γ-γ' eutectic liquids and (2) the isolating effect induced by dendrite arms' morphologies. The study also proved that conducting research to find the optimal withdrawal rates for different alloys is a very effective method to minimise porosities in castings, especially in large-scale production. The composition of certain alloying elements can also influence the formation of porosities. This was investigated in a study [76] that examined the role of elements like zirconium, boron, and carbon in porosity creation. The chemical compositions of alloying elements for the alloys used in the study were 20.2Cr-13.7Co-4.78Mo-1.19Al-0.69Ti-0.08C-2.34Fe for Alloy 1 and 20.5Cr-15.6Co5.03Mo-1.57Al-3.42Ti-0.15C-1.64Fe-0.076Zr-0.01%B for Alloy 2. Since the alloys used in the study were made under vacuum conditions, the porosities detected in the structure of the alloys were seen to be due to microshrinkages and not due to gas evolution during the solidification process. The presence of small amounts of B and Zr and higher C content in alloy 2 was seen to reduce porosity formation due to the segregating effect of these elements which helps in alleviating microshrinkages during solidification. These elements were also seen to increase the carbide content in the interdendritic region by their segregation and formation of carbides. The study also showed that an increasing Ti and C content increased the MC carbide and γ/γ' eutectic, volume fraction, with alloy 2 having 4 times the carbide volume fraction of alloy 1.

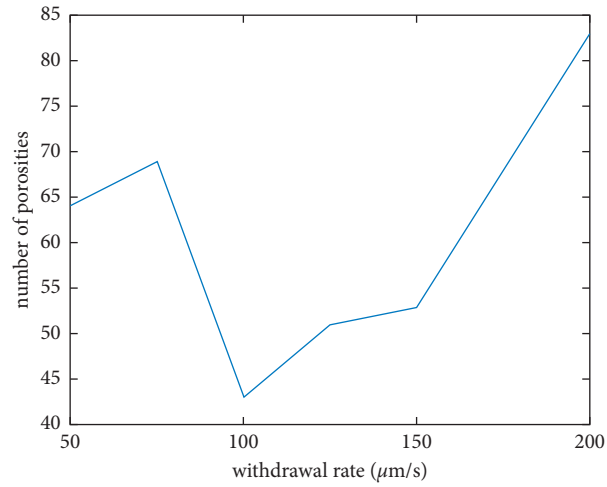

Figure 65: The variation in the number of porosities formed as the rate of withdrawal increases.

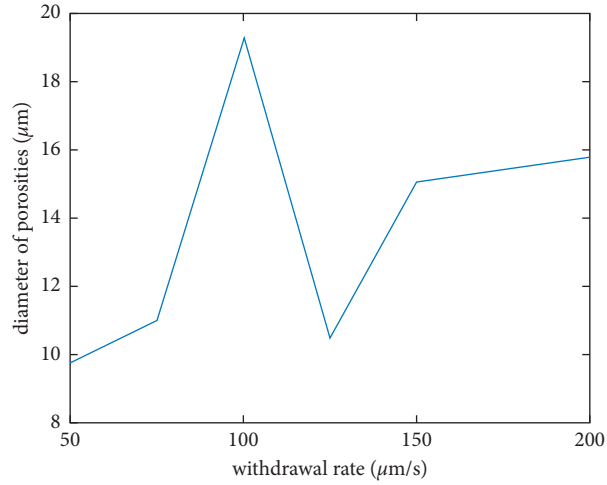

Figure 66: The variation in the diameter of porosities formed as the rate of withdrawal increases.

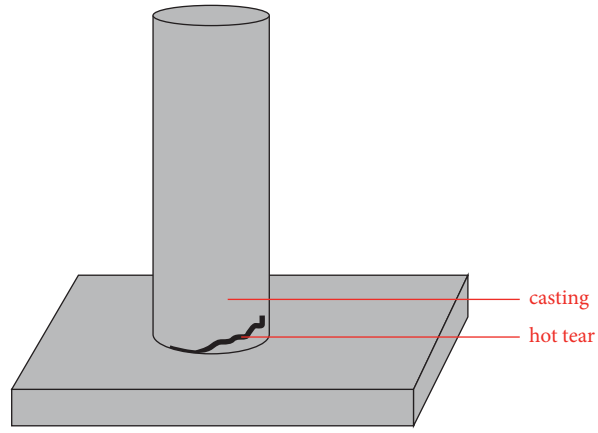

Figure 67: Hot crack formed in a cast component.

6.3. Hot Cracking in Cast Ni-Based Superalloys. Hot cracking is another defect that is a major problem while casting Ni-based superalloys. Because of their outstanding performance at high temperatures and pressures, SX Ni-superalloys are widely employed in the production of blades for turbines. However, after working in very awful conditions for quite

some time, formation of tip defections like, tip deformation and tip cracking, can occur. This process is called hot cracking. Figure 67 shows how a hot tear looks like. Once the defects start to form on the blades, they will mostly be abandoned. It was found via many experiments that if and when hot cracks are formed, they most often occur along the GBs, thus indicating their effect on solidification crack behaviour. According to studies [38, 40], the formation of cracks called as solidification cracks, hot tears, and hot cracks occur in last phases of the solidification process, when the dendritic arms' coalescence has already occurred, and is now leading to problems with melt feeding. And when strain occurred in such situations, as a result of solidification shrinkage or contraction caused by the thermal conditions, hot tears were seen to have formed along GBs. These results showed us importance of studies that investigated what kind of influence GBs have on hot cracking. One study [38] took this approach and investigated how GB-misorientation affects the hot cracking susceptibility of DD6, a 2^{nd}-gen Ni-superalloy that has a considerably high Re content. Large deviation angles were observed to aid in the development of a stable liquid film in the GBs, indicating that the GB-misorientation angle is a key parameter that regulates the formation of hot cracks. The temperature for which the expansion of the liquid film was observed decreased as the misorientation angle increased. Hot cracks were seen to appear only in places where the strain localised and a critical temperature was present. The solidification cracking susceptibility influenced by GB-misorientation angles was further examined in the study, and it was found that critical angle for superalloy DD6 is 16°. The calculation of the dendritic grains' coalescence under cooling led to the finding that it was significantly bigger than the temperature gap relating to the region inside the grain. So, if GBs are existent, then the liquid layer developed along the GBs was the seen to be the primary reason for hot tearing and not that formed in the intradendritic region. The concentration and presence of certain alloying elements which are susceptible towards interdendritic segregation was also seen influence the hot cracking behaviour of a material. This was the subject of one study [40], which looked into the influence of Ta and Ti on the hot cracking behaviour of IN792 that is made with the help of the DS process. The time when the casting temperature lies within the temperature of carbide formation and final solidification was seen to be the most favourable time for the formation of hot cracks. IN792 castings having a Ti/Ta ratio that was greater than 1 or less than 0.7 were seen to exhibit good castability, and a Ti content decrease from 3.9% to 3%, followed by either a reduction or a gain in Ta content, was observed to result in a reduction in the fraction of interdendritic liquid present when solidification finishes, thus restricting the possibility for hot crack formation. Another research [94] found that decreasing Ti content reduced hot cracking in IN792, thus confirming the influence of Ti on hot cracking. In this study, reducing Ti content to 2% was seen to eliminate hot cracks altogether. Increase in the Ti content was seen to induce severe hot cracks. The presence of interdendritic liquid between GB's leading promoting hot cracking was also proved by this study. In IN792 and CM247, another superalloy that is Ni-based and is utilized in this study, a decrease in the Ti content was also observed to minimise interdendritic liquid. But the Ti content's effect on CM247 was not seen to have been as significant as it was in IN792. One other study [7] looked at how the proportion of zirconium (Zr) in IN738LC, a polycrystalline Ni-superalloy, affected hot tearing. Zr is added to Ni-superalloys as it helps in enhancing the alloys' creep properties. As a result, it can always be found in Ni-based superalloys. The influence of very tiny Zr additions (0.01–0.04 wt. % or 100–400 parts per million) on the development of hot cracks in the same superalloy was investigated in this study. Even though Zr is a trace element, it was found to have very profound effects on hot tearing of cast during solidification. Four specimens with varying Zr content (0.01–0.04% wt) were prepared. The study proved the significant impact that even tiny variations in the trace element Zr's content can have on hot cracking. Hot cracks were seen to appear when Zr content reached 0.03 wt.%, and the hot cracking was seen to worsen when the Zr composition was increased to 0.04 wt.%. On studying the microstructure of sample I (0.01%wt Zr) and sample IV (0.04%wt Zr), it was found that there was not any significant difference in the grain size or SDAS. These values were rather found to be almost identical. This proved that the grain size or the SDAS have no impact on the hot tearing of solidifying metal. But the study showed an increase in γ/γ' volume fraction and its spreading increased with increasing Zr content. Further study showed that there were intragranular eutectics formed in the sample where hot tearing was observed, along with Zr segregation and shrinkage porosities appearing in the coarse γ/γ' eutectic regions. It was observed that the solidification crack began in a micropore and spread across the intergranular eutectic, eventually stopping when the eutectic vanished, which is when the GB became phase free. Despite the increased volume fraction of the eutectic γ/γ' phase, a local shortage of feeding of liquid when solidification occurred was observed. And this was seen to cause the formation of microporosity in the eutectic phase. Zr was seen to segregate at the GBs. When the Zr content was found to increase, the volume fraction of the eutectic phase and its growth along the GBs was seen to rise significantly. This was seen to hinder the coalescence of grains at GBs covered with interdendritic phases, and as a result making the castings more prone to the formation of hot cracks. Both eutectic phase and isolated carbides were seen to act as hindrances for the flow of intergranular liquid that feeds the mushy zone's deep regions. Micropores were also seen to form in isolated liquid pools and function as origin point or source for hot cracks.

6.4. Sliver Defects in Ni-Based Superalloy Castings. Another important issue with Ni-based superalloy castings is sliver defects. It is a typical grain defect observed in castings made of SX Ni-superalloys and produced using the Bridgman DS method. It is recognized as a grain defect caused due to misoriented dendrites observed on the casting's surface. In one study [68], the formation of sliver defects was

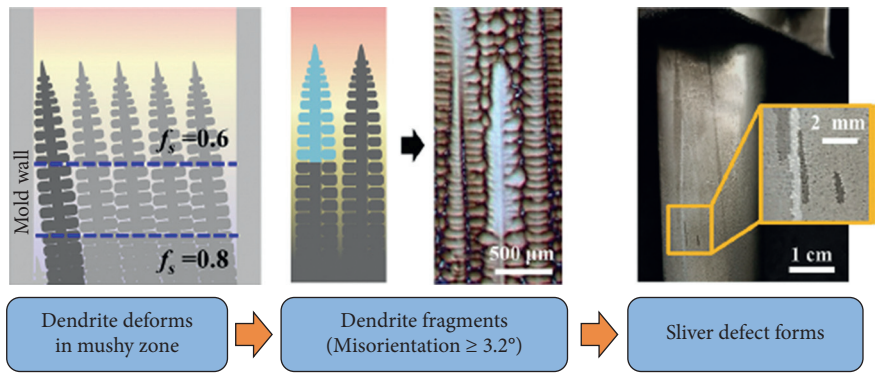

Figure 68: Summary of how sliver defects are formed (figure is taken from [68]).

investigated (the findings are briefly summarised pictorially in Figure 68). Grain selection techniques and Bridgman DS process were used to create a variety of SX castings. CMSX-4, a commercial Ni-superalloy, was the material chosen for the study. The formation of sliver defects was detected during the SX castings' DS process, and fragmented dendrites were shown to be the cause. Sliver grains were found to have a deviation/misorientation angle ranging from 3.2° to 12°. The critical value for dendritic fragmentation was determined to be 3.2 degrees, which is the least deviation/misorientation angle. TEM and EBSD results showed that fragmentation of dendrites took place in brittle fashion instead of undergoing huge plastic deformations. The fragmentation of dendrites was seen to be caused by micro and macroscopic nonuniform stresses, and the dendrite deformation was seen to include bending and torsion. The presence of pores and oxide inclusions were also seen to bring about the fragmentation of dendrites. The lower level of misorientation of sliver grains demonstrated conclusively that dendrite fragmentation occurred when the mushy zone's solid fraction reached a higher level. According to the dendrite morphologies of the various solid fractions in the mushy zone, the solid fraction range in which dendrite fragmentation occurred was found to be 0.6–0.8. The findings of this investigation also revealed that slivers formed mostly on the side where the major dendrites converged on the inner wall of the mould. The development of a converging interface was blamed for the inclination of sliver defects to occur on the convex surface of a blade. Another study [101] mentioned the impact thermal gradient during casting of Ni-based superalloys can have on sliver defect formation. In this study, 3 types of castings made in Bridgman furnace with the help of standard, adjusted, and inner radiation baffles were made in order to obtain 3 types of castings made with varying thermal gradient. Samples made with SRB had the least thermal gradient, while sample made with IRB had the highest thermal gradient. Among samples that had sliver defects in them, in the ones made with SRB, the sliver defect formation was more pronounced, due to low thermal gradient. As we used ARB, the higher thermal gradient was seen to suppress sliver defect formation, and using IRB was seen to increase the thermal gradient even higher and thus suppress sliver defect formation even more.

7. Conclusion

In our paper, we have reviewed many papers that have studied various aspects of Ni-based superalloys like their manufacturing, elemental composition, physical and mechanical properties, and defects. The various achievements and advancements regarding these aspects in the field of Ni-based superalloy technology were reviewed and highlighted in this article. And from reviewing these papers, it was made clear that the potential held by this special class of alloy is exceptional and further extensive research in this field can help improve them much more. Such research has so far helped in finding 2nd, 3rd, and recently even experimental 4th generation superalloys that exhibit highly superior physical and mechanical properties, along with excellent creep performance of highly elevated temperatures exceeding 1500°C. Thus, following this path and pursuing further research can lead to finding even a potential 5th generation superalloy with vastly superior properties. Following are some of the ideas that can be useful while considering future research:

(i) Ni-based superalloys are still mainly manufactured using casting methods, particularly investment casting. But recently, various alternative methods for their manufacturing are also being investigated. Thus, research on unconventional methods of manufacturing like AM and powder metallurgy is one possibility for future research.

(ii) Today, lots of metal and alloy components are being made using 3D printing technology. Thus, research on the feasibility and possibility of using this method to manufacture Ni-based superalloy parts is another possibility for future research. This research can be very useful in the aerospace field due to various benefits.

(iii) Castability of Ni-based superalloys is one aspect that is extensively researched but another aspect that not so meticulously investigated is the machinability of these alloys. Ni-based superalloys are known to be notoriously difficult to machine so research on this aspect can be extremely helpful.

(iv) Ni-based superalloys are made of a number of different alloying elements. Varying the composition of some of these elements can bring about significant changes in the properties of the final casting, or even lead to making a variation or a totally different Ni superalloy. Research on how these changes can affect the various physical and mechanical properties and how it can aid in developing special variations or new Ni superalloys is another possibility for future research.

(v) Many defects occurring in Ni-based superalloys like freckles and slivers are still unknown, and methods and techniques to completely eliminate them in parts produced via certain manufacturing methods are yet to be found. So creating such novel techniques is yet another possibility for future research.

(vi) In this article, we have reviewed the properties and behaviour of various Ni-based superalloys. But most studies done are conducted and spoke about in a generalized perspective. So examining the properties of different Ni superalloys individually and not from a generalized perspective can help us find the optimal applications for the different Ni superalloys out there.

(vii) Since Ni-based superalloys mostly work under very high temperatures, pressures, and highly erosive/corrosive environments, recently applying thermal or anti-erosive/corrosive coats has come into practice. But the application of such coats can change the substrate's physical and mechanical properties and behaviour, i.e., the Ni superalloy. Very few research regarding has been done. So pursuing this aspect is another possibility for future research.

(viii) Seeing if Ni-superalloys can be used in producing composite materials or not is something that is yet to be researched about as number of researches on this aspect is little to none, thus making this a topic for possible future research.

(ix) Research on 5^{th} and 6^{th} generation Ni-superalloys is very scarce. Thus, this is one very potential and quite untouched area of research.

Data Availability

The data used to support this study are included within the article.

Conflicts of Interest

The authors declare that they have no conflicts of interest.

References

[1] S. Steuer, P. Villechaise, T. M. Pollock, and J. Cormier, "Benefits of high gradient solidification for creep and low cycle fatigue of AM1 single crystal superalloy," *Materials Science and Engineering A*, vol. 645, pp. 109–115, 2015.

[2] H. Lin, H. P. Geng, Y. Y. Zhang et al., "Fatigue strength and life prediction of a MAR-m247 nickel-base superalloy gas turbine blade with multiple carbide inclusions," *Strength of Materials*, vol. 51, no. 1, pp. 102–112, 2019.

[3] V. Horník, S. Fintová, M. Šmíd, P. Hutař, K. Hrbáček, and L. Kunz, "Fatigue properties of B1914 superalloy at high temperatures," *Procedia Structural Integrity*, vol. 23, pp. 191–196, 2019.

[4] X. Zhu, F. Wang, D. Ma, and A. Bührig-Polaczek, "Grain selection in a high-efficiency 2D grain selector during casting of single-crystal superalloys," *Materials*, vol. 12, no. 5, pp. 789–798, 2019.

[5] J. Hong, D. Ma, J. Wang et al., "Freckle defect formation near the casting interfaces of directionally solidified superalloys," *Materials*, vol. 9, no. 11, pp. 929–1017, 2016.

[6] X. Zhu, Q. Yang, F. Wang, and D. Ma, "Grain orientation optimization of two-dimensional grain selector during directional solidification of Ni-based superalloys," *Materials*, vol. 13, no. 5, pp. 1121–1210, 2020.

[7] D. Heydari, A. S. Fard, A. Bakhshi, and J. M. Drezet, "Hot tearing in polycrystalline Ni-based IN738LC superalloy: influence of Zr content," *Journal of Materials Processing Technology*, vol. 214, no. 3, pp. 681–687, 2014.

[8] D. Han, W. Jiang, J. Xiao et al., "Investigation on freckle formation and evolution of single-crystal nickel-based superalloy specimens with different thicknesses and abrupt cross-section changes," *Journal of Alloys and Compounds*, vol. 805, pp. 218–228, 2019.

[9] Y. Zhao, K. Li, M. Gargani, and W. Xiong, "A comparative analysis of Inconel 718 made by additive manufacturing and suction casting: microstructure evolution in homogenization," *Additive Manufacturing*, vol. 36, Article ID 101404, 2020.

[10] B. Vieille, C. Keller, M. Mokhtari et al., "Investigations on the fracture behavior of Inconel 718 superalloys obtained from cast and additive manufacturing processes," *Materials Science and Engineering A*, vol. 790, Article ID 139666, 2020.

[11] J. Salvat Cantó, S. Winwood, K. Rhodes, and S. Birosca, "A study of low cycle fatigue life and its correlation with microstructural parameters in IN713C nickel based superalloy," *Materials Science and Engineering A*, vol. 718, pp. 19–32, 2018.

[12] I. Šulák, K. Obrtlík, S. Hutařová, M. Juliš, T. Podrábský, and L. Čelko, "Low cycle fatigue and dwell-fatigue of diffusion coated superalloy Inconel 713LC at 800 °C," *Materials Characterization*, vol. 169, Article ID 110599, 2020.

[13] I. Šulák, K. Obrtlík, L. Čelko, T. Chráska, D. Jech, and P. Gejdoš, "Low cycle fatigue performance of Ni-based superalloy coated with complex thermal barrier coating," *Materials Characterization*, vol. 139, pp. 347–354, 2018.

[14] L. Kunz, P. Lukáš, R. Konečná, and S. Fintová, "Casting defects and high temperature fatigue life of in 713LC superalloy," *International Journal of Fatigue*, vol. 41, pp. 47–51, 2012.

[15] D. Szeliga, K. Kubiak, M. Motyka, and J. Sieniawski, "Directional solidification of Ni-based superalloy castings: thermal analysis," *Vacuum*, vol. 131, pp. 327–342, 2016.

[16] M. Lamm and R. F. Singer, "The effect of casting conditions on the high-cycle fatigue properties of the single-crystal nickel-base superalloy PWA 1483," *Metallurgical and Materials Transactions A*, vol. 38, no. 6, pp. 1177–1183, 2007.

[17] C. Del Vecchio, G. Fenu, F. A. Pellegrino et al., "Support Vector Representation Machine for superalloy investment casting optimization," *Applied Mathematical Modelling*, vol. 72, pp. 324–336, 2019.

[18] K. Gancarczyk, M. Zubko, A. Hanc-Kuczkowska et al., "The effect of withdrawal rate on crystal structure perfection, microstructure and creep resistance of single crystal castings made of CMSX-4 nickel-based superalloy," *Materials*, vol. 12, no. 20, pp. 3422–20, 2019.

[19] B. G. Choi, I. S. Kim, H. U. Hong, J. Do, J. E. Jung, and C. Y. Jo, "Effect of Ti content on creep properties of Ni-base single crystal superalloys," *Metals and Materials International*, vol. 23, no. 5, pp. 877–883, 2017.

[20] A. Cervellon, J. Cormier, F. Mauget, and Z. Hervier, "VHCF life evolution after microstructure degradation of a Ni-based single crystal superalloy," *International Journal of Fatigue*, vol. 104, pp. 251–262, 2017.

[21] L. M. Bortoluci Ormastroni, L. Mataveli Suave, A. Cervellon, P. Villechaise, and J. Cormier, "LCF, HCF and VHCF life sensitivity to solution heat treatment of a third-generation Ni-based single crystal superalloy," *International Journal of Fatigue*, vol. 130, Article ID 105247, 2020.

[22] A. Cervellon, L. M. Bortoluci Ormastroni, Z. Hervier, T. M. Pollock, F. Pedraza, and J. Cormier, "Damage mechanisms during very high cycle fatigue of a coated and grit-blasted Ni-based single-crystal superalloy," *International Journal of Fatigue*, vol. 142, Article ID 105962, 2021.

[23] M. V. Nathal, J. Bierer, L. Evans, E. A. Pogue, F. Ritzert, and T. P. Gabb, "Stress relaxation behavior in single crystal superalloys," *Materials Science and Engineering A*, vol. 640, pp. 295–304, 2015.

[24] C. Qiu, N. D'Souza, J. Kelleher, and C. Panwisawas, "An experimental investigation into the stress and strain development of a Ni-base single crystal superalloy during cooling from solidification," *Materials & Design*, vol. 114, pp. 475–483, 2017.

[25] C. Vorkötter, D. E. Mack, O. Guillon, and R. Vaßen, "Superior cyclic life of thermal barrier coatings with advanced bond coats on single-crystal superalloys," *Surface and Coatings Technology*, vol. 361, pp. 150–158, 2019.

[26] F. Wang, D. X. Ma, and A. Bührig-Polaczek, "Effect of ceramic cores on the freckle formation during casting Ni-based single crystal superalloys," *Metallurgical and Materials Transactions A*, vol. 50, no. 2, pp. 804–815, 2019.

[27] Q. Li, J. Shen, L. Qin, Y. Xiong, and X. a. Yue, "Effect of traveling magnetic field on freckle formation in directionally solidified CMSX-4 superalloy," *Journal of Materials Processing Technology*, vol. 274, Article ID 116308, 2019.

[28] Q. Li, J. Shen, Y. Xiong, L. Qin, and X. a. Yue, "Prediction of freckle formation in directionally solidified CMSX-4 superalloy," *Materials Letters*, vol. 228, pp. 281–284, 2018.

[29] N. Stanford, A. Djakovic, B. A. Shollock, M. McLean, N. D'Souza, and P. A. Jennings, "Seeding of single crystal superalloys--role of seed melt-back on casting defects," *Scripta Materialia*, vol. 50, no. 1, pp. 159–163, 2004.

[30] J. Yu, D. Wang, D. Li et al., "Physical simulation of investment casting for GTD-222 Ni-based superalloy processed by controlled cooling rates," *International Journal of Advanced Manufacturing Technology*, vol. 105, no. 7-8, pp. 3531–3542, 2019.

[31] J. Strößner, C. H. Konrad, M. Brunner, R. Völkl, and U. Glatzel, "Influence of casting surface on creep behaviour of thin-wall Ni-base superalloy Inconel100," *Journal of Materials Processing Technology*, vol. 213, no. 5, pp. 722–727, 2013.

[32] W. Jin, T. Li, and G. Yin, "Research on vacuum-electromagnetic casting of IN100 superalloy ingots," *Science and Technology of Advanced Materials*, vol. 8, no. 1-2, pp. 1–4, 2007.

[33] B.-p. Wu, L.-h. Li, J.-t. Wu et al., "Microstructure and stress rupture properties of polycrystal and directionally solidified castings of nickel-based superalloys," *International Journal of Minerals, Metallurgy, and Materials*, vol. 21, no. 1, pp. 58–64, 2014.

[34] L. Liu, T. Huang, Y. Xiong et al., "Grain refinement of superalloy K4169 by addition of refiners: cast structure and refinement mechanisms," *Materials Science and Engineering A*, vol. 394, no. 1-2, pp. 1–8, 2005.

[35] A. J. Elliott, T. M. Pollock, S. Tin, W. T. King, S.-C. Huang, and M. F. X. Gigliotti, "Directional solidification of large superalloy castings with radiation and liquid-metal cooling: a comparative assessment," *Metallurgical and Materials Transactions A*, vol. 35, no. 10, pp. 3221–3231, 2004.

[36] X. Yan, R. N. Wang, Q. Xu, and B. Liu, "Numerical simulation and experimental casting of nickel-based single-crystal Superalloys by HRS and LMC directional solidification processes," *High Temperature Materials and Processes*, vol. 36, no. 4, pp. 327–337, 2017.

[37] Z. Xu, B. Britton, and Y. Guo, "Casting voids in nickel superalloy and the mechanical behaviour under room temperature tensile deformation," *Materials Science and Engineering A*, vol. 806, Article ID 140800, 2021.

[38] P. Rong, N. Wang, L. Wang, R. N. Yang, and W. J. Yao, "The influence of grain boundary angle on the hot cracking of single crystal superalloy DD6," *Journal of Alloys and Compounds*, vol. 676, pp. 181–186, 2016.

[39] D. Szeliga, W. Ziaja, M. Motyka, K. Kubiak, and J. Sieniawski, "Application of inner radiation baffles in the bridgman process for flattening the temperature profile and controlling the columnar grain structure of directionally solidified Ni-based superalloys," *Materials*, vol. 12, no. 6, pp. 935–6, 2019.

[40] J. Zhang, "Effect of Ti and Ta on hot cracking susceptibility of directionally solidified Ni-based superalloy IN792," *Scripta Materialia*, vol. 48, no. 6, pp. 677–681, 2003.

[41] L. Rémy, M. Geuffrard, A. Alam, A. Köster, and E. Fleury, "Effects of microstructure in high temperature fatigue: lifetime to crack initiation of a single crystal superalloy in high temperature low cycle fatigue," *International Journal of Fatigue*, vol. 57, pp. 37–49, 2013.

[42] Q. Y. Sun, Y. Ren, and D.-R. Liu, "Numerical investigations of freckles in directionally solidified nickel-based superalloy casting with abrupt contraction in cross section," *Results in Physics*, vol. 12, pp. 1547–1558, 2019.

[43] K. Pang and H. Yuan, "Fatigue life assessment of a porous casting nickel-based superalloy based on fracture mechanics methodology," *International Journal of Fatigue*, vol. 136, p. 105575, Article ID 105575, 2020.

[44] L. Zheng, G. Zhang, C. Xiao et al., "The interdendritic-melt solidification control (IMSC) and its effects on the porosity and phase change of a Ni-based superalloy," *Scripta Materialia*, vol. 74, pp. 84–87, 2014.

[45] C. Labergère, M. Long, H. Badreddine, N.-T. Niane, D. Grange, and K. Saanouni, "Thermomechanical model for solidification and cooling simulation of Ni-based superalloy components," *International Journal of Solids and Structures*, vol. 212, pp. 202–219, 2021.

[46] A. Szczotok and H. Matysiak, "Influence of constituents of shell mold on the morphology and chemical composition of carbides occurring in IN 713C superalloy castings," *Journal of Materials Engineering and Performance*, vol. 23, no. 8, pp. 2748–2759, 2014.

[47] D. Gelmedin and K.-H. Lang, "Fatigue behaviour of the superalloy in 713C under LCF-, HCF- and superimposed LCF/HCF-loading," *Procedia Engineering*, vol. 2, no. 1, pp. 1343–1352, 2010.

[48] E. M. Visik, E. V. Kolyadov, O. G. Ospennikova, V. V. Gerasimov, and E. V. Filonova, "Effect of technological casting conditions on the structure of single-crystal blades made of a carbon-free nickel superalloy," *Russian Metallurgy*, vol. 2018, no. 13, pp. 1222–1228, 2018.

[49] S. F. Gao, L. Liu, N. Wang, X. B. Zhao, J. Zhang, and H. Z. Fu, "Grain selection during casting Ni-base, single-crystal superalloys with spiral grain selector," *Metallurgical and Materials Transactions A*, vol. 43, no. 10, pp. 3767–3775, 2012.

[50] Q. Yue, L. Liu, W. Yang et al., "Influence of withdrawal rate on the porosity in a third-generation Ni-based single crystal superalloy," *Progress in Natural Science: Materials International*, vol. 27, no. 2, pp. 236–243, 2017.

[51] Y. S. Huang, X. G. Wang, C. Y. Cui et al., "The effect of coarsening of γ' precipitate on creep properties of Ni-based single crystal superalloys during long-term aging," *Materials Science and Engineering A*, vol. 773, Article ID 138886, 2020.

[52] A. H. V. Pavan, R. L. Narayan, M. Swamy, K. Singh, and U. Ramamurty, "Stress rupture embrittlement in cast Ni-based superalloy 625," *Materials Science and Engineering A*, vol. 793, Article ID 139811, 2020.

[53] M. Kopec, D. Kukla, X. Yuan, W. Rejmer, Z. L. Kowalewski, and C. Senderowski, "Aluminide thermal barrier coating for high temperature performance of MAR 247 nickel based superalloy," *Coatings*, vol. 11, no. 1, pp. 48–12, 2021.

[54] L. Gong, B. Chen, L. Zhang, Y. Ma, and K. Liu, "Effect of cooling rate on microstructure, microsegregation and mechanical properties of cast Ni-based superalloy K417G," *Journal of Materials Science & Technology*, vol. 34, no. 5, pp. 811–820, 2018.

[55] K. Hou, M. Wang, M. Ou et al., "Effects of microstructure evolution on the deformation mechanisms and tensile properties of a new Ni-base superalloy during aging at 800 °C," *Journal of Materials Science & Technology*, vol. 68, pp. 40–52, 2021.

[56] X. Meng, J. Li, T. Jin, X. Sun, C. Sun, and Z. Hu, "Evolution of grain selection in spiral selector during directional solidification of nickel-base superalloys," *Journal of Materials Science & Technology*, vol. 27, no. 2, pp. 118–126, 2011.

[57] M. T. Jovanović, Z. Mišković, and B. Lukić, "Microstructure and stress-rupture life of polycrystal, directionally solidified, and single crystal castings of nickel-based IN 939 superalloy," *Materials Characterization*, vol. 40, no. 4–5, pp. 261–268, 1998.

[58] B. Nie, Z. Zhao, S. Liu et al., "Very high cycle fatigue behavior of a directionally solidified Ni-base superalloy DZ4," *Materials*, vol. 11, no. 1, pp. 98–12, 2018.

[59] G. Xiao, J. Jiang, Y. Wang, Y. Liu, and Y. Zhang, "Microstructure and mechanical properties of nickel-based superalloy GH4037 parts formed by thixoforming," *Materials Science and Engineering A*, vol. 780, Article ID 139196, 2020.

[60] H. Zhang, Q. Xu, and B. Liu, "Numerical simulation and optimization of directional solidification process of single crystal superalloy casting," *Materials*, vol. 7, no. 3, pp. 1625–1639, 2014.

[61] X.-w. Yan, X. Guo, Y.-l. Liu, X.-f. Gong, Q.-y. Xu, and B.-c. Liu, "Numerical simulation of dendrite growth in Ni-based superalloy casting during directional solidification process," *Transactions of Nonferrous Metals Society of China*, vol. 29, no. 2, pp. 338–348, 2019.

[62] D. Pan, Q. Xu, B. Liu, J. Li, H. Yuan, and H. Jin, "Modeling of grain selection during directional solidification of single crystal superalloy turbine blade castings," *Journal of Occupational Medicine*, vol. 62, no. 5, pp. 30–34, 2010.

[63] X. Yan, Q. Xu, G. Tian, Q. Liu, J. Hou, and B. Liu, "Multiscale modeling of liquid-metal cooling directional solidification and solidification behavior of nickel-based superalloy casting," *Journal of Materials Science & Technology*, vol. 67, pp. 36–49, 2021.

[64] A. Durga, H. Dai, S. Huang, I. Spinelli, and L. Yuan, "Grain structure prediction for directionally solidified superalloy castings," *Journal of Occupational Medicine*, vol. 72, no. 5, pp. 1785–1793, 2020.

[65] H. Farhangi, S. Norouzi, and M. Nili-Ahmadabadi, "Effects of casting process variables on the residual stress in Ni-base superalloys," *Journal of Materials Processing Technology*, vol. 153-154, no. 1–3, pp. 209–212, 2004.

[66] V. Kavoosi, S. M. Abbasi, S. M. G. Mirsaed, and M. Mostafaei, "Influence of cooling rate on the solidification behavior and microstructure of IN738LC superalloy," *Journal of Alloys and Compounds*, vol. 680, pp. 291–300, 2016.

[67] Y. Liu, M. Kang, Y. Wu et al., "Crack formation and microstructure-sensitive propagation in low cycle fatigue of a polycrystalline nickel-based superalloy with different heat treatments," *International Journal of Fatigue*, vol. 108, no. 800, pp. 79–89, 2018.

[68] W. Xu, F. Wang, D. Ma, X. Zhu, D. Li, and A. Bührig-Polaczek, "Sliver defect formation in single crystal Ni-based superalloy castings," *Materials & Design*, vol. 196, Article ID 109138, 2020.

[69] D. Szeliga, "Manufacturing of thin-walled Ni-based superalloy castings using alternative thermal insulating module to control solidification," *Journal of Materials Processing Technology*, vol. 278, Article ID 116503, 2020.

[70] M. Rahimian, S. Milenkovic, L. Maestro, A. Eguidazu Ruiz De Azua, and I. Sabirov, "Development of tool for physical simulation of skin formation during investment casting of nickel-based superalloys," *Materials & Design*, vol. 87, pp. 712–720, 2015.

[71] M. M. Franke, R. M. Hilbinger, A. Lohmüller, and R. F. Singer, "The effect of liquid metal cooling on thermal gradients in directional solidification of superalloys: thermal analysis," *Journal of Materials Processing Technology*, vol. 213, no. 12, pp. 2081–2088, 2013.

[72] G. Shang, P. Gao, F. Luo, J. Yuan, J. Liao, and H. Wang, "Effect of Ca on the Y content and cyclic oxidation behavior of Ni-based single-crystal superalloy," *International Journal of Metalcasting*, vol. 12, no. 3, pp. 607–613, 2018.

[73] P. G. Min, V. V. Sidorov, and V. E. Vadeev, "Reduction of silicon from a ceramic mold during directional solidification of single-crystal nickel superalloys," *Russian Metallurgy*, vol. 2018, no. 13, pp. 1288–1292, 2018.

[74] W.-J. Zhang, "Thermal mechanical fatigue of single crystal superalloys: achievements and challenges," *Materials Science and Engineering A*, vol. 650, pp. 389–395, 2016.

[75] Ł. Rakoczy, M. Grudzień, and R. Cygan, "Influence of melt-pouring temperature and composition of primary coating of

shell mold on tensile strength and creep resistance of Ni-based superalloy," *Journal of Materials Engineering and Performance*, vol. 28, no. 7, pp. 3826–3834, 2019.

[76] E. Cortes, A. Bedolla-Jacuinde, M. Rainforth et al., "Role of titanium, carbon, boron, and zirconium in carbide and porosity formation during equiaxed solidification of nickel-based superalloys," *Journal of Materials Engineering and Performance*, vol. 28, no. 7, pp. 4171–4186, 2019.

[77] W. Song, X. G. Wang, J. G. Li et al., "Effect of ruthenium on microstructure and high-temperature creep properties of fourth generation Ni-based single-crystal superalloys," *Materials Science and Engineering A*, vol. 772, Article ID 138646, 2020.

[78] D. Bürger, A. B. Parsa, M. Ramsperger, C. Körner, and G. Eggeler, "Creep properties of single crystal Ni-base superalloys (SX): a comparison between conventionally cast and additive manufactured CMSX-4 materials," *Materials Science and Engineering A*, vol. 762, Article ID 138098, 2019.

[79] J. Nawrocki, M. Motyka, D. Szeliga, W. Ziaja, R. Cygan, and J. Sieniawski, "Effect of cooling rate on macro- and microstructure of thin-walled nickel superalloy precision castings," *Journal of Manufacturing Processes*, vol. 49, pp. 153–161, 2020.

[80] N. El-Bagoury and A. Nofal, "Microstructure of an experimental Ni base superalloy under various casting conditions," *Materials Science and Engineering A*, vol. 527, no. 29-30, pp. 7793–7800, 2010.

[81] S. Barella, A. Gruttadauria, C. Mapelli et al., "Solidification microstructure of centrifugally cast Inconel 625," *China Foundry*, vol. 14, no. 4, pp. 304–312, 2017.

[82] R. Eriş, M. V. Akdeniz, and A. O. Mekhrabov, "Atomic size effect of alloying elements on the formation, evolution and strengthening of γ'-Ni3Al precipitates in Ni-based superalloys," *Intermetallics*, vol. 109, pp. 37–47, 2019.

[83] L. Zheng, C. Xiao, G. Zhang, B. Han, and D. Tang, "Primary α phase and its effect on the impact ductility of a high Cr content cast Ni-base superalloy," *Journal of Alloys and Compounds*, vol. 527, pp. 176–183, 2012.

[84] Y. Liu, J. Wang, M. Kang et al., "Microstructure evolution and mechanical performance of nickel based superalloy C1023 at elevated temperatures," *Materials Characterization*, vol. 138, no. 800, pp. 174–185, 2018.

[85] D. X. Ma, Z. H. Dong, F. Wang, and H. B. Dong, "A phenomenological analysis of freckling in directional solidification of Ni-base superalloy: the role of edge and curvature in casting components," *Metallurgical and Materials Transactions A*, vol. 51, no. 1, pp. 88–92, 2020.

[86] G. Liu, S. Winwood, K. Rhodes, and S. Birosca, "The effects of grain size, dendritic structure and crystallographic orientation on fatigue crack propagation in IN713C nickel-based superalloy," *International Journal of Plasticity*, vol. 125, pp. 150–168, 2020.

[87] M. S. Varfolomeev and G. I. Shcherbakova, "Interaction of a ceramic casting mold material of the Al2O3-Al2O3 composition with a nickel-based superalloy," *International Journal of Metalcasting*, vol. 15, no. 4, pp. 1309–1316, 2021.

[88] Z.-q. Jie, J. Zhang, T.-w. Huang et al., "Effects of grain refinement on cast structure and tensile properties of superalloy K4169 at high pouring temperature," *China Foundry*, vol. 13, no. 2, pp. 101–106, 2016.

[89] X.-M. Wang, Y. Zhou, Z.-H. Zhao, and Z. Zhang, "Microstructural evolution of creep-induced cavities and casting porosities for a damaged Ni-based superalloy under various hot isostatic pressing conditions," *Acta Metallurgica Sinica*, vol. 28, no. 5, pp. 628–633, 2015.

[90] Y. Amouyal and D. N. Seidman, "The role of hafnium in the formation of misoriented defects in Ni-based superalloys: an atom-probe tomographic study," *Acta Materialia*, vol. 59, no. 9, pp. 3321–3333, 2011.

[91] J. Hong, D. Ma, J. Wang et al., "Geometrical effect of freckle formation on directionally solidified superalloy CM247 LC components," *Journal of Alloys and Compounds*, vol. 648, pp. 1076–1082, 2015.

[92] N. Ren, J. Li, C. Panwisawas, M. Xia, H. Dong, and J. Li, "Thermal-solutal-fluid flow of channel segregation during directional solidification of single-crystal nickel-based superalloys," *Acta Materialia*, vol. 206, Article ID 116620, 2021.

[93] L. Qin, J. Shen, Q. Li, and Z. Shang, "Effects of convection patterns on freckle formation of directionally solidified Nickel-based superalloy casting with abruptly varying cross-sections," *Journal of Crystal Growth*, vol. 466, pp. 45–55, 2017.

[94] J. Zhang and R. F. Singer, "Hot tearing of nickel-based superalloys during directional solidification," *Acta Materialia*, vol. 50, no. 7, pp. 1869–1879, 2002.

[95] X. Zhu, F. Wang, T. Wittenzellner et al., "Investigation of start block and corresponding influence for grain selection during casting of single-crystal superalloys," *Materials*, vol. 12, no. 10, p. 1717, 2019.

[96] X. Ma, H. Shi, J. Gu, Z. Wang, H. Harders, and T. Malow, "Temperature effect on low-cycle fatigue behavior of nickel-based single crystalline superalloy," *Acta Mechanica Solida Sinica*, vol. 21, no. 4, pp. 289–297, 2008.

[97] H. Zhang and Q. Xu, "Simulation and experimental studies on grain selection and structure design of the spiral selector for casting single crystal Ni-based superalloy," *Materials*, vol. 10, no. 11, pp. 1236–11, 2017.

[98] T. F. Baranova, S. A. Valiakhmetov, G. V. Gogolev et al., "Experience of using silica-free alumox binder in technology for preparing composite ceramic investment casting molds for superalloy directional solidification," *Refractories and Industrial Ceramics*, vol. 57, no. 4, pp. 335–341, 2016.

[99] W.-d. Bian, H.-r. Zhang, M. Gao et al., "Influence of yttrium and vacuum degree on the purification of K417 superalloy," *Vacuum*, vol. 152, pp. 57–64, 2018.

[100] F. Wang, D. X. Ma, J. Zhang, S. Bogner, and A. Bührig-Polaczek, "A high thermal gradient directional solidification method for growing superalloy single crystals," *Journal of Materials Processing Technology*, vol. 214, no. 12, pp. 3112–3121, 2014.

[101] D. Szeliga, "Microstructure refinement of single crystal Ni-based superalloy by improvement of thermal radiation shielding in the industrial-scale Bridgman solidification process," *International Communications in Heat and Mass Transfer*, vol. 118, Article ID 104868, 2020.

[102] D. Zhang, Z. Feng, C. Wang, W. Wang, Z. Liu, and W. Niu, "Comparison of microstructures and mechanical properties of Inconel 718 alloy processed by selective laser melting and casting," *Materials Science and Engineering A*, vol. 724, no. 100, pp. 357–367, 2018.